An Experimental and Analytical Exploration of the Effects of Manufacturing Parameters on Ceramic Pot Filter Performance

by

Amelia Tepper Servi

B.S. Massachusetts Institute of Technology 2010

SUBMITTED TO THE DEPARTMENT OF MECHANICAL ENGINEERING IN PARTIAL FULFILLMENT OF THE REQUIREMENTS FOR THE DEGREE OF

MASTERS OF SCIENCE IN MECHANICAL ENGINEERING
AT THE
MASSACHUSETTS INSTITUTE OF TECHNOLOGY

JUNE 2013

Author_____
Department of Mechanical Engineering
May 17, 2013

Certified by_____
Susan Murcott
Senior Lecturer of Environmental Engineering
Thesis Supervisor

Certified by_____
Daniel Frey
Professor of Mechanical Engineering
Thesis Supervisor

Accepted by_____
David Hardt
Professor of Mechanical Engineering
Graduate Officer

An Experimental and Analytical Exploration of the Effects of Manufacturing Parameters on Ceramic Pot Filter Performance

by

Amelia Tepper Servi

Submitted to the Department of Mechanical Engineering
on May 17, 2013 in partial fulfillment of the
Requirements for the Degree of Master of Science in
Mechanical Engineering

ABSTRACT

Ceramic pot filters (CPF) are a promising low-cost option for household water treatment, providing a barrier of protection against microbiological contaminants for households with or without reliable piped water supplies. The goal of this thesis is to provide CPF manufacturers with tools to increase their ability to reach performance objectives for CPF flow rate, bacteria removal and strength. This is achieved by experimentally determining relationships between these three aspects of performance and three manufacturing values: percentage rice husk, rice husk size and wall thickness. These relationships are used to run a series of optimizations that result in design recommendations including the recommendation to increase wall thickness to improve bacteria removal and to tightly control rice husk size to maintain consistent flow rates. In addition to the experimental relationships, this author seeks a theoretical explanation of filter performance. Through this process, the author determined that hydraulic head can be increased without decreasing bacteria removal and that incomplete combustion should not be of primary concern to manufacturers. While the results in this study are preliminary, the systematic approach to the CPF design shown here can be used in future studies to further analyze and improve the CPF design.

Thesis Supervisors: Senior Lecturer Susan Murcott, Professor Daniel Frey

ACKNOWLEDGEMENTS

There are so many people whom I want to thank for making this thesis happen and for making it such a meaningful experience along the way.

First, I want to thank Susan Murcott for supporting me in so many ways. She has been an amazing mentor, and I enjoyed our personal talks as much as our technical ones. The attention and interest she takes in her students is inspiring and her office was an oasis within MIT. I am grateful for the time and effort she spent working with me.

I want to thank Dan Frey, who took me on as a graduate student and encouraged me to pursue a project that I was passionate about – that encouragement made all the difference.

I want to thank Amos Winters for steering me toward the big issues within international development and for emphasizing the importance of discovering science in addition to working on design. He picked me up when I was a wandering first year and I cannot thank him enough.

I want to thank the many wonderful and supportive staff at MIT, especially Leslie Regan, Joan Kravit and Una Sheehan, who helped me through the hoops, and Mary Rowe, who was a great sounding board when I got existential. I am sure I would not have made it to graduation without them.

I want to thank my fellow graduate students (some of them now post-graduate) who shared in camaraderie and support both technical and personal: Daniela Faas, Shane Colton, Charles Guan, Rachel Batzer, Faye Wu and Nevan Hanumara.

I want to especially thank the members of D-Grads: Amy Banzaert, Mark Jeunnette, Amit Gandhi, Lennon Rodgers, Greg Tao and David Taylor. They created a valuable forum for discussion and the sharing of knowledge.

I want to thank the hardworking and brilliant staff at IDE-Cambodia, especially Ros Kimsan, Chea Saroeun, Sarath Ouk, Kuoch Tol, Mariko Takeuchi and Mike Roberts, who were wonderful hosts and taught me so much. I am inspired by their hard work and passion. I also want to thank Gretchen Yuan for making my time in Cambodia that much more fun.

I want to thank the staff at Pure Home Water, especially Abraham Musah, Awal Iddrisu, Alhassan Iddrisu and Abdul-Karim Alale. In addition, Mary Kay and Charlie Jackson were great hosts in Accra. I also want to thank the woman potters and clay pounders, whose spirit and strength are inspiring. I want to thank the Ghana team: Deborah Vacs Renwick, Kristine Cheng, Shen Yang, Abel Manangi and honorary members Prakesh, Jaya and Bhavna Ramchandani for making the time in Ghana memorable. I also want to thank Matt Miller with whom I shared early experiments in the lab, and Mark Williams with whom I had some interesting and enlightening chats.

I want to thank the people who read and reviewed this thesis. Peter Kang gave me insightful feedback, articulately delivered. Ezra Glenn talked me through the data, Vishal Gupta

gave me a crash course on optimization techniques and Travis Reed Miller gave a thorough read for clarity. Their efforts helped me organize the work and hopefully make it a more useful product.

I also want to thank the people who helped with my many hands-on experiments: Steve Rudolph is a wizard and helped me many times when I was in a jam. He set up the strength experiment rig in record time. The Pappalardo shop guys, especially Bill Cormier and Jimmy Dudly, have been there my whole graduate school career and were always good for letting me use the machines, giving design advice or having a chat. Amy Tatem and Steven Kooi at the MIT Institute for Soldier Nanotechnologies ran the mercury intrusion samples, and I am still amazed at their generosity. Patrick Boisvert at the Center for Materials Science and Engineering at MIT helped me run the SEM, and I am thankful for his skill and patience. Mike Tarkanian was generous as well, giving me access to a kiln when I needed one. Barbara Hughey was also a huge help, always able to produce the right sensor at the right time. Also, a few people got me started with the daunting task of learning how to culture *E. coli*. Without the help from Deepak Dugar, Andrew Jones and Isabelle Gensburger my bacteria would have died before they reached the filters!

I want to thank my family: Mom, Dad, Jim, Susan, Joe, Jesse, Grandma and Grandpa, who are always there for me and who provide me with a haven away from MIT. In particular, my father, Les Servi, has in some ways been like a third advisor to me. I also want to thank Grandma Deborah, who passed away, but who I am sure would be proud. I want to thank my friends from home, pika and beyond. I'm so lucky to have all of you! And I want to thank Tamzin too, who makes everything better always.

This thesis builds on the work of many others. I am in awe of the many researchers, manufacturers and distributers who have taken this once obscure technology and made it into a product that saves lives every day. I have greatly enjoyed being a part of this project.

This work was funded in part by SUTD/MIT International Design Center and by the Public Service Center at MIT.

Table of Contents

List of Abbreviations

cfu: Colony-forming unit
CPF: Ceramic pot filter
E. coli: *Escherichia coli*
IDE: International Development Enterprises
LB: Lysogeny broth (also called Luria broth)
LRV: Logarithmic reduction value
MIT: Massachusetts Institute of Technology
PBS: Phosphate buffered saline
PHW: Pure Home Water
SEM: Scanning electron microscope
UNICEF: United Nations Children's Fund
USAID: United States Agency for International Development
WHO: World Health Organization

List of Variables

A: cross-sectional area of a filter disk [m^2]
a: half crack length [m]
α: removal constant [ ]
B: bacteria removal [ ]
C(x): concentration of contaminants at a position x [m^{-3}]
C_{in}: concentration of contaminants entering the filter [m^{-3}]
C_{out}: concentration of contaminants leaving the filter [m^{-3}]
D: rice husk size [m]
d: characteristic pore size [m]
d_c: grain diameter [m]
d_h: pore height [m]
d_b: diameter of bacteria [m]
E: Young's modulus [N/m^2]
ε: porosity by volume [ ]
F_{max}: load at rupture
G: total removal in a layer [m^{-1}]
G_c: strain energy release rate [J/m^2]
h: hydraulic head [m]
η: collision percentage [ ]
K: hydraulic conductivity [m/s]
l: length of the pipe [m]
L: wall thickness [m]
μ: dynamic viscosity [kg/ms]
M_{crit}: moment at rupture [Nm]
N: number of pipes [ ]
N': scaled number of pipes [ ]
n: number of pores in a layer of the filter [ ]
P: percentage combustible by mass [ ], pressure [Pa]
ΔP: pressure drop [Pa]
ϕ: contact angle [radian]
Q: volumetric flow rate [m^3/s]
q: volumetric flow rate of a single pipe [m^3/s]
R: probability per unit length that contaminant will be removed from solution [m^{-1}]
r_c: capillary radius [m]
S: strength normalized to the PHW filter [ ]

σ: surface tension [N/m]
σ_{max}: modulus of rupture [N/m^2]
T: tortuosity [ ]
w: sample width [m]
Δx: a single step in the direction of x [m]

List of Figures

List of Tables

Chapter 1: Introduction

1.1 Motivation

According to the WHO/UNICEF *Progress on Drinking Water and Sanitation 2012 update*, over 780 million people worldwide do not have access to improved sources of drinking-water[1] with 84% of that population living in rural areas [1] (Figure 1-1). The disease burden from lack of safe water, sanitation and hygiene accounts for 4.0% of all deaths and 5.7% of the total disease burden worldwide [2]. Children are especially vulnerable with 21% of deaths of children under five years in developing countries occurring from diarrheal disease [3] (Figure 1-2). Since diarrheal diseases are transmitted mainly through the fecal-oral route, of which drinking water is a part, water quality interventions can reduce the disease burden by as much as 42% [4].

Figure 1-1: Highly turbid drinking water source near the city of Tamale in Northern Ghana.

Figure 1-2: Child infected with worms living in Northern Ghana.

Ceramic pot filters (CPF) are one of many options for household water treatment [5] (Figures 1-3, 1-4 and 1-5). One of the advantages of the CPF is its utilization of the worldwide availability of local clays and ceramic manufacturing traditions. The design includes a method of safe water storage, and the filter can effectively treat highly turbid water. It is one of the less

[1] The definition of "improved drinking water" and many other specialized words in this study can be found in the glossary at the end of this document.

expensive forms of water treatment, costing $8-$40 for filters that last multiple years [6]. The design has traction in the international community, gaining support from international agencies such as USAID and UNICEF and being the subject of academic studies at several major universities. In a 2007 study by Joe Brown in Cambodia, the CPF was shown to reduce diarrheal diseases by 40% in areas where it was used [7]. A meta-regression by Hunter in 2009 found that "with the currently available evidence, ceramic water filters are the most effective form of household water treatment in the long term" [8]. For these reasons, the CPF is an important technology to study.

Figure 1-3: Ceramic filter element.

Figure 1-4: Assembled filters.

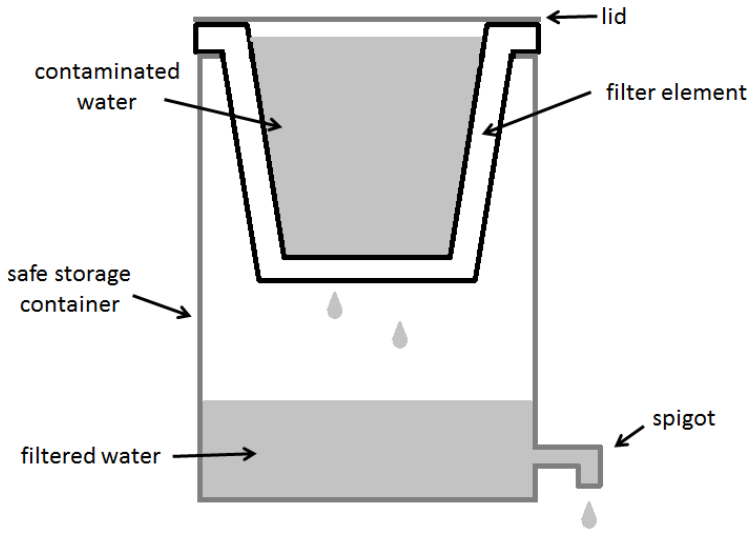

Figure 1-5: Schematic of the assembled CPF.

1.2 Background

The CPF was invented by Fernando Mazariegos in Guatemala in 1981. Since 1998, the NGOs, Potters for Peace and Potters without Borders among others, have promoted the production of CPFs based on Mazariegos' design [9]. These filters are currently produced in 52 independently run factories in 31 countries (personal communication with Susan Murcott, March, 2013). In 2001, an MIT student team supervised by Susan Murcott conducted the first independent, academic research study of the filters, and subsequently Daniele Lantagne, supported by USAID, wrote a report that brought the CPF into the English-language published sphere [10].

The CPF filter element is made out of porous ceramic. The ceramic is produced from a mixture of clay powder, water and either rice husk or sawdust all sourced locally. The mixture is typically formed into a pot shape that can hold from 6 to 11 liters [6] and allowed to dry before being fired in a kiln. During the firing process, the rice husk or sawdust combusts as the clay sets, producing pores in the filter (Figure 1-6). Upon removal from the kiln, the filter is tested for quality. If it passes inspection, it is painted with a silver compound which acts as a biocide and packaged along with a safe storage container for shipment. Factories vary in their level of mechanization, recipe, filter shape and type of silver, among other parameters, but the basic process and design is generally the same.

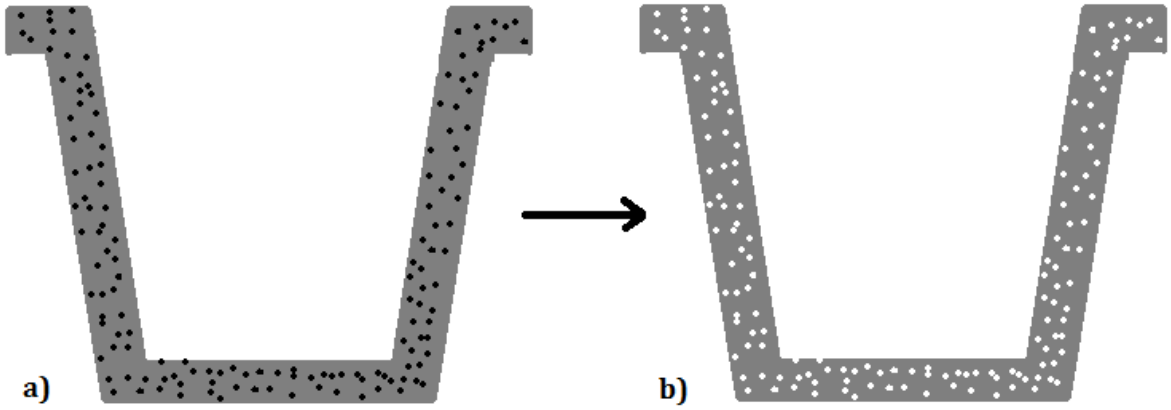

Figure 1-6: Schematic of the CPF Before (a) and after (b) firing. The black dots represent rice husk or sawdust particles. The white dots represent pores.

Many studies of the efficacy of the CPF have been conducted over the years. These have included studies of filter performance in the laboratory and in the field, as well as studies of health impact and user acceptance. Many of these studies are discussed in [11]. More recently, several new studies have been conducted in order to determine the effects of various manufacturing parameters on CPF performance. The "Best Practice Recommendations for Local Manufacturing of Ceramic Pot Filters for Household Water Treatment," referred to in this document as the "Best Practices Guide", was created in 2011 to bring together information about the design and manufacturing decisions made at factories around the world [6]. Together, the efforts of the many researchers and manufacturers worldwide have steadily developed and improved the effectiveness of the CPF as a product.

1.3 Performance requirements

Ceramic pot filters were designed for a challenging environment. Among other factors, they must be extremely low-cost, easy to use, robust and able to handle very turbid water. Ideally, they should remove a variety of pathogens including bacteria, viruses and protozoa, and they should be a product that users find attractive and want in their homes. In this thesis the author focuses on understanding and optimizing for three aspects of filter performance which reflect the basic functioning of the CPF. The three performance metrics addressed in this thesis are **flow rate**, **bacteria removal** (in this study, indicated by *E. coli* removal) and **strength**. These performance metrics as they relate to the CPF are described in more detail below:

1.3.1 Flow rate

CPF factories around the world have different standards for the amount of water that must filtered per hour. Figure 1-7, reprinted from the *Best Practices Guide*, shows the ranges of flow rates that have been deemed acceptable by various factories around the world [6]. Ranges are given instead of single values because manufacturers are often unable to control flow rates within a tight tolerance. Out of the set of factories that responded to the survey, acceptable flow rates ranged from 1L/hr to 5L/hr. However, this author knows of at least one

factory that allows filters with flow rates up to 7L/hr. While each factory has chosen ranges for flow rate that are acceptable to them, a common complaint from users about the CPF is that filtration is too slow. This is especially a problem after the system has started to clog with contaminants. For this reason, many users would benefit if manufacturers could produce a faster filter.

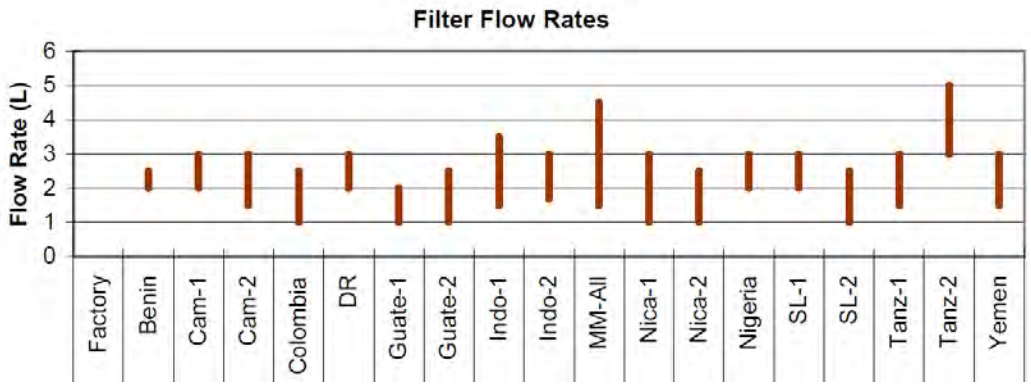

Figure 1-7: Allowable flow rates at factories around the world measured in L/hr [6].

1.3.2 Bacteria removal

CPFs from factories around the world also display different levels of bacteria removal. While data for this aspect of performance have not yet been consolidated in the same way as the flow rate information, manufacturers can reference the *WHO Guidelines for Drinking Water Quality 4th Edition* when deciding on acceptable microbiological removal levels [12] (Figure 1-8). These guidelines do not require 100% removal of biological contaminants, but rather high enough removal to reduce the contaminant load to a level that can be tolerated by the human body. While different factories sell filters that achieve different levels of bacteria removal, not all factories are satisfied with the levels of bacteria removal that they are achieving. Thus, the factories and customers would benefit from increased bacteria removal. In addition, due to the high cost, logisitical challenges and technical skill requirements of microbiological testing, many factories do not conduct regular water quality testing [6] making it very important that the manufacturing process be well controlled for the parameters that affect contaminant removal.

Target	Log_{10} reduction required: **Bacteria**	Log_{10} reduction required: **Viruses**	Log_{10} reduction required: **Protozoa**
Highly protective	≥ **4**	≥ **5**	≥ **4**
Protective	≥ **2**	≥ **3**	≥ **2**
Interim	Achieves "protective" target for two classes of pathogens and results in health gains		

Figure 1-8: WHO drinking water guideline expressed as log reduction values[2] [12].

1.3.3 Strength

Data for filter strength have not been consolidated across the many CPF factories. However, despite the lack of data, breakage of filters is an acknowledged problem. In surveys conducted in Cambodia in 2007, Brown found that 65% of disuse of CPFs after distribution or sale was due to filter breakage [7], emphasizing the need for stronger filters.

1.4 Thesis goal and objectives

While many studies of the CPF have focused on specific factories and their manufacturing decisions, this author adds to the field by taking a step back and considering the effects of the manufacturing parameters at a level that is applicable across factories. The goal of this thesis is to provide a framework for understanding the effects of manufacturing parameters on filter perforamance and so give ceramic pot filter manufacturers the tools

[2] Log reduction value is defined in Section 1.4.1 as well as in the glossary.

needed to achieve their performance targets. In pursuit of this goal, the author hopes to serve the many people around the world who lack access to safe drinking water.

The goal of this thesis is approached through three objectives:

Objective one: Determine the relationships between three key manufacturing parameters and three key metrics of filter performance (see Figure 1-9).

Objective two: Examine the internal structure and filtration mechanisms of the CPF and develop a theoretical model to describe it.

Objective three: Use the results from Objectives one and two to produce recommendations about the design of the CPF.

Objective one is addressed in Chapters 2-4. Chapter 2 introduces data from existing studies of the relationships between various manufacturing parameters and filter performance. Chapters 3 and 4 describe the methods and results from this author's own experiments which fill in the gaps in the existing literature. Objective two is addressed in Chapter 5, introducing additional experimental results and anlaysis which build our understanding of the internal mechanisms of the CPF. Objective three is addressed in Chapters 6 and 7 with formal optimizations presented in Chapter 6 and design recommendations and areas for future work presented in Chapter 7.

1.4.1 Objective one: Manufacturing parameters/performance relationships

Flow rate, bacteria removal and strength are interrelated and often in conflict with each other; increasing one often decreases the other two, forcing manufacturers to choose between them based on their relative importance. In the case of CPFs manufactured with rice husk, these three aspects of filter performance are largely determined by three manufacturing parameters: **percentage rice husk**, **rice husk size** and **wall thickness** (Figure 1-9). In this thesis, the author will investigate the relationships between each manufacturing parameter and the three performance metrics, while building a framework into which additional manufacturing parameters and metrics of performance could be added.

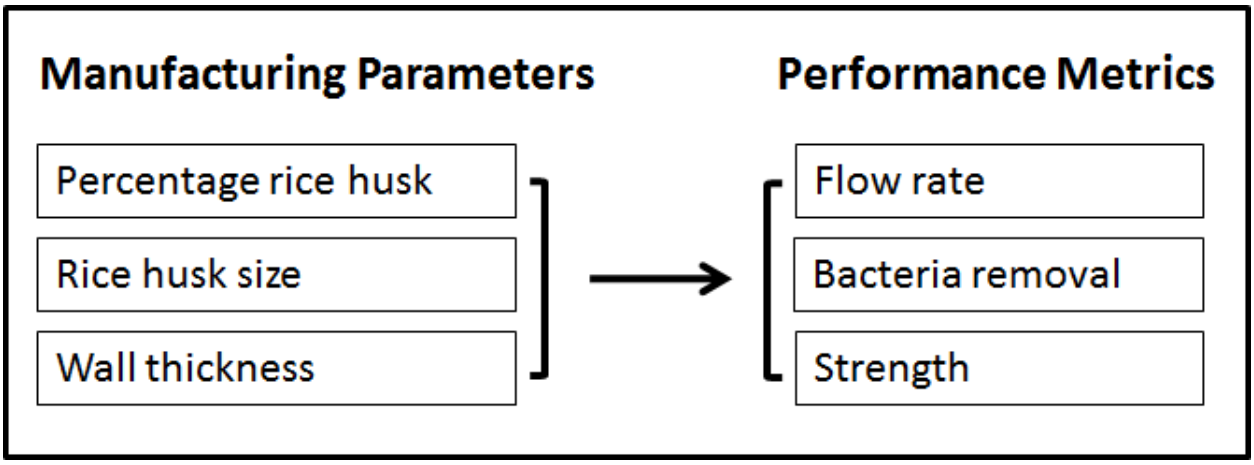

Figure 1-9: Three key manufacturing parameters and three key metrics of performance.

The three manufacturing parameters were chosen for their importance in determining performance, their controllability by the manufacturer and their applicability across many factories. Additional parameters such as the effects of silver, other types of combustibles, clay parameters and firing parameters are left for future studies. Definitions of the manufacturing parameters and the metrics of performance are described below.

Definitions of the manufacturing parameters:

Percentage rice husk: Percentage rice husk is the mass of rice husk as a fraction of the total mass of dry materials (clay powder and rice husk) incorporated in the filter. The percentage rice husk contributes to the porosity of the fired filter, where porosity is defined as the volume percentage of void space.

Rice husk size: In this study, the effects of rice husk size were studied by sieving the rice husk for each filter between two different sized meshes. During sieving, rice husk particles that were larger than the openings of the courser mesh or smaller than the openings of the finer mesh were discarded. In this study, rice husk size for a filter is reported as the average of its courser and finer mesh diameters. Rice husk size is also sometimes expressed as a range between the courser and finer mesh diameters. Figure 1-10 shows rice husk sieved to 400-500µm. Milled, unsieved rice husk is typically in the range of 0-2000µm.

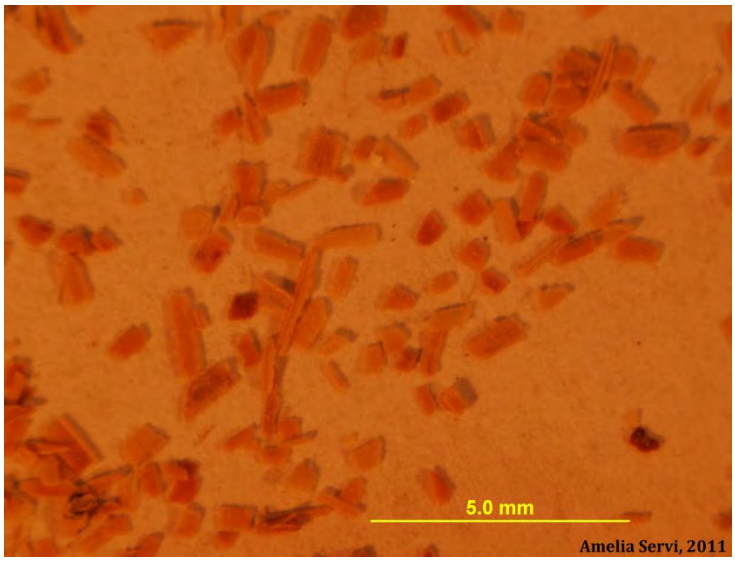

Figure 1-10: Rice husk that was sieved between 400 and 500µm meshes.

Wall thickness: Wall thickness is defined as the distance between the inside and outside surface of a CPF. When working with filter disks (as will be described in Chapter 3) wall thickness is the height of the disk (Figure 1-11).

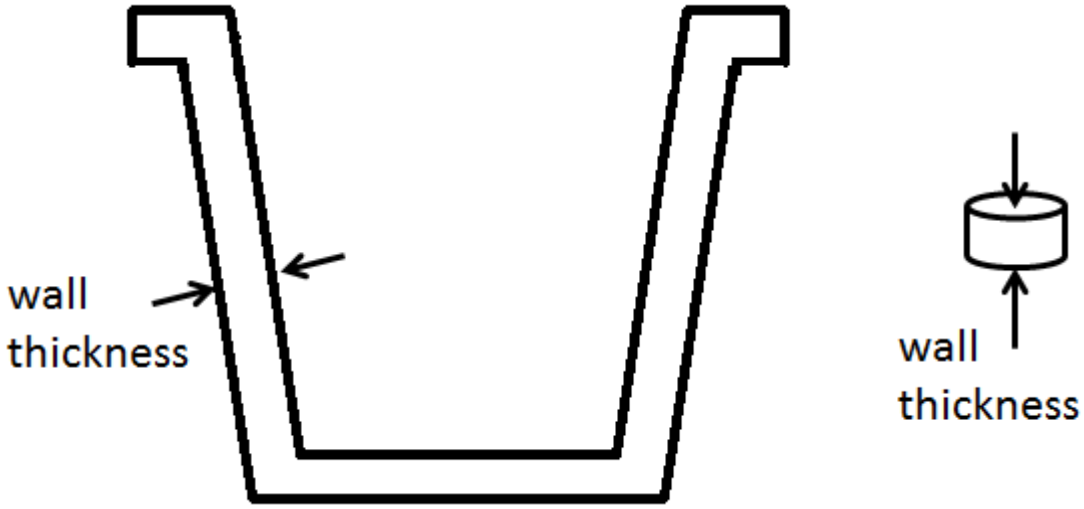

Figure 1-11: Wall thickness of a filter and a disk.

Definitions of the metrics of performance:

Flow rate: Flow rate equals the volume of liquid per unit time exiting the CPF.

Bacteria removal: Removal of bacteria is expressed as a logarithmic reduction value (LRV) where

$$LRV = -\log\left(\frac{\#\ cfu\ in\ influent}{\#\ cfu\ in\ effluent}\right)$$

Equation 1-1

and colony forming units (cfu) is the number of viable bacterial cells per unit volume. This is a standard metric of bacteriological drinking water quality [13].

Strength: Reported as the moment at rupture, strength of the CPF is defined as the amount of torque that must be applied to the filter wall to cause it to fail. Strength is also sometimes reported as the modulus of rupture which is the maximum stress that can be sustained within the filter wall before failure.

The outcome from Objective one is a full description of the relationships between the three manufacturing parameters and the three performance metrics.

1.4.2 Objective two: Internal mechanisms

The author explores fine-grained models of the CPF in order to relate the performance metrics to the manufacturing parameters. In the process, the author addresses a number of aspects of the internal structure and behavior of the CPF including:

- The relationship between flow rate and bacteria removal;
- The effects of incomplete combustion of the rice husk on flow rate and bacteria removal;
- The relationship between hydraulic head and flow rate;
- The relationship between rice husk size and pore size/shape;
- The role of a removal constant in bacteria removal;
- The relationship between rice husk size and tortuosity.

These areas of inquiry will be described in more detail in Chapter 5.

The outcomes of Objective two are models describing flow rate, bacteria removal and strength as functions of the manufacturing parameters. These models are not definitive but provide a starting point to be built upon. Preliminary results regarding the internal structure of the CPF are also presented along with directions for future investigation.

1.4.3 Objective three: Design recommendations

The author uses her understanding of the CPF, based on the results of Objectives one and two, to conduct a series of optimizations to determine the limiting factors of the CPF design and the ways to improve the choices of parameter values. The optimization methods presented in Chapter 6 can be expanded to include additional manufacturing parameters and performance metrics. The design recommendations presented in Chapter 7 reflect the author's current understanding of the CPF and could be tested in the laboratory or in a pilot factory setting. The author expects these recommendations to be expanded and modified as more experimental data becomes available.

Chapter 2: Literature review

2.1 Prior experimental studies

The first objective of this thesis is to determine the relationships between three manufacturing parameters (percentage rice husk, rice husk size and wall thickness) and three metrics of filter performance (flow rate, bacteria removal and strength). These manufacturing parameters and performance metrics are organized by the author into a matrix as shown in Table 2-1. In this matrix, the author summarizes some of the experimental results of Rayner [14], Gensburger [15], Plappally [16], Miller [17], Lantagne [18], Watters [19], and Miller [20]. The ovals in Table 2-1 are the areas where this author will add new data, as presented in Chapter 4.

Table 2-1: Parameter/performance matrix filled with data from the literature[3].

Performance metrics

Manufacturing parameters	Flow rate	Bacteria removal	Strength
Percentage rice husk	Gensburger[15]: positive linear	Gensburger[15]: no correlation	Plappally[16]: negative correlation[1]
	Miller[17]: positive linear	Miller[17]: no correlation[3]	Watters[19]: negative correlation
	Rayner[14] : positive correlation		
	Plappally[16]: positive correlation[1]		
	Lantagne[18]: positive correlation[1,2]		
	Miller[20]: positive correlation[2]		
Rice husk size	Rayner[14]: positive correlation	Rayner[14]: negative correlation	
Wall thickness		Rayner[14]: positive correlation	Watters[19]: power relationship

The author chose this matrix configuration in order to see where prior studies exist and where more work is needed. This framework can be easily expanded to include other parameters and performance metrics as further progress is made in the study of the CPF.

[3] Explanations of the superscripts are found on the next page.

For this thesis, only studies with more than two distinct values of the manufacturing parameter are included in the matrix. In addition, this author only included studies where an explicit conclusion was drawn by the author for the relationship of interest.

Since every study is conducted differently, a number of distinctions should be made. While this thesis focuses on filters produced with rice husk as the combustible, data from Plappally[16] and Lantagne[18] who used sawdust as the combustible were considered relevant and so were included in Table 2-1 (denoted by superscript 1). In addition, while this thesis focuses on filters that were not painted with silver, flow rate results from Lantagne[18] and Miller[20] who did use silver, are still included (superscript 2). While this study focuses on the removal of *Escherichia coli* (*E. coli*) as the indicator of bacteria removal, this author includes the results of Miller[17] who used total coliform as a biological indicator (superscript 3).

Appendix A contains quotations, details and figures from the studies in Table 2-1. While this author does not fully explain the methods or the results in all of the figures, the reader can inspect the data for themselves in the original documents.

2.2 Prior theoretical studies

2.2.1 Characteristic pore size

Van Halem conducted an interesting study regarding the flow and filtration mechanisms of the CPF [21]. In particular, she worked towards an understanding of characteristic pore size, the importance of which this author discusses in more detail in Section 5.1. Van Halem investigated characteristic pore size via mercury intrusion porosimetry and the "bubble point test." Both of these methods can be used to calculate a "characteristic pore length" which is one interpretation of characteristic pore size. Characteristic pore length corresponds to the minimum diameter through which a liquid needs to pass in order to breach the filter. The results from Van Halem's tests are shown in Table 2-2. The first column shows the country of origin of the filter samples. The values in the second column were determined using mercury intrusion porosimetry, details about which method can be found in Webb [22]. The values in the third column were determined using the bubble point test, a test where air is forced against

the inside of a submerged filter, and the pressure corresponding to the first bubbles seen on the outside of the filter is used to calculate a characteristic pore length. Details about the bubble point test can be found in Van Halem's report [21].

Table 2-2: Characteristic pore lengths for filters from three countries. Adapted from [21].

Characteristic length (µm) determined by:		
	Mercury Intrusion Porosimetry	Bubble Point Test
Cambodia	13	20
Ghana	12	22
Nicaragua	9	20

Van Halem's work showed that the characteristic pore lengths of the CPFs, contrary to previous assumptions, are larger than bacteria which typically range in size from two to five microns. Her work also indicated that the characteristic pore length is larger than the pores found in ceramics in the absence of rice husk or sawdust. These pores, which this author calls the "intrinsic clay pores," are typically on the order of two to five microns as can be seen in the SEM image in Figure 5-4. Thus the intrinsic pores are smaller than the characteristic pore lengths found by Van Halem. In addition, Van Halem's results show that the characteristic pore lengths are smaller than the size of rice husk or sawdust particles which are typically on the order of 100-2000µm in diameter. Together her results imply that flow through the CPF is more complicated than a straight path through the pores made by the rice husk or sawdust or a straight path through the intrinsic clay pores. Table 2-3 summarizes these relevant sizes.

Table 2-3: Relevant size scales.

Relative sizes in microns			
bacteria size	intrinsic pores	characteristic pore length	rice husk size
2 - 5µm	2 - 5µm	9 - 22µm	100 - 2000µm

2.2.2 Flow rate

Van Halem also discussed a model for flow rate through the CPF based on the theory of packed columns. This model is described by the Carman-Kozeny equation:

$$r_c = \sqrt{\frac{8\mu LQ}{\varepsilon \Delta P A}}$$

Equation 2-1

where r_c is the capillary radius, μ is dynamic viscosity, L is wall thickness, Q is volumetric flow rate, ε is porosity, ΔP is pressure drop across the surface and A is surface area. This hydrodynamic model for flow rate will be discussed further in Section 5.4 of this thesis.

This form of Equation 2-1 can be used to calculate a capillary radius based on the measured values of the variables on the right hand side of the equation. Using her experimental values, Van Halem calculated values for r_c ranging from 12 to 17 microns for the filters described in Table 2-2. These values are of the same order of magnitude as the characteristic pore lengths calculated from mercury intrusion porosimetry and the bubble point test, indicating that the Carman-Kozeny model may accurately describe flow through the CPF. This subject is addressed further in Section 5.4 of this thesis.

2.2.3 Contaminant removal

Van Halem began the process of modeling contaminant removal of the CPF by proposing a list of possible mechanisms of filtration [21]. These mechanisms include sedimentation, diffusion, inertia, turbulence and adsorption all of which will be described in more detail in Section 5.5.1 of this thesis. This author builds on Van Halem's work to further investigate the candidate mechanisms of bacteria removal.

2.2.4 Strength modeling

Watters [19] considered the theoretical relationship between moment at rupture and wall thickness of the CPF, determining that theoretically

$$M_{crit} = \frac{\sigma_{max} w L^2}{6}$$

Equation 2-2

where M_{crit} is the moment at rupture (a property of an object), $\sigma_{max}$is the modulus of rupture (a property of a material), w is the width of the sample and $L$is the wall thickness [19]. In his thesis, Watters reported experimental data showing that strength increased more with additional wall thickness than predicted by the theoretical model. He found experimentally that

$$M_{crit} \sim L^{2.6}$$

Equation 2-3

leaving this area open for debate.

Chapter 3: Methods

A number of experiments were conducted by this author in order to fill in the holes in the parameter/performance matrix introduced in Section 2.1. The results from these experiments are presented in Chapter 4. Additional experiments were conducted in order to better understand the internal mechanisms of the filters. Those results are presented in Chapter 5.

3.1 The factories

The work done by this author was made possible through collaborations with two CPF factories, Hydrologic in Cambodia and Pure Home Water (PHW) in Ghana. Hydrologic, spun off of IDE-Cambodia, builds on more than ten years of production experience. This author spent June-August of 2011 at Hydrologic, and many of the experiments in this study were conducted using samples from filters produced at that factory.

Pure Home Water, located in Tamale in Northern Ghana, was founded in 2005 by Susan Murcott, Senior Lecturer at MIT, together with Mary Kay Jackson PE, a water engineer who is the Managing Director of PHW. Pure Home Water's factory was built between 2010 and 2012 with production beginning in February 2012. The author spent January of 2013 at the Pure Home Water factory. Many of the samples used in this study were made from clay and rice husk brought back to MIT from the Pure Home Water factory.

The author's time at the factories largely informed the work presented in this thesis. In particular, the author's focus on rice husk size was a direct result of observations made at the Hydrologic factory. Similarly, the author's choice to study filter strength was due to observations at the Pure Home Water factory. In addition, at the factories the author gained an appreciation for the challenges faced by manufacturers of the CPF who not only have to make design decisions but also need to develop and run a full production enterprise.

3.2 List of experiments

Wall thickness test: The purpose of these experiments was to determine the relationship between wall thickness and flow rate and bacteria removal. Filter samples were produced at Hydrologic in August, 2011 using a special composition as requested by this author. Samples were not painted with silver. Experiments were conducted in Susan Murcott's laboratory at MIT from November, 2011-January, 2012.

Rice husk size test: The purpose of these experiments was to determine the relationship between rice husk size and flow rate and bacteria removal. Filter samples were produced using clay and rice husk imported from the PHW factory in September, 2012. Samples were produced at MIT in September, 2012 and experiments were conducted from September-December, 2012 in Susan Murcott's laboratory at MIT. Samples were not painted with silver.

Hydraulic head test: The purpose of these experiments was to determine the relationship between hydraulic head and flow rate and bacteria removal. The same samples were used as for the rice husk size tests and the experiments took place within the same time frame and location as the rice husk size tests.

Wall strength test: The purpose of these experiments was to determine the relationship between rice husk size and wall strength. The same samples were used as for the rice husk size tests. Experiments were conducted in the MIT Civil and Environmental Engineering Laboratory with help from Steven Rudolph in March, 2013.

Droplet test: The purpose of these experiments was to determine the number of independent paths that the water takes to flow through the filter. Experiments were conducted at the IDE office in Phnom Penh, Cambodia using filters that were made during regular production at Hydrologic. The filters were not painted with silver. Experiments were conducted in August, 2011.

Mercury intrusion porosimetry: The purpose of these experiments was to learn more about the internal structure of the CPF material, especially how that internal structure is affected by rice husk size. The same samples were used as for the rice husk size tests.

Experiments were conducted at the Institute for Soldier Nanotechnologies at MIT by Amy Tatem-Bannister and Steven Kooi in March-May, 2013.

Scanning electron microscopy: The purpose of these experiments was to learn more about the internal structure of the CPF material. Filter samples were produced at Hydrologic in August, 2011 according to Hydrologic's standard composition. The samples were not painted with silver. Experiments were conducted at the MIT Center for Materials Science and Engineering with help from Patrick Boisvert in November, 2011.

3.3 Wall thickness test

3.3.1 Samples

This author spent June-August, 2011 at the Hydrologic factory in the Kampong Chhnang Province in Cambodia. The purpose of this research period was to understand the effects of manufacturing parameters at the factory in order to improve quality assurance. During this time, at the request of the author, a set of filters were produced by the factory for use in the author's research.

As per Hydrologic's standard composition, the filters consisted of 73.6% local clay and 26.4% rice husk by mass. While Hydrologic's standard filters are made with rice husk sieved to within the 0-1000µm range, the special filters produced for this author were of four variations with rice husk size ranges of 0-400µm, 400-500µm, 500-1000µm and 400-1000µm. Ten filters of the first three types along with 90 filters of the fourth type were produced. Samples were manufactured as full filters and tested for flow rate while still at the factory. The bottoms of five of each type of filter were then sawed off and transported back to MIT though only some of these filters were ever tested at MIT. In addition, one filter from Hydrologic's regular production was brought back to MIT for analysis using a scanning electron microscope.

At MIT, a hole-saw was used to produce disks of average diameter 27.6mm (tolerance ± 1.05mm) (Figure 3-1). All data used in analysis was normalized to a standard disk diameter to make the results comparable. The starting wall thicknesses of the disks ranged from 14.7 to 20.2mm due to two different molds being used at the Hydrologic factory at that time.

Figure 3-1: Disk cut from the bottom of the filter. The disk is used in the experiments.

The disks were coated around the sides with two coats of clear marine silicone sealant and cemented using PC-11 epoxy paste to the bottom of 33cm long, 27mm diameter PVC pipes. In this configuration, when the pipes were filled, water would flow through the disks (Figures 3-2 and 3-3).

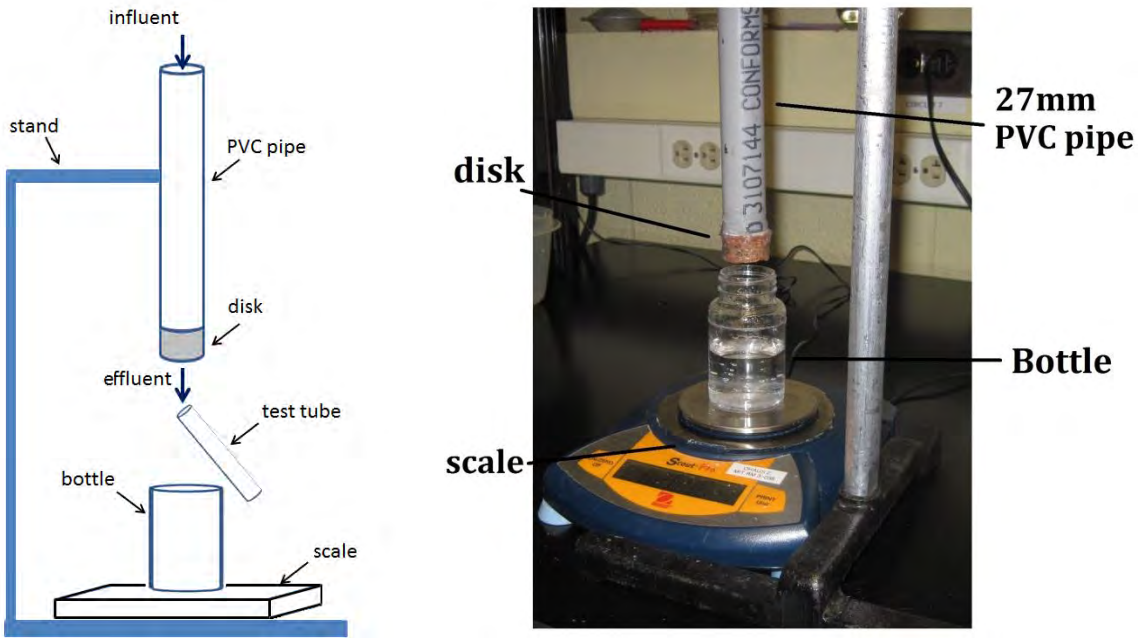

Figures 3-2 and 3-3: Disk attached to the PVC pipe and held over a bottle on the scale.

Experiments were conducted using small disks instead of full filters in order to facilitate doing the experiments at MIT where the author could benefit from full laboratory facilities. Bringing back only the bottoms of the filters from Cambodia allowed the author to transport many more samples then if full filters had been used. Using small disks also decreased the laboratory space and influent needed to run the experiments. The wall thicknesses of the disks could also be manipulated more easily than would be possible for full filters. In addition, the simple geometry of the disks makes the results more generalizable to the varied geometries of the filters produced around the world.

The disadvantages of using the disks was that preparing the samples was time-consuming, and the experiments themselves often took many hours due to the small surface areas of the disks causing low flow rates. In addition, the use of disks required a more complex experimental setup than would be needed if full filters were used.

During each experiment, a disk/PVC unit was placed in a lab stand over a bottle atop a Vernier Ohaus Scout Pro scale with 120g capacity and 0.001g precision. The scale was connected to a computer, and LabPro software was used to continuously record the weight of the effluent over the course of the experiment so that the flow rate of the disk could be calculated. When the author needed to test the bacterial load in the effluent, a sterile test tube was used to collect drops from the bottom of the disk as shown in Figure 3-2. Samples of the influent were taken with a sterile pipette from the top of the PVC pipe.

3.3.2 *E. coli* influent preparation

All bacterial experiments conducted by the author used *Escherichia coli* K12, bought from ATCC, a private, nonprofit biological resource center[4]. The *E. coli* was prepared in Luria Broth (LB) to produce a slurry containing 10^9 colony forming units (cfu) per 1mL. The slurry was diluted in phosphate buffered saline (PBS) made with deionized water to 10^5 cfu/mL to be used as the influent in the experiments. The author used prepared influent instead of water from a

[4] http://www.atcc.org/

natural source in order to control the amount and type of bacteria in the influent and to avoid the clogging that occurs when using turbid water from a river or pond.

In order to determine the *E. coli* concentration of the influent in units of cfu/mL, samples were diluted by 100 times (50µL of sample pipetted into 5mL deionized water), and 50µL of the dilution was pipetted and spread onto an LB agar plate. After incubation, the number of colonies on the plate was counted to determine the concentration of bacteria in the influent.

In order to determine the *E. coli* concentration of the effluent in units of cfu/mL, samples were diluted by 100 times (50µL of sample pipetted into 5mL deionized water) and 50µL of the original sample and 50µL of the dilution were pipetted and spread onto separate LB agar plates. Using this method, generally one of the dilutions would produce too many or too few colonies on the plate, and the other dilution would produce a countable number. In this way, the author was able to determine the cfu/mL of the effluent despite varying bacteria removal levels between experiments. By measuring the cfu/mL in both the influent and effluent, the LRV of the disks could be calculated.

All bacteriological tests were conducted in triplicate (three independent samples taken and plated at a time) so that the median value could be selected for use in the LRV calculations. This was done to protect the data from the noise that is often present in bacteriological data as an artifact of the measurement process. Details about culturing the *E. coli* and making the agar plates can be found in Appendix B.

3.3.3 Preliminary test

Before conducting the wall thickness tests, a preliminary test was done on a disk from the 400-1000µm rice husk size group. The purpose of the test was to determine the total amount of throughput that needs to pass through a clean disk before the flow rate and LRV become constant. This was done to ensure that the data collected for the future tests would not be influenced by transient effects.

Before beginning the test, the disk was soaked in clean PBS for 24 hours in order to saturate. This was done in order to be comparable to the many studies of CPFs which saturate the filters in clean water or PBS before taking measurements. After soaking, the disk/PVC unit was placed in a lab stand over a scale, and the PVC attachment was filled with the influent to a height of 30cm. This height of 30cm was maintained manually for the duration of the experiment using a pipette. Samples of the influent and effluent were collected and plated at increments of throughput as shown in Figure 3-4. Flow rates were also measured concurrently as shown in Figure 3-5.

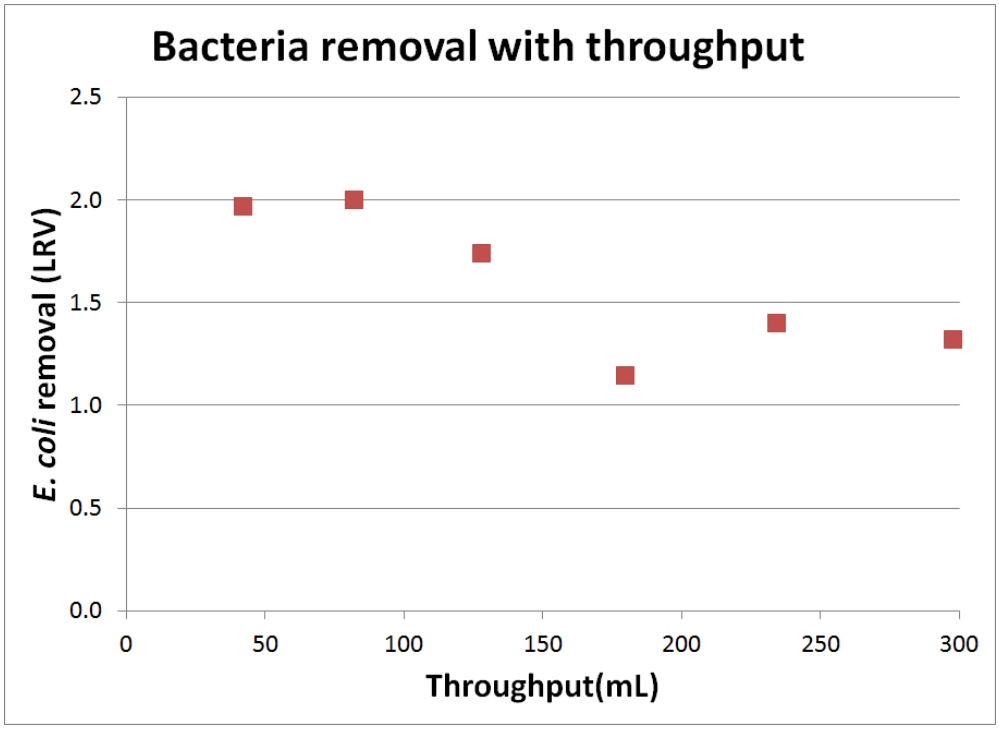

Figure 3-4: Bacteria removal with respect to throughput (preliminary test).

Figure 3-4 shows that the measured *E. coli* removal for this sample decreased over the first 175mL of throughput before stabilizing. This is likely due to the contaminated influent initially mixing with clean PBS that was left inside of the disk after soaking. The effluent is thus less concentrated initially because the PBS solution dilutes the effluent, causing an apparent larger LRV. As more contaminated influent passes through the filter, this effect diminishes and

the measured *E. coli* removal approaches the true value, and it is safe to start running the actual experiments.

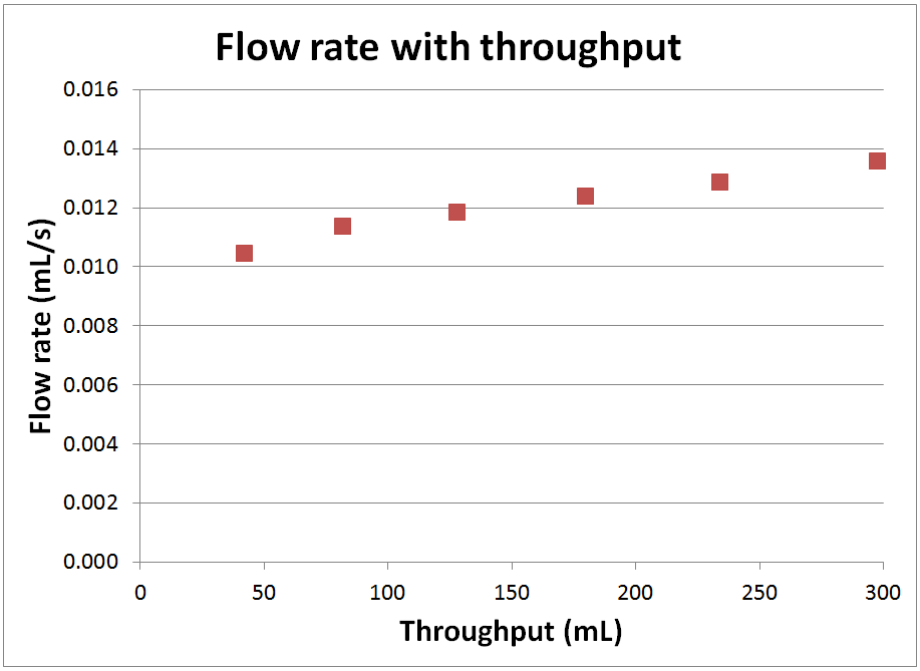

Figure 3-5: Flow rate with respect to throughput (preliminary test).

Figure 3-5 shows the flow rates measured at the same time as the data points in Figure 3-4. The data show flow rate increasing with throughput indicating an initial instability. Due to time constraints, even though the flow rates had not stabilized after 300mL as shown in Figure 3-5, the researcher decided to conduct the subsequent experiments after the 300mL throughput mark. This may have caused inaccurate flow rate measurements, but it is hoped that the errors are small and comparable between experiments.

The results from this test are important because they illustrate that filters that were saturated in clean PBS will not show accurate bacteria removal or flow rates initially. This means that researchers should wait until the system stabilizes before taking measurements for their experiments. While at least 300mL was needed to pass through the small disks, much larger amounts should be allowed to pass through full filters before taking measurements.

3.3.4 Wall thickness protocol

The wall thickness tests were performed in order to determine the relationship between wall thickness and bacteria removal and flow rate. The researcher started with full thickness disks and then reduced their wall thicknesses incrementally over the course of the experiment using a dremel with a sanding attachment (Figure 3-6). After dremeling, the wall thickness of the samples was measured with calipers.

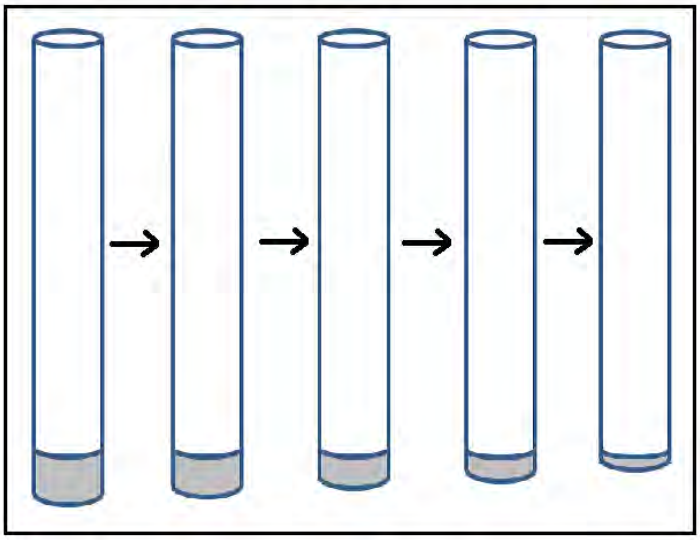

Figure 3-6: Progressively decreased wall thickness.

The author chose to incrementally decrease wall thickness instead of starting with disks manufactured to varying wall thickness for a number of reasons. When initially conducting the experiment, the author did not know where within the disks the bacteria were being caught. By removing a layer of the disk at a time, the author was able to determine the contribution to bacteria removal of each layer of a single disk. In addition, working with full disks from filters produced at Hydrologic allowed the author to explore the effects of incomplete combustion as will be discussed further in Section 5.3 of this thesis.

As with the preliminary tests, the disks were soaked for 24 hours in clean PBS before starting the experiment. The disk/PVC unit was then placed in a lab stand with the PVC pipe filled to a height of 30cm. This height was maintained for the duration of the experiment. After

300mL of influent had passed through the filter, samples of the influent and effluent were collected, and flow rate was measured.

After taking measurements, the PVC pipe was emptied and a dremel with a sanding attachment was used to shave off a prescribed thickness from the bottom surface of the disk. The first round of dremeling only took off minimal thickness in order to establish a baseline "post-dremel" LRV and flow rate. The disk was then rinsed briefly in clean PBS and placed back into the lab stand. The PVC pipe was filled with influent to 30cm and the test was run again waiting 15mL before taking samples of the influent and effluent and measuring the flow rate. The PVC was emptied again, and another round of dremeling was conducted. This procedure was repeated until the disk was too thin to continue testing.

During this experiment, 15mL of contaminated influent was allowed to wash through the sample between dremeling rounds in order to remove any contamination and dust from the surface of the disk that may have been added during the dremeling and rinsing process. The author was also careful to keep the disk from being contaminated during dremeling by keeping the area sterile and sterilizing the sanding attachment between rounds.

3.4 Rice husk size test

3.4.1 Samples

The filter samples for the rice husk size tests were produced at MIT using clay and rice husk from the Pure Home Water factory in Northern Ghana. The change from using filters produced at Hydrologic to using materials from Pure Home Water was due to logistical and funding reasons. The change from importing filters produced at a factory to producing the filters at MIT was done to allow more flexibility in filter composition than would be possible at a factory. Since the results of the various tests are reported separately, the change in disk source should not affect the validity of the conclusions.

Making the disks at MIT instead of at a factory introduces some issues that should be addressed. The most important is the difference in molding technique. While filters produced in the factories are typically shaped using a hydraulic press and mold, the disks made at MIT

were formed by packing clay into a wooden mold by hand and then pushing them out with a flat disk. This could cause the rice husk in the samples made at MIT to be less well aligned than they would be for filters made at a factory. More discussion on rice husk alignment can be found in Section 5.1.4 of this thesis. In addition, pressing the disks by hand may affect the structure of the intrinsic clay pores due to the lower compression force. However, these factors were outweighed by the ability afforded to control the composition and firing parameters of filter production by producing the disks at MIT.

The disks used in the rice husk size tests matched the PHW standard composition of 80% local clay and 20% rice husk by mass. Before mixing the dry ingredients, the clay was sieved using a 710µm mesh, a step that was not undertaken at the PHW factory at the time of the author's fieldwork in January, 2013. The author added this step to improve the consistency of the disks. While filters made during standard production at Pure Home Water are made with rice husk sieved to between 0 and 1500µm, the samples made by this author were tightly controlled for rice husk size. Six variations of disks were produced, sieving the rice husk to the following size ranges: 208-355µm, 355-420µm, 420-590µm, 590-710µm, 710-850µm and 850-1000µm. In addition, four disks with a rice husk size range of 590-850µm were also produced. Figures 3-7 and 3-8 show the inside surfaces of a 208-355µm and a 710-850µm disk.

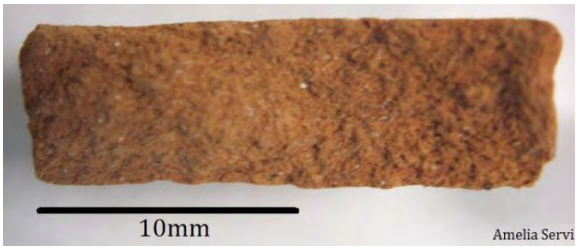

Figure 3-7: Inside surface of a disk produced with risk husk sieved to 208-355µm.

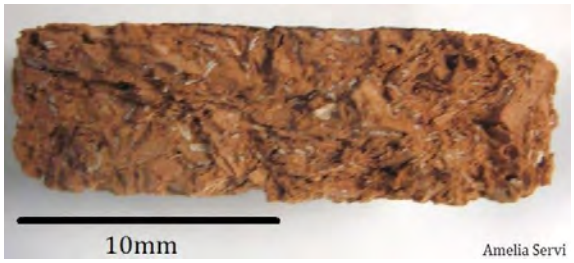

Figure 3-8: Inside surface of a disk produced with risk husk sieved to 710-850µm.

The disks were fired in a Nabertherm N200 oven at the MIT Department of Material Science and Engineering foundry managed by Mike Tarkanian. The Nabertherm N200 has a maximum temperature of 1300°C and is heated from five sides. Its inner dimensions (centimeters) are 50 x 53 x 59.

The firing profile for the disks consisted of a linear ramp of 73°C/hr up to 830°C and then an immediate down-ramp of 50°C/hr back to room temperature. This firing profile is similar in maximum temperature and ramping speed to the profile used at the Hydrologic factory. Using this profile, all disks were fired through completely.

At least four disks of each type were produced with an average diameter of 23.5mm (tolerance ±0.85mm) and an average wall thickness of 20.7mm (tolerance ±1.35mm). The variations were due to the nature of the manufacturing process, and all data used in analysis was normalized to standard diameter and wall thickness as needed to make the results comparable.

After firing, the disks were coated around the sides with two coats of clear marine silicone sealant and cemented using PC-11 epoxy paste to brass fittings so that water could pass through the fitting and disk (Figure 3-9). While the silicone and cement may have reduced the effective diameters of the disks, this effect is consistent across the disks and so was not factored into the analysis. During the experiments, the fittings were screwed onto a four-prong connection which was attached to a hose attached to a bucket. The bucket was hoisted to the ceiling using a pulley so that the bottom of the bucket was 2.74m above the bottoms of the lower two disks (Figures 3-10, 3-11, 3-12 and 3-13). This meant that when the bucket was filled with water, there would be at least 2.74m of hydraulic head above the disks.

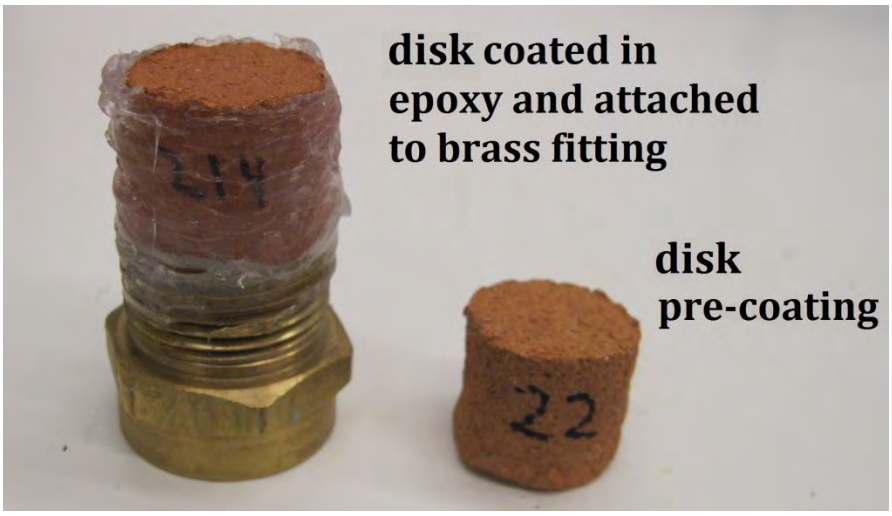

Figure 3-9: Coated and uncoated filter disks.

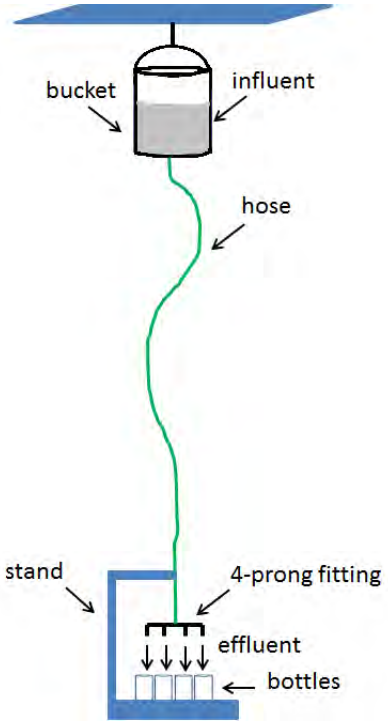

Figures 3-10 and 3-11: Bucket and hose raised 2.74 meters above the filter disks.

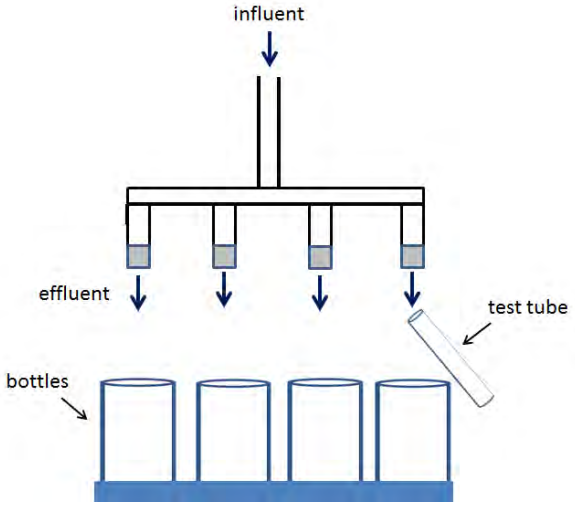

Figures 3-12 and 3-13: Four-prong fitting for the rice husk size test.

Similarly to the wall thickness tests, the hose was held in a lab stand so that the disks were over bottles. A scale was not placed under the bottles except during the preliminary test described in Section 3.4.3. Instead, flow rates were measured by weighing the cumulative effluent collected in the bottles over a set time-period. This was done because the scale could not be used for four disks at the same time. Samples of the effluent for bacteriological testing were collected in sterile test tubes as the water dripped from the bottoms of the disks. Samples of the influent were taken after conducting the experiments by removing the brass fitting and using a sterile pipette to take a sample from the influent sitting inside the fitting.

The author changed the test set-up between the wall thickness and the rice husk size tests in response to what she learned from her experiences with the wall thickness tests. In particular, the author increased the hydraulic head from 30cm to 2.74m in order to increase the flow rates so that the experiments would run more quickly. In addition, the pulley system for the bucket allowed the hydraulic head to be adjustable, a feature needed for the hydraulic head tests described in Section 3.5. Brass fittings were used instead of cementing the samples onto PVC pipes so that the samples could be swapped out easily between tests. The four-prong fitting was added so that four samples could be tested at the same time.

Another benefit of the new experimental setup was that due to the large volume of the bucket, the water level could decrease over the course of the experiments with only a fractional

reduction in hydraulic head. For example, if 2L flowed out of the bucket and through the samples, there would only be a 5% change in hydraulic head. However, the author still normalized the data for any differences in hydraulic head between tests when doing the analysis.

3.4.2 *E. coli* influent preparation

The same *E. coli* K12 in LB broth was used as for the wall thickness tests. The broth was diluted to 10^5 cfu/mL for all tests except for the two sets of disks with the smallest rice husk sizes. For those two sets of disks, the broth was diluted to 10^7 cfu/mL in order to avoid zero readings in the effluent if removal levels were higher than 10^5. It is possible that this inconsistency could compromise these data points. However the author has never seen a study showing that the influent concentration affects log reduction values for the CPFs. Rather, the many studies conducted to date by various researchers have yielded similar LRV values despite widely ranging protocols regarding influent concentration. The effect of this protocol irregularity is left as an open question.

3.4.3 Preliminary test

Similarly to the wall thickness tests, a preliminary test was done to determine the amount of throughput needed to pass through a clean disk before the flow rate and bacteria removal would stabilize. Unlike for the wall thickness tests, for this preliminary test and for the subsequent rice husk size tests, the disks were not soaked in clean PBS before conducting the experiments. This change of protocol was made in an effort to reduce the amount of throughput needed for flow rate and LRV to stabilize.

The disks used for the preliminary tests were produced at MIT out of material from PHW as described in Section 3.4.1 and had a rice husk size range of 590-850µm. The bucket was filled with 3L of *E. coli* broth and raised to 2.74m above the bottom of the lower disks. Samples of the influent and effluent were collected and plated at throughput increments as shown in Figure 3-14. Flow rate was measured continuously using a scale as shown in Figure 3-15.

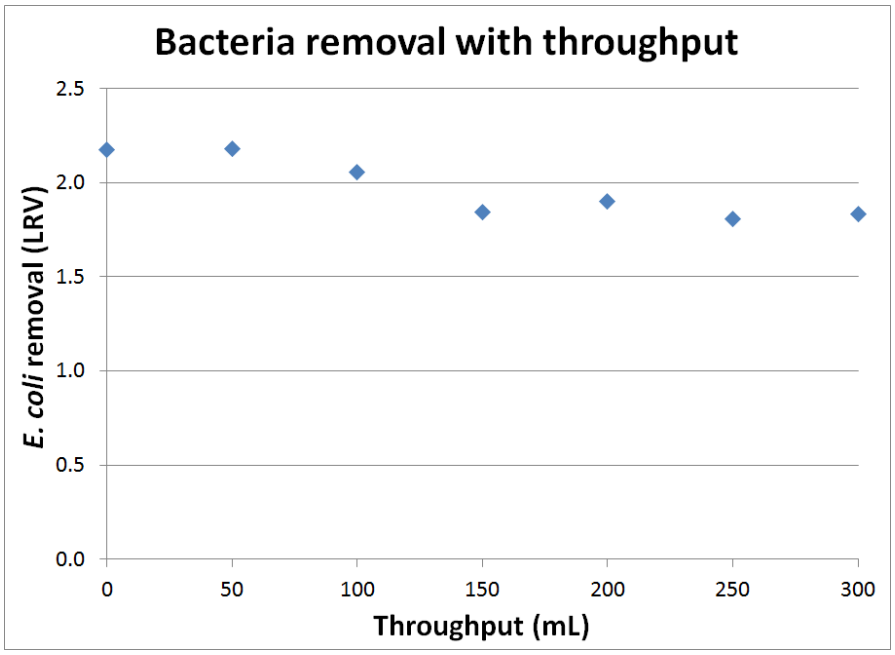

Figure 3-14: Bacteria removal with respect to throughput (preliminary test).

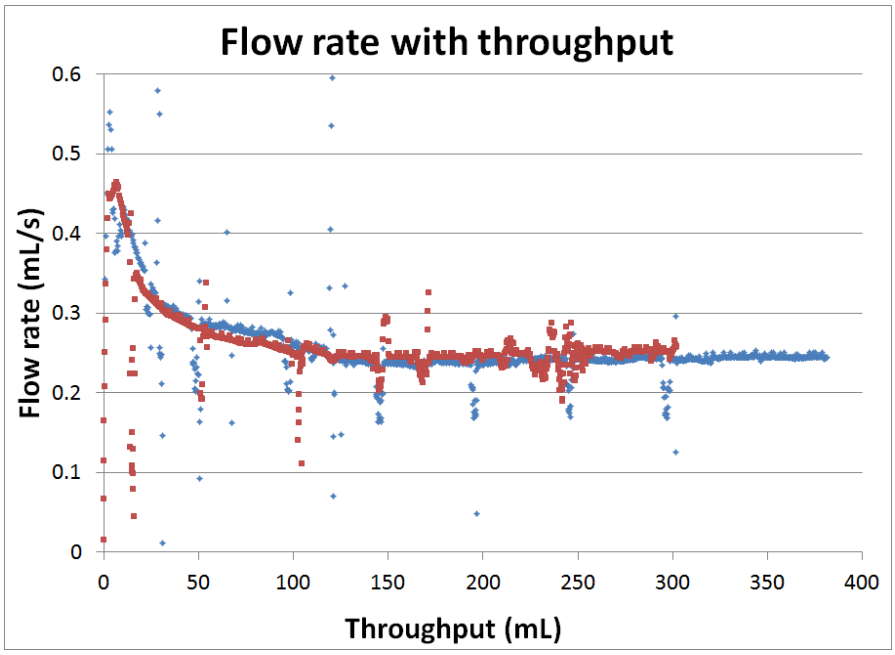

Figure 3-15: Flow rate with respect to throughput (preliminary test).

The results for this preliminary test were different in some ways than for the wall thickness preliminary test. Bacteria removal stabilized in a similar amount of time, but the change from the initial LRV to the final LRV was much less dramatic than for the previous test

setup. Flow rate stabilized much faster than for the pre-soaked case, though in this case it decreased over time instead of increasing. The author does not know the cause of this. Based on the results from this test, the author continued with the protocol of not pre-soaking, and 300mL was allowed to pass through each disk before all subsequent experiments.

3.4.4 Protocol

The rice husk size tests were conducted as follows: At the start of each round, four disks with the same rice husk size were screwed onto the four-prong attachment. The valves on the attachment were opened and 300mL of liquid was allowed to pass through each disk as measured by collecting the effluent in bottles below the samples as shown in Figure 3-12. Once 300mL had been collected in the bottles, samples of influent and effluent were collected in sterile test tubes to be plated and flow rate was measured and recorded. After collecting the influent and effluent samples and measuring flow rate, the bucket was lowered and the remaining height left in the bucket was recorded in order to calculate the hydraulic head over each disk at the time of sample collection.

3.5 Hydraulic head test

The hydraulic head tests were performed identically to the rice husk size tests except that after the first flow rate and bacteria samples were taken, the bucket was lowered from 2.74m to 2.13m. 50mL were allowed to pass through each disk in order to let the system stabilize before a second set of samples was collected. The same procedure was repeated as the bucket was lowered in increments of 61cm until it reached 30cm above the bottoms of the disks. The samples for these experiments had a rice husk size range of 590-850µm.

3.6 Wall strength test

The wall strength tests were conducted with unused disks from the rice husk size tests. These disks were reduced to a wall thickness of 0.74cm using sandpaper (Figure 3-16) in order to increase the importance of bending as opposed to shear as the failure mechanism.

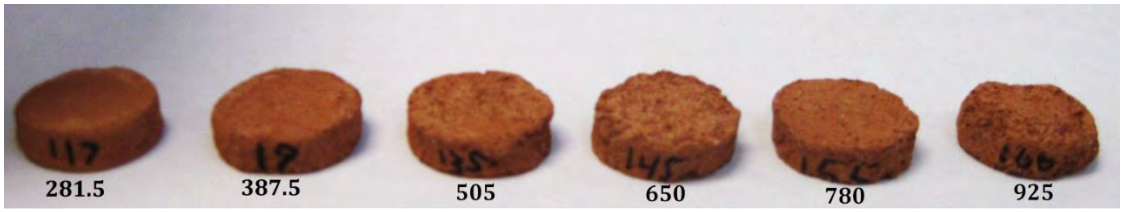

Figure 3-16: Strength test disks with their respective rice husk sizes (microns). All samples have the same wall thickness.

During the wall thickness tests, the disks were held in a vice so that one half was supported and the other half was free (Figures 3-17 and 3-18). A worm gear jack was used to lower a load cell onto a specified point on the free end of the disk as a displacement sensor recorded the position of the worm jack.

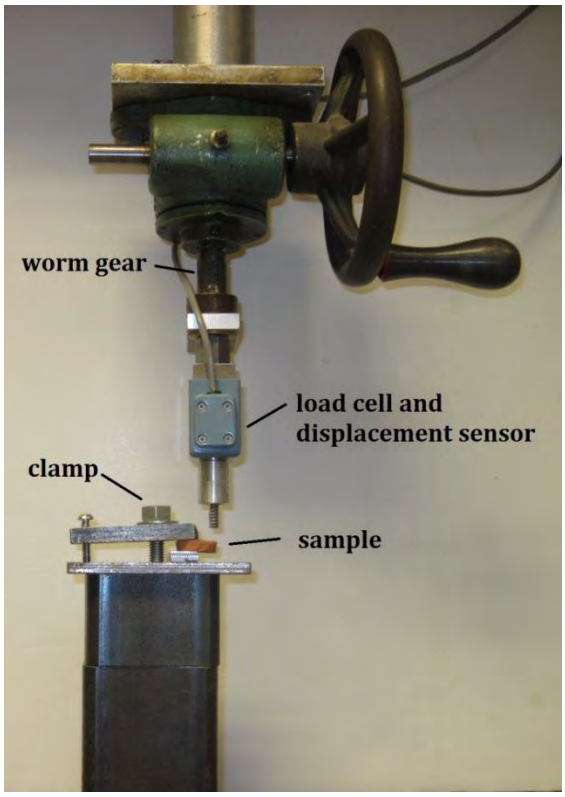

Figure 3-17: Worm gear jack, load cell and displacement sensor.

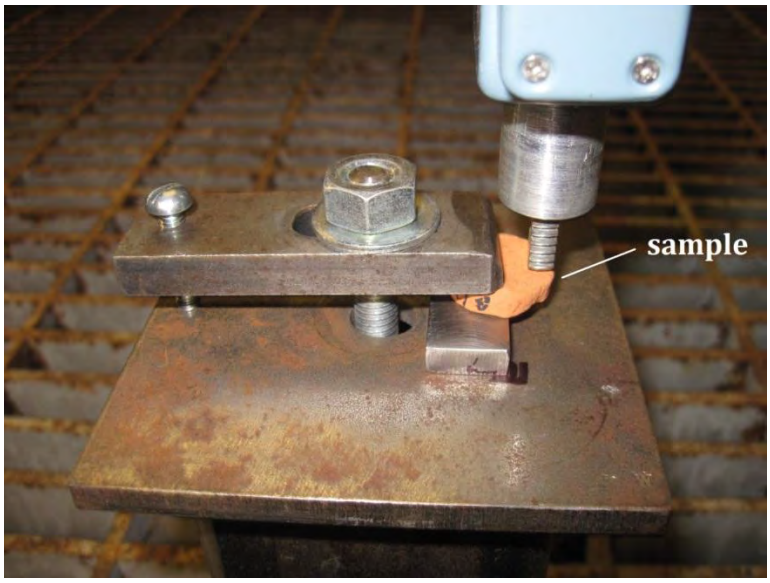

Figure 3-18: Disk clamped in the vice (close-up).

This disk geometry is not ideal for bending tests, and beam-shaped samples would yield more accurate results. However, the purpose of this test was to get a baseline set of data for

the relationship between rice husk size and filter strength, an area where no data were previously available. The author thus used the resources available to her within her time constraints. In Section 4.5 the data from these tests are reported as load at failure instead of moment at rupture due to the unorthodox geometries of the disks.

3.7 Droplet test

The purpose of these experiments was to learn more about the paths that the water takes when it flows through the filter. Experiments were conducted at the IDE office in Phnom Penh, Cambodia using filters that were made during regular production at Hydrologic. During this experiment, freshly made filters were submerged in buckets of water such that the water could seep up from the bucket and into the filter through the walls (Figure 3-19). A video camera was used to record the number of independent droplets that emerged over time.

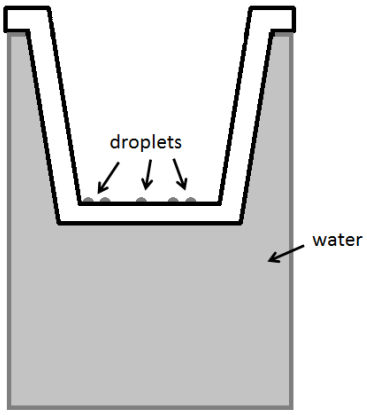

Figure 3-19: Droplet test setup.

This method for determining the number of paths through the filter was developed by this author, and the experiment was quick and easy to conduct. The filter was submerged from the bottom as opposed to being filled from the top to make it easier for the observer to record the number of droplets. While eventually, the droplets merged, it was observed that large areas of the filter surface had no droplets after much time, indicating that there are distinct paths through the filter, even if the distinct paths are not visible during regular operation.

3.8 Mercury intrusion porosimetry

Mercury intrusion porosimetry is a technique for learning about the internal pore structure of a material. For this technique, a sample is placed in a sealed chamber containing mercury vapor. Since mercury is non-wetting on most surfaces, it resists entry into the pore-network of the material. As the pressure in the chamber is increased, mercury vapor is forcibly pushed into the porous material, and the volume of absorbed mercury with respect to chamber pressure is recorded. The pressure data is then converted to pore sizes using Washburn's equation:

$$P = \frac{2\sigma}{r_c}\cos\phi$$

Equation 3-1

where P is pressure, $\sigma$is surface tension, $\phi$is contact angle and r_c is the capillary radius. The information gathered in this way can be used to draw many conclusions about the internal structure of the material. More information about mercury intrusion porosimetry can be found in Webb [22].

Filter samples were taken from unused samples from the rice husk tests. They were broken into pieces to fit into the sample holder (Figure 3-20). In addition, a sample from a filter made in January, 2013 at the Pure Home Water factory in Ghana was also tested. Breaking the filter samples into pieces possibly affects the results of the test. This is because one of the main uses of mercury intrusion porosimetry is to determine the characteristic pore length, the minimum pore size through which the mercury must pass in order to breach the sample. Since the broken pieces were not at full wall thickness, the results may not be indicative of the values for a full filter.

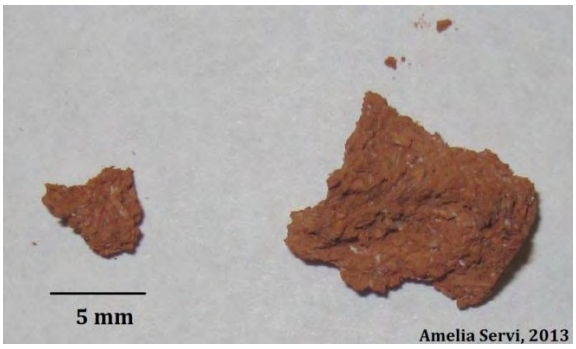

Figure 3-20: Sample for the mercury intrusion machine.

The mercury intrusion tests were conducted courtesy of the Institute for Soldier Nanotechnologies at MIT using a Micromeritics AutoPore IV 9500. Sample pieces were placed into a penetrometer as shown in Figure 3-21 and pressure was increased from 0.53psi, the pressure associated with a pore size of 400µm, to 30,000psi, the pressure associated with a pore size of 0.007µm.

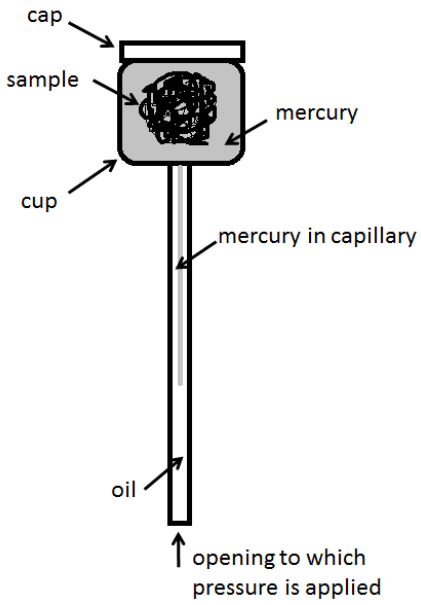

Figure 3-21: Penetrometer containing a filter sample.

3.9 Scanning electron microscope (SEM)

Scanning electron images were obtained for samples from filters produced at the Hydrologic factory in Cambodia. Images were taken of the rough, internal surface produced by breaking off a piece from the full filter (Figure 3-22). The images were taken using an FEI XL30

SEM in the MIT Center for Materials Science and Engineering. The FEI XL30 has a resolution of 3.5nm. Images for this study were taken at 250x and 2500x magnification at 15.0kV using Gaseous Secondary Electron (GSE) detection. A working distance of 10.4mm and a spot size of 3.0nm were used. More information about SEM imaging can be found in Jeol [23].

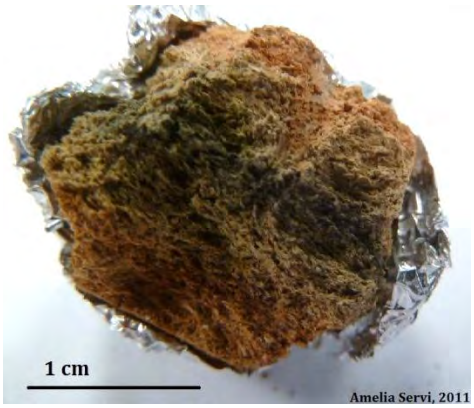

Figure 3-22: Sample for the SEM.

Chapter 4: Results

This chapter presents the data collected by this author using the experimental methods described in Chapter 3. The results presented in this chapter fill the gaps in the parameter/performance matrix introduced in Chapter 2. Additional data relevant to the theoretical discussion of the CPF are presented in Chapter 5. Tables containing the experimental data for this chapter and others can be found in Appendix C.

This chapter contains results for the relationships between:

- Wall thickness and flow rate;
- Wall thickness and bacteria removal;
- Rice husk size and flow rate;
- Rice husk size and bacteria removal;
- Rice husk size and strength.

4.1 Wall thickness and flow rate

The author first addresses flow rate with respect to wall thickness. Sample preparation and protocol were conducted as described in Section 3.3. All samples used in this experiment were produced at the Hydrologic factory in Cambodia and consisted of 26.4% rice husk by mass with a rice husk size of 400-1000µm and an average surface area of 600mm^2. The hydraulic head above the disks was 30cm. Data from four disks are plotted in Figure 4-1.

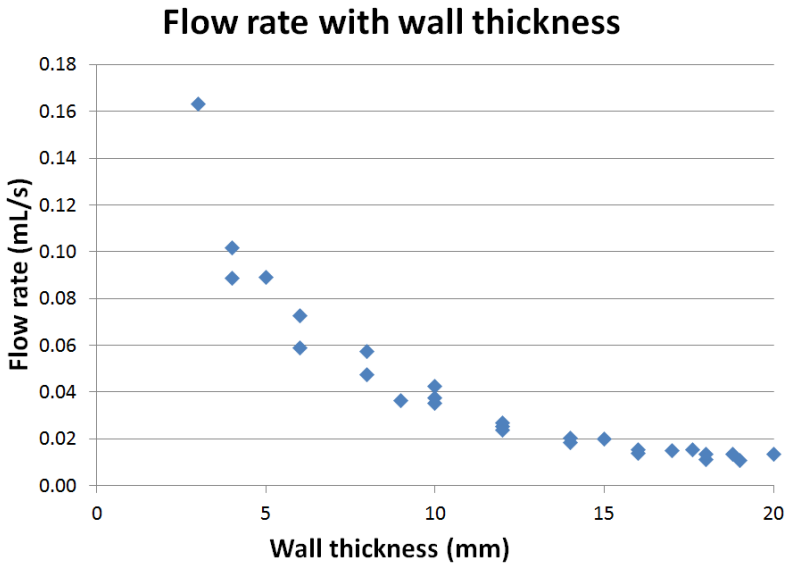

Figure 4-1: Flow rate with respect to wall thickness.

This data confirms that flow rate through the CPF is proportional to the inverse of the wall thickness. This is easier to see when the same data are plotted with respect to the inverse of wall thickness as shown in Figure 4-2.

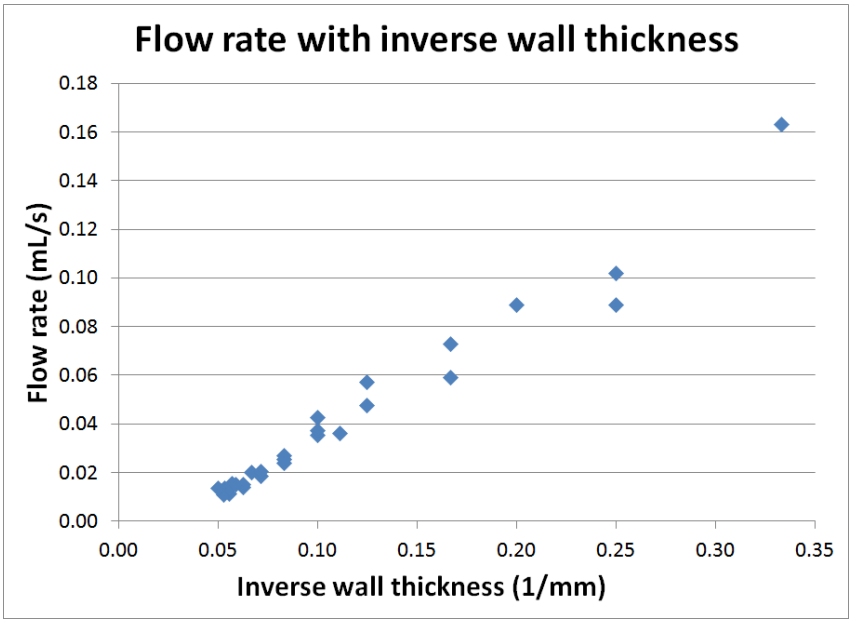

Figure 4-2: Flow rate with respect to the inverse of wall thickness.

This inversely proportional relationship between wall thickness and flow rate shows that the CPF acts in a way that is consistent with Darcy's law for laminar flow through porous media given by

$$Q = \frac{KAh}{L}$$

Equation 4-1

where Q is volumetric flow rate, $K$is hydraulic conductivity, A is the cross-sectional area, h is the hydraulic head in meters and L is wall thickness. Darcy's Law is useful in that it allows a hydraulic conductivity to be calculated that is independent of the geometry of the sample or hydraulic head used in the experiment. The fact that the CPF is consistent with Darcy's law with respect to wall thickness has often been assumed but not experimentally demonstrated in the published literature about the CPF.

4.2 Wall thickness and bacteria removal

The author next addresses bacteria removal with respect to wall thickness. Sample preparation and protocol were conducted as described in Section 3.3. All samples were produced at the Hydrologic factory in Cambodia and consisted of 26.4% rice husk by mass. The three series in Figure 4-3 represent three separate filter disks with rice husk ranges of 400-500µm, 400-1000µm and 500-1000µm. These three disks were chosen in order to determine if the relationship between bacteria removal and wall thickness held across different disk compositions. The average surface area of the disks was 600mm^2, and the hydraulic head above the disks was 30 centimeters. Two of the disks started at 20mm wall thickness and the third one started at 15mm wall thickness. The results from this experiment are plotted in Figure 4-3.

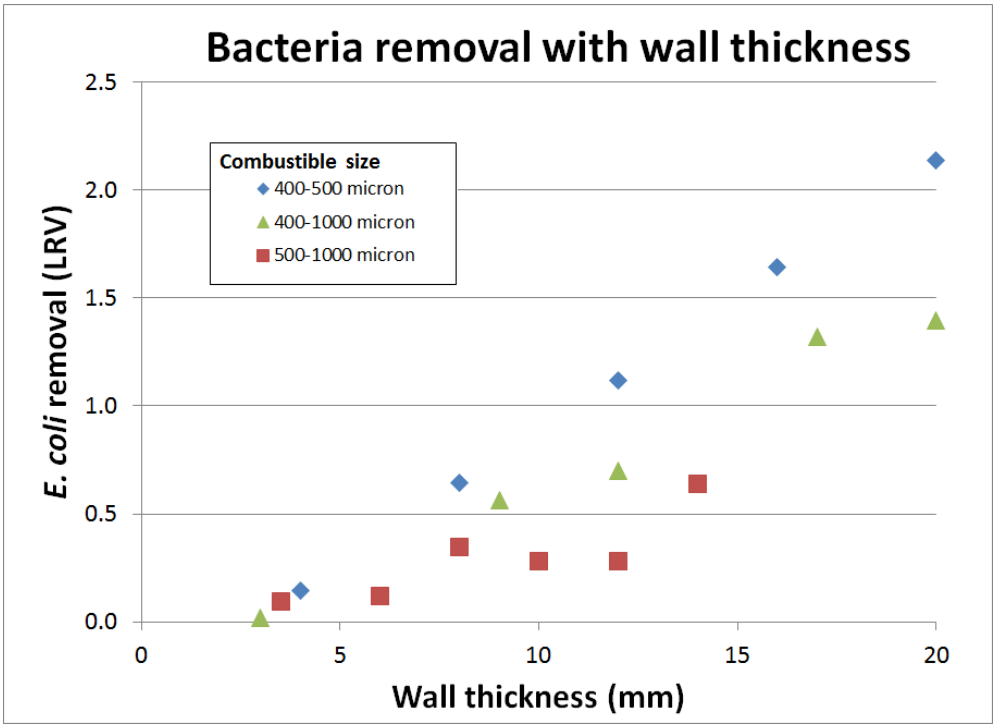

Figure 4-3: Bacteria removal with respect to wall thickness.

The relationship between wall thickness and bacteria removal appears to be linear with the slopes varying according the size of the disk's rice husk. This implies that bacteria are caught throughout the thickness of the sample. All curves have an x-intercept at approximately 2.8mm indicating a minimum thickness that allows for bacteria removal.

4.3 Rice husk size and flow rate

Flow rate with respect to rice husk size is addressed next. Sample preparation and protocol were conducted as described in Section 3.4. All disks were produced at MIT out of clay and rice husk from the Pure Home Water factory and consisted of 20% rice husk by mass. The hydraulic head above the samples at the time the data was collected ranged from 2.77-2.88m. Before plotting, flow rates were normalized to a hydraulic head of 2.74m in order to make the results comparable. Each point in Figure 4-4 corresponds to a single disk and is plotted at the x-value that represents the average rice husk size of the disk.

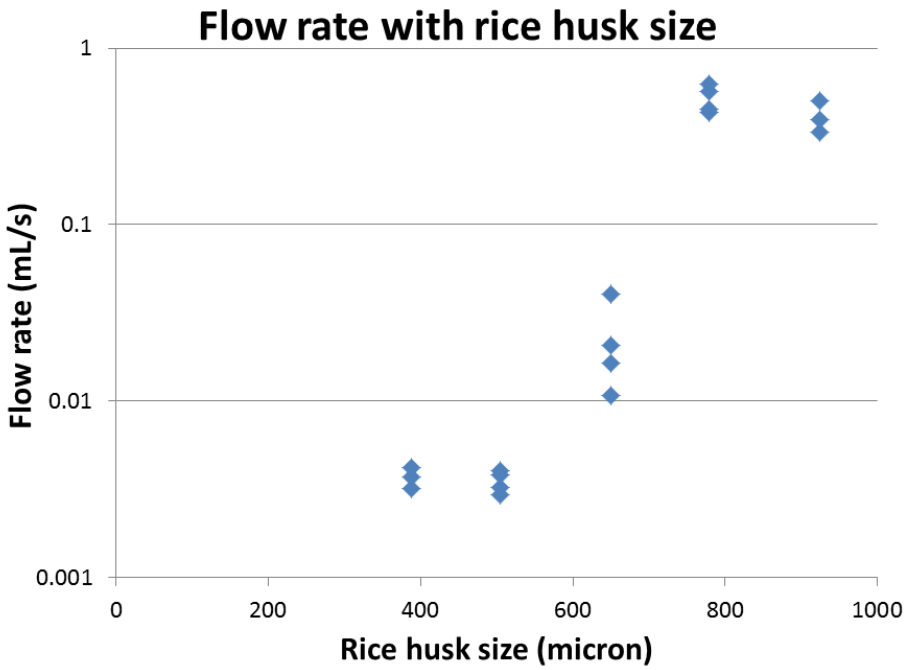

Figure 4-4: Flow rate with respect to rice husk size.

In Figure 4-4, flow rate is plotted on a logarithmic scale in order to show the full range of the measured flow rates. The data suggests an exponential relationship between rice husk size and flow rate. Another interpretation is that there are two regimes for flow rate, one relatively low (approximately 0.003mL/s) and the other relatively high (approximately 0.43mL/s) with a transition occurring at a rice husk size of about 650µm. This interpretation is sketched in Figure 4-5.

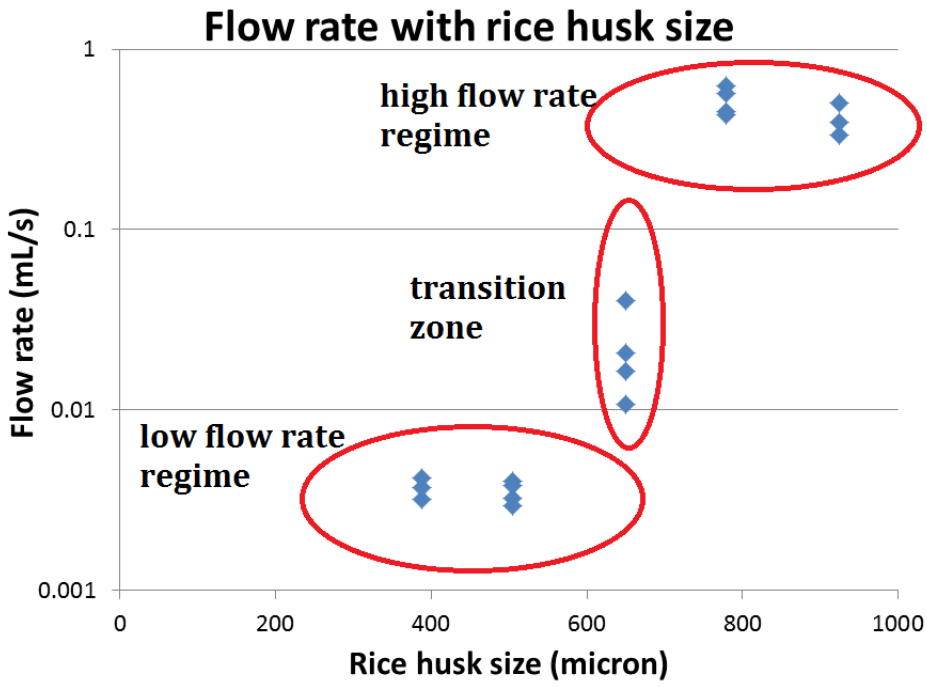

Figure 4-5: Flow rate with respect to rice husk size interpreted as distinct regions.

The flow rates reported in various studies of the CPF range widely for many reasons, but mainly because the geometries of the filters studied are not consistent. Referring to Darcy's Law in Equation 4-1, hydraulic conductivity, K, for a sample can be calculated based on flow rate, geometry and hydraulic head. Calculating hydraulic conductivity removes the geometric dependence of the results allowing for comparison across filters of different geometries.

Figure 4-6 shows the data from Figure 4-4, plotted as hydraulic conductivities. The hydraulic conductivity values presented in Figure 4-6 can be compared to values calculated in the literature for full filters. For example, Miller [20] calculated hydraulic conductivities in the range of 0.00175-0.00432m/hr for full filters produced during regular production at PHW. These values fall in the middle of the range found by this author during the rice husk size tests.

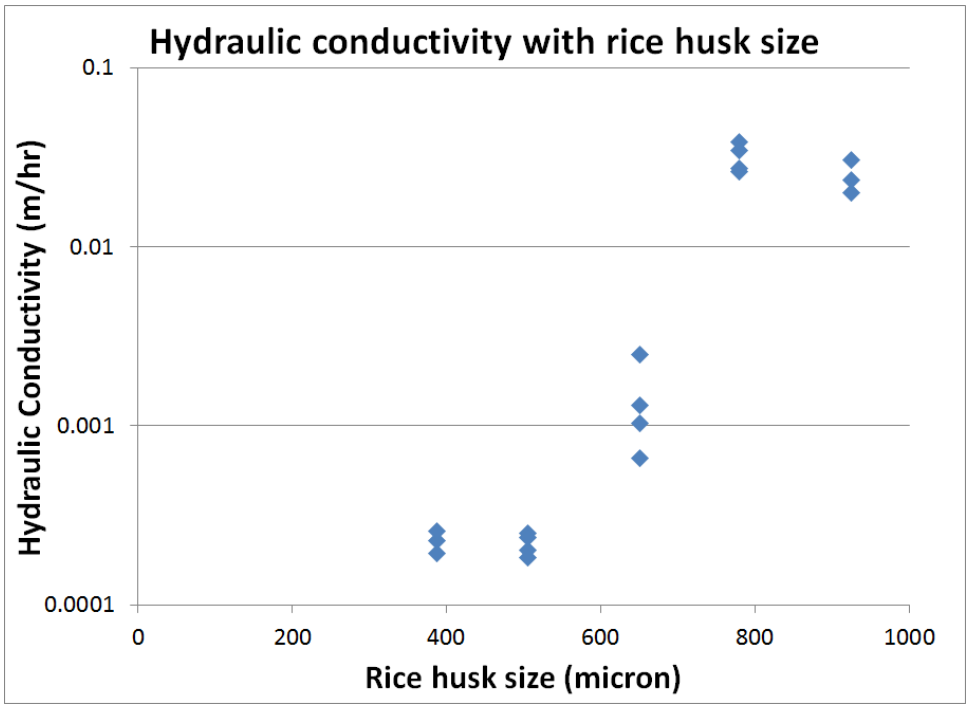

Figure 4-6: Hydraulic conductivity with respect to rice husk size.

4.4 Rice husk size and bacteria removal

Next, bacteria removal with respect to rice husk size is addressed in Figure 4-7. This data was collected concurrently with the data in Figure 4-4 using the same filter disks and according to the same protocol as described Section 3.4. Each point represents a single disk. For each disk, three measurements were taken of the influent and effluent with the top and bottom values discarded in order to reduce the influence of contamination or user error which, at times, resulted in a zero or too numerous to count result. The remaining values were used to calculate the LRVs which are plotted in Figure 4-7.

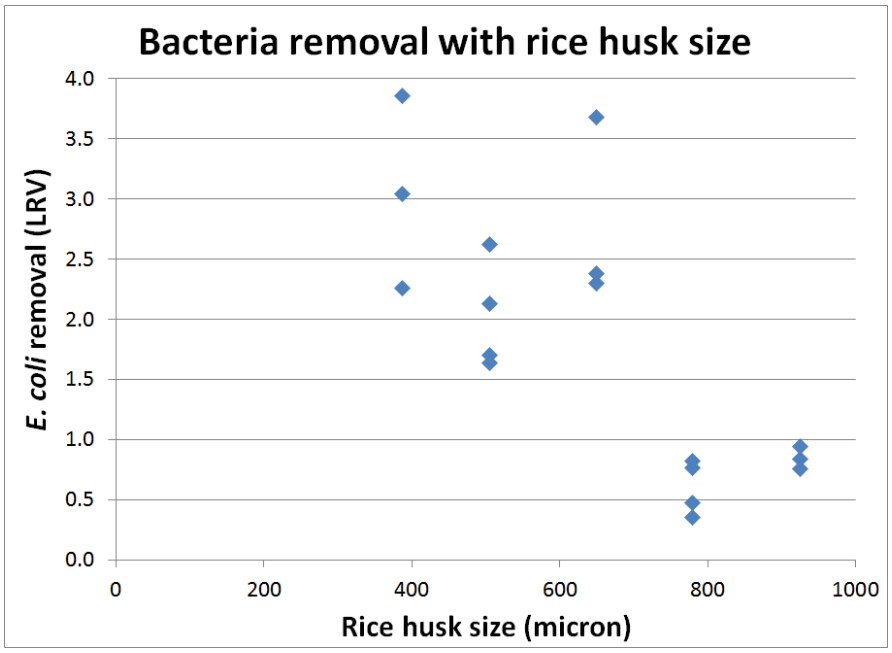

Figure 4-7: Bacteria removal with respect to rice husk size.

Figure 4-7 suggests a linear correlation with a negative slope. In light of the flow rate results in Figure 4-4, another interpretation is that bacteria removal switches from a zone of high removal (approximately 2.6 LRV) to a zone of low removal (approximately 0.75mL/s) at a rice husks size of approximately 650µm. This interpretation is sketched in Figure 4-8.

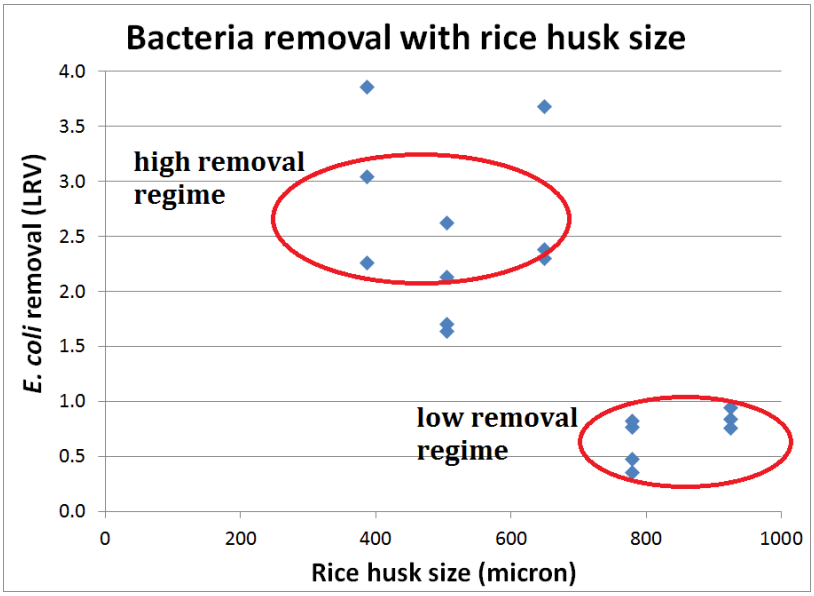

Figure 4-8: Bacteria removal with respect to rice husk size interpreted as two distinct regions.

4.5 Rice husk size and wall strength

Lastly, wall strength with respect to rice husk size is addressed in Figure 4-9. The disks were prepared and the experiments were conducted as described in Section 3.6. The results are presented as the applied load at rupture with each point corresponding to a single filter. All samples were made out of clay and rice husk from the Pure Home Water factory in Ghana and consisted of 20% rice husk by mass. Wall thickness for all samples was 7.4mm.

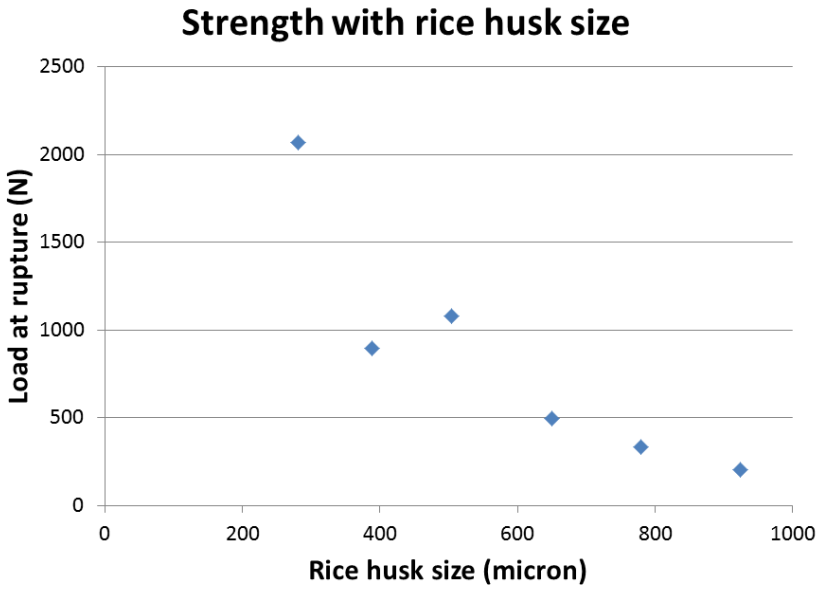

Figure 4-9: Strength with respect to rice husk size.

The strengths of the disks appear to reduce with increased rice husk size, flattening out as rice husk size increases, with a mathematical description of the shape of the curve left to be determined.

Chapter 5: Theoretical models

Experimental data can only take us so far and often does not tell us which directions of inquiry to follow to make the most progress. Developing theoretical models to describe observed behavior forces us to address many questions about the subject of study. This chapter contains a discussion regarding the internal structure of the CPF and how an understanding of that structure can be translated into theoretical models of its performance.

The objective of this chapter is to build fine-grained models of flow rate, bacteria removal and strength as functions of the three manufacturing parameters. In this endeavor, the author was largely starting from a blank slate, as models of filter performance with respect to the manufacturing parameters are lacking in the literature. For this reason, the author sought to present full models for these three performance metrics, however imperfect, which could serve as a starting point to be disputed and improved upon by future researchers.

Before building these models, it is first necessary to relate the manufacturing parameters to the physical properties of the filter (Figure 5-1). Where the manufacturing parameters represent choices made at the factory during production, the physical properties are measurable characteristics of the filters as they come out of the production process. Together, the physical properties determine filter performance. Only when a better physical understanding of the filter exists, can we hypothesize about how the filter works.

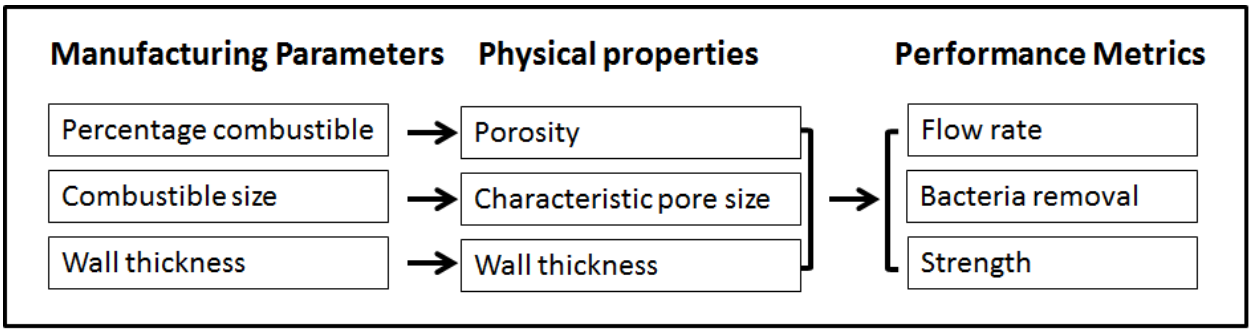

Figure 5-1: Manufacturing parameters, physical properties and performance metrics.

5.1 Characteristic pore size

5.1.1 Overview

While models of porous media often involve a term for characteristic pore size, determining an appropriate size for the CPF is a challenge. A variety of methods have been developed to determine pore size distributions in porous media including visual imaging, resin molding and capillary filling techniques including mercury intrusion porosimetry. In a paper published in 2004, Nimmo explores a variety of these methods in the context of the pores in soil [24].

Based on the experimental results showing a strong dependence of flow rate on rice husk size (Figure 4-4), we can conclude that the characteristic pore size is related to rice husk size. However, while the "rice husk size" corresponds to the associated mesh size used to sieve the rice husk particles, this size would not be accurate to use as the characteristic pore size for a number of reasons. By this author's observations, the rice husk particles are not spheres or cubes but are rather square flakes whose height is approximately 100µm regardless of the other two dimensions (Figure 5-2). A possible explanation for the constant height is that the rice husk particles, regardless of size, come from the shell of the rice which has a uniform thickness. The flat shape of the rice husks means that the characteristic pore size should be smaller than the mesh size.

Figure 5-2: Flat flake dimensions of a rice husk particle.

Second, the rice husk leaves behind a residue after it combusts, further reducing the expected pore size. This occurs because it contains other materials including silica in addition to carbon. Third, the filter shrinks during firing, and the chemical reactions that cause the clay to harden also cause the pores inside the filter to change in shape and size and to coalesce. While not explored in detail in this study, this dependence on firing parameters has been studied by others, including Gensburger [15]. Fourth, the CPF material is heterogeneous and

the path through the filter likely traverses both the pores left by the rice husk particles as well as the intrinsic pores in the clay. In addition, since the pores in this complex network are not in alignment, this means that the openings between the pores will be smaller than the pores themselves.

Because of these complexities of the material, additional data is needed to understand the pore structure and how it relates to rice husk size. Therefore, scanning electron microscopy (SEM), visual microscopy and mercury intrusion porosimetry were used by the author to gain additional information about characteristic pore sizes. Informed by these results, geometric arguments are made for the analytical relationship between rice husk size and characteristic pore size.

5.1.2 SEM and visual microscopy

Images of a piece of a filter produced at Hydrologic were taken using an SEM at MIT as described in Section 3.9. The filter was produced with 26.4% rice husk with rice husk size sieved through a 1000µm mesh such that the rice husk particles inside the filter ranged from 0-1000µm. The SEM images are shown in Figures 5-3 and 5-4. Figure 5-3 reveals smaller pores on the scale of several microns as well as larger pores on the scale of hundreds of microns. This author thinks that the smaller pores are the microscopic pores intrinsic to the clay formed by the open spaces in the alignment of clay particles during firing. The author thinks that the larger pores are the voids formed by combustion of the rice husk. The long, flat dimensions of the larger pores reflect the long flat dimensions of the rice husks.

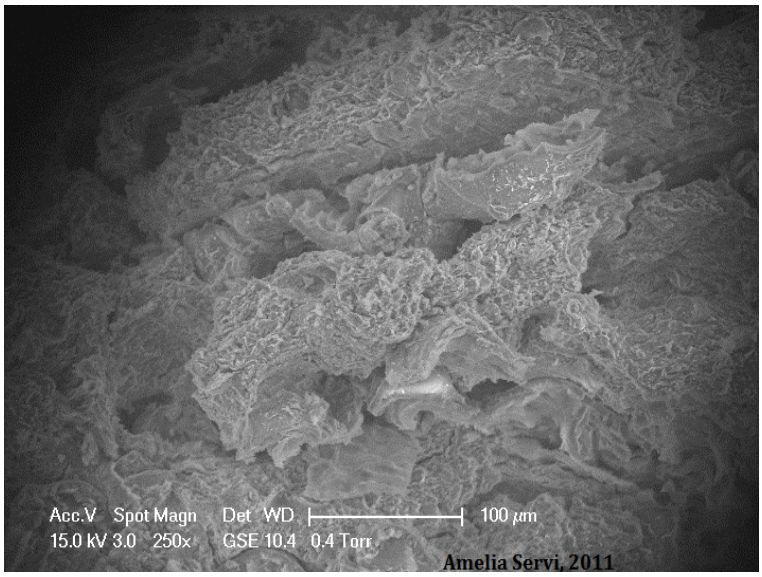

Figure 5-3: SEM image of a filter produced at Hydrologic using rice husk as the combustible.

Figure 5-4 is a close-up of the same sample as Figure 5-3. This image better shows the intrinsic micron-scale pores in the clay. By visual inspection, this author observes these pores to be in the range of 2-5µm.

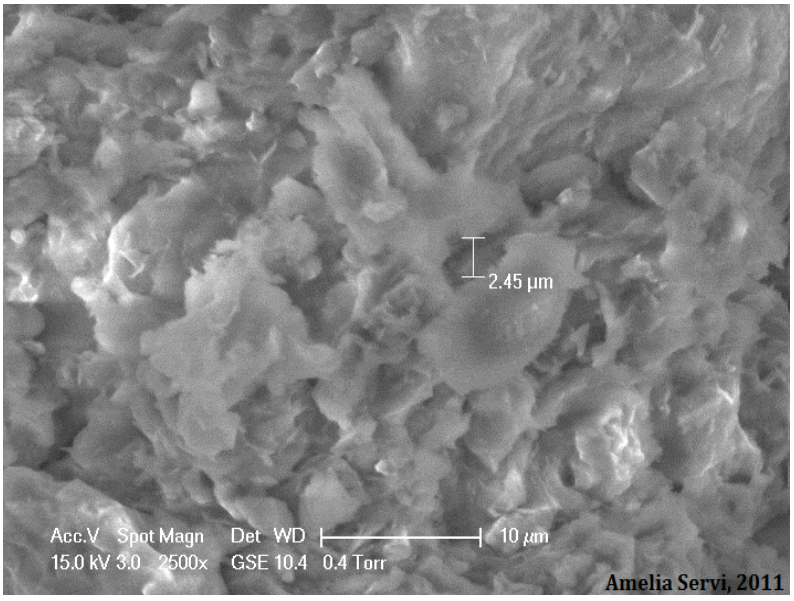

Figure 5-4: SEM image of the same filter (close up).

An optical microscope was used to provide a third view of the same filter sample (Figure 5-5). Like Figure 5-3, this image shows many pores on the order of several hundred microns, comparable to the size of the rice husk.

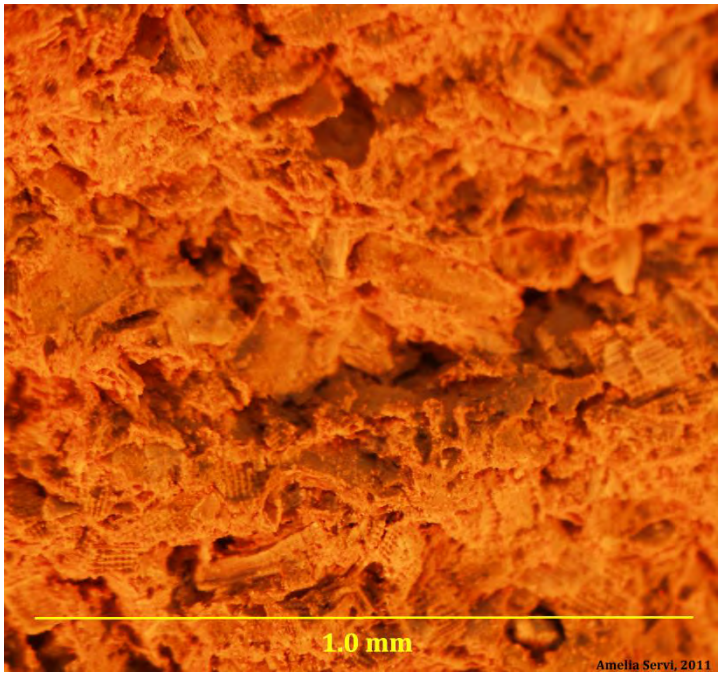

Figure 5-5: Microscope image of the same filter.

These three images reveal the range of pore sizes present in a single filter sample, highlighting the challenges of determining a single characteristic pore size for flow, filtration and strength models.

5.1.3 Mercury intrusion porosimetry

In order to gain a better understanding about the internal structure of the CPF, mercury intrusion porosimetry was conducted on pieces from six filter samples of different rice husk sizes. These samples were produced at MIT using materials from Pure Home Water as described in Section 3.4.1. Using the data from the mercury intrusion experiments, many aspects of the samples' internal structure could be determined. The data are available, upon request, from the author.

Four traits of the internal structure of the CPF were of particular interest to this author. These traits are defined as follows:

- **Characteristic length**: Characteristic length corresponds to the minimum diameter through which mercury needs to pass in order to breach the sample. More information about characteristic length can be found in Webb [22]. Characteristic length is reported in units of microns.
- **Permeability:** The ability of a sample to allow fluids to pass through it. Permeability is dependent on the characteristics of the fluid as well as the characteristics of the porous media. It is reported here in units of mDarcy which are approximately equivalent to 0.001 μm^2.
- **Porosity**: The volume percentage of void space in the sample.
- **Tortuosity**: The ratio between the length of a continuous path traversing the sample and the wall thickness of the sample.

Values of characteristic length, tortuosity, porosity and permeability were calculated for each sample using the software that accompanies the AutoPore IV mercury intrusion porosimeter. The following plots show these values plotted against the rice husk sizes of the six samples.

Characteristic length is plotted in Figure 5-6 along with a linear trend line. It appears that characteristic length is linearly correlated with rice husk size, a result that this author finds surprisingly simple given the complexity of the material.

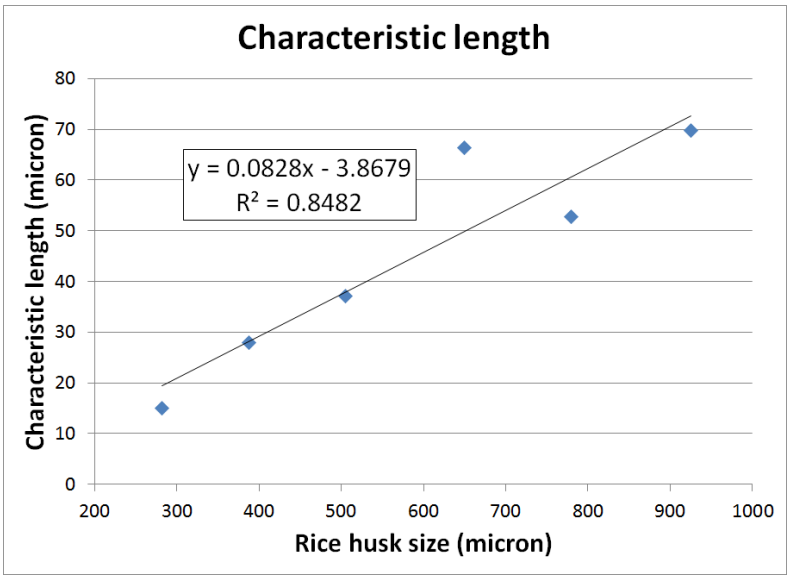

Figure 5-6: Characteristic length as calculated by the AutoPore IV mercury intrusion porosimeter.

The permeability of the samples to mercury vapor is plotted in Figure 5-7. This author was also surprised at this apparently linear relationship with respect to rice husk size. This result is in sharp contrast to the exponential increase of hydraulic conductivity, which is linearly proportional to permeability. An explanation of this result is left for future work.

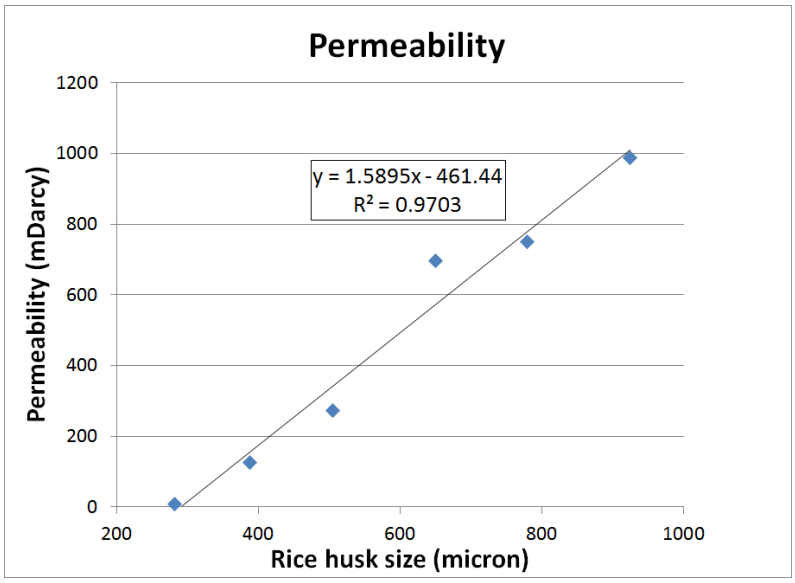

Figure 5-7: Permeability as calculated by the AutoPore IV mercury intrusion porosimeter.

The porosity of the filter samples is plotted in Figure 5-8. Since all samples tested contained the same percentage rice husk, it was expected that porosity would be constant for these sample. However, the data in Figure 5-8 suggest a slight increase in porosity with increased rice husk size. One possible explanation for this is that the smaller rice husk particles may leave behind a larger percentage of residue during combustion. This effect is slight enough that this author considers porosity to be constant with rice husk size for the purposes of her analysis.

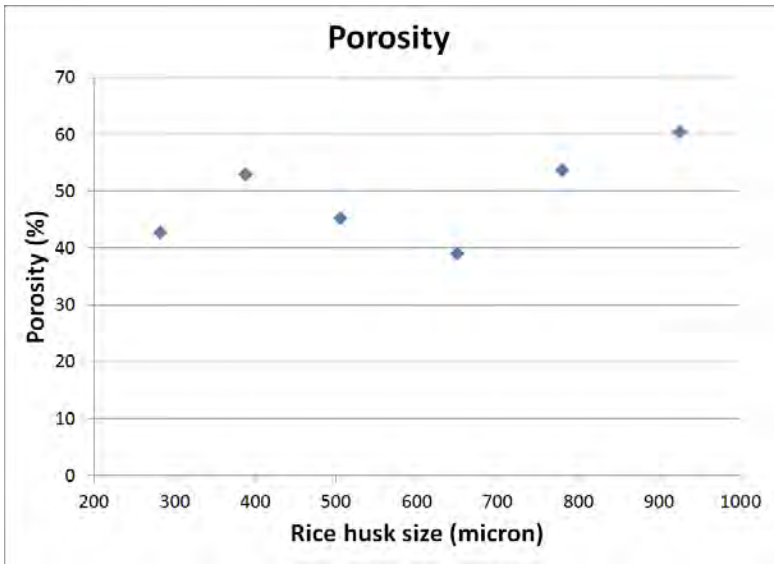

Figure 5-8: Porosity as calculated by the AutoPore IV mercury intrusion porosimeter.

Figure 5-9 shows tortuosity as a function of rice husk size. This relationship appears to be an exponential decay that settles at a constant value at approximately 400µm rice husk size. Since the sample with the smallest rice husk size was not included in this author's flow rate or bacteria removal experiments, tortuosity is treated as a constant in the analysis of this thesis.

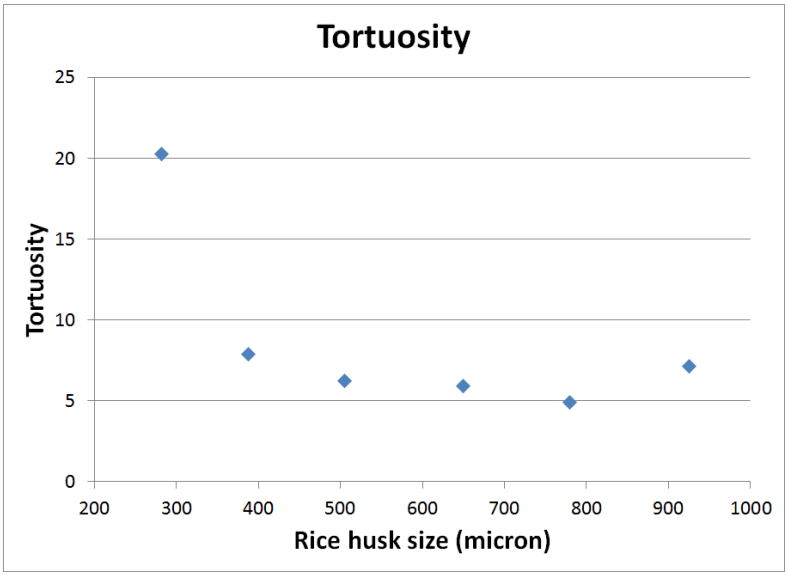

Figure 5-9: Tortuosity as calculated by the AutoPore IV mercury intrusion porosimeter.

5.1.4 Geometric analysis

While visual images and mercury intrusion provide observations about the characteristic pore size and the internal structure of the CPF material, an analytical relationship between rice husk size and characteristic pore size is still needed if we want a theoretical model of filter performance. Three relationships are suggested below based on geometric arguments. The "hydraulic diameter" and "fractional diameter" interpretations assume that flow through the filter is dominated by flow through the pores left by the rice husk particles. The "intrinsic clay pore" interpretation assumes that flow through the filter is dominated by flow through the intrinsic clay pores. These interpretations of characteristic pore size are described below.

Hydraulic diameter:

As described in Section 5.1.1, the height of the rice husk particles is approximately 100µm regardless of the other dimensions. It has been observed by this author as well as others that the rice husks align themselves such that their long dimensions run parallel to the surface of the filter. This is likely caused by the pressing process when the clay is stretched into the final filter shape, thus pulling the rice husks along the axis of stretching. Figure 5-10 shows a photograph of a filter from Hydrologic with horizontal striations.

Figure 5-10: Filter cross-section with horizontal striations.

Based on this observation of rice husk alignment, the path that the water takes through the filter is expected to look something like the sketch in Figure 5-11 with the water jumping from pore to pore on through the thickness of the filter. The level of tortuosity of the filter is reflected in the windiness of the path.

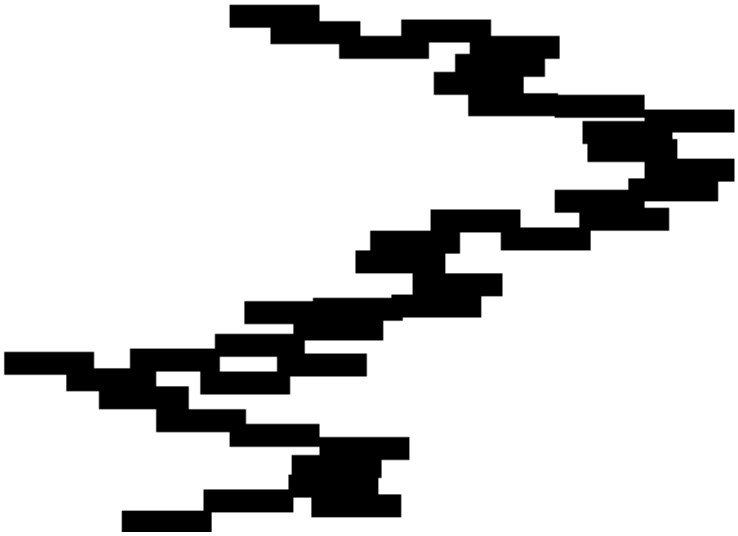

Figure 5-11: Schematic of rice husk path.

If flow is expected to be dominated by lengthwise movement as shown in Figure 5-12, the use of hydraulic diameter for characteristic pore size would be applicable. That is

$$d = \frac{4A}{P} = \frac{4D * 100\mu m}{2D + 2 * 100\mu m}$$

Equation 5-1

where d is characteristic pore size, A is cross-sectional area, $P$is perimeter and D is rice husk size. Here d and D are both expressed in units of microns.

Figure 5-12: Lengthwise fluid movement.

Fractional diameter:

If flow through the pores left by the rice husk is more like Figure 5-13, the characteristic pore size would have to be evaluated differently. It is conceivable that the characteristic pore size would be some fraction of the rice husk size, called the "fractional rice husk size" in this thesis. Since the mercury intrusion data shows characteristic length to be equal to approximately one twelfth of the rice husk size, the factor of one twelfth is used to define fractional rice husk size as

$$d = \frac{D}{12}$$

Equation 5-2

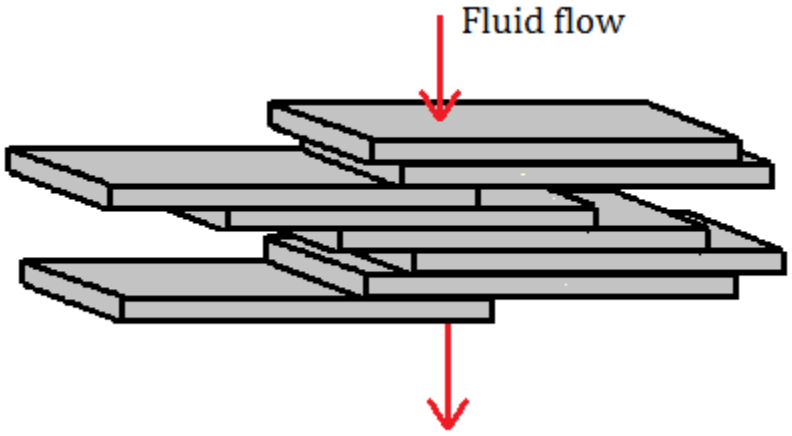

Figure 5-13: Vertical fluid movement.

While Figures 5-12 and 5-13 show extreme cases, the true flow path though the pores left by the rice husks may lie somewhere in the middle.

Intrinsic pore size:

A third option for characteristic pore size assumes that water flows through a combination of rice husk pores and intrinsic clay pores arranged in series. If this is the case, since the clay pores are so much smaller than the rice husk pores, the flow should be completely dominated by the intrinsic clay pores. Based on the Figure 5-4, a characteristic intrinsic clay pore size is estimated by this author as approximately 2.5µm. Thus this value of characteristic pore size is given by

$$d = 2.5\mu m.$$

Equation 5-3

Figure 5-14 shows these three interpretations of characteristic pore sizes plotted against their corresponding rice husk sizes.

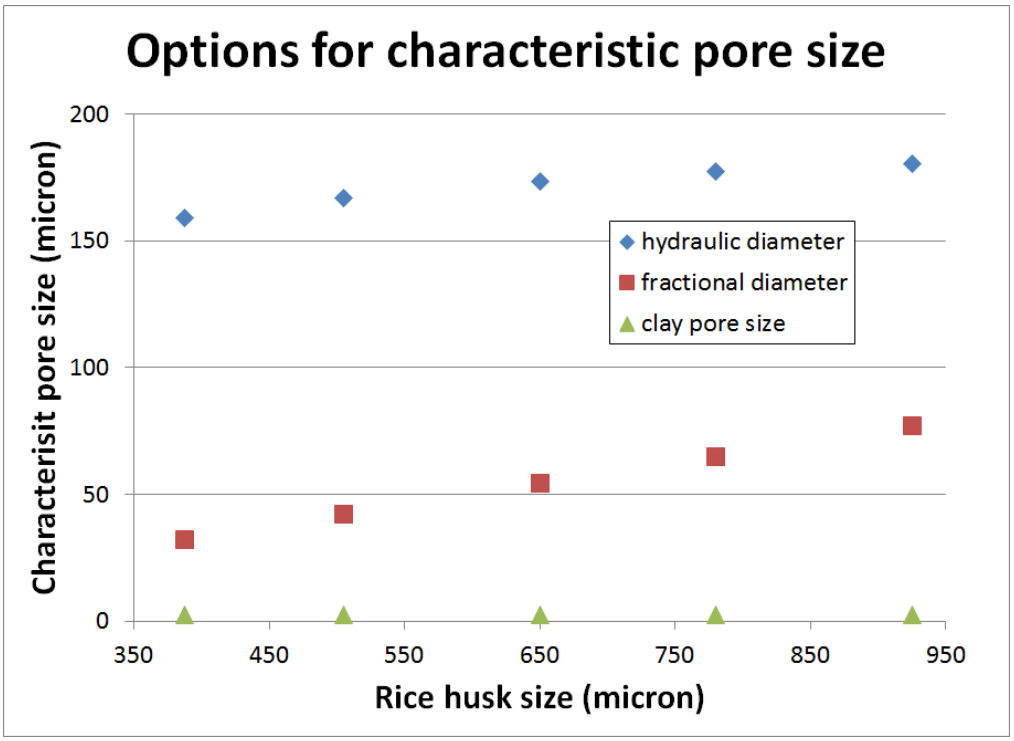

Figure 5-14: Possible interpretations of characteristic pore size.

The three interpretations of characteristic pore size have different behaviors with respect to rice husk size. The hydraulic diameter values are relatively flat compared to the rice husk size, only spanning 13% of their average value over a threefold increase in rice husk size.

On the other hand, the fractional diameters vary more, spanning 83% of their total value over the same increase in rice husk size. Meanwhile, the intrinsic clay pore size is constant with rice husk size and so small that it barely shows on the chart. Considering the uncertainty for characteristic pore size, the three options are evaluated in the following models.

5.2 Porosity, wall thickness and flow regime

5.2.1 Porosity

Porosity, the volume percentage of void space in the sample, has been previously shown to be linearly correlated with percentage rice husk [16] [17]. Miller's findings are depicted in Figure 5-15 [17].

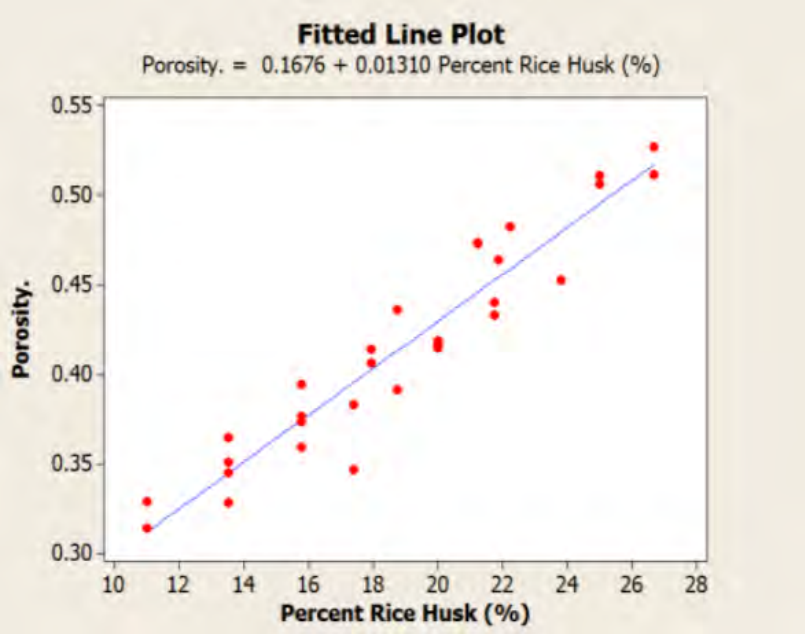

Figure 5-15: Porosity with respect to percent rice husk. Reprinted from [17] Figure 7-5.

Based on Miller's fitted line plot in Figure 5-15, this author uses the following relationship in her subsequent analysis:

$$\varepsilon(P) = 0.16 + 1.3P$$

Equation 5-4

where ε is the total porosity by volume and P is the percentage of rice husk by mass represented as a fraction of unity. The coefficient of P captures the difference in density

between the clay and the rice husk as well the residue volume left in the pores when the rice husk combusts. The constant term likely reflects the porosity caused by the intrinsic clay pores whose existence is independent of the presence of rice husk. While these coefficients may vary with changes in manufacturing parameters such as clay type and firing profile, the form of the relationship is expected to remain the same.

5.2.2 Wall thickness

While the filter shrinks during firing, manufacturers typically size their molds based on the desired size of the fired filter. Because of this, the manufacturing parameter of wall thickness is considered by this author to be equivalent to the physical property of wall thickness. When modeling flow rate and bacteria removal, wall thickness is multiplied by a factor of tortuosity in order to better reflect the distance that the water travels through the filter. When modeling strength, the wall thickness is not multiplied by tortuosity.

5.2.3 Verifying laminar flow

While not a physical property, it is important to determine whether flow in the filter is laminar or turbulent in order to know which models to use. Determining the flow regime can be achieved directly by calculating the bulk Reynold's number. However, given that there is no definite velocity or pore diameter to use, this approach is inadequate. Therefore an indirect experiment was conducted using the hydraulic head tests as described in Section 3.5. Figure 5-16 shows flow rate as a function of hydraulic head for two filter disks. Both disks were produced using clay and rice husk from the Pure Home Water factory in Ghana and consisted of 20% rice husk by mass. Wall thickness of both samples was normalized to 20mm and surface area was normalized to 430mm^2. The rice husk size was 590-850µm.

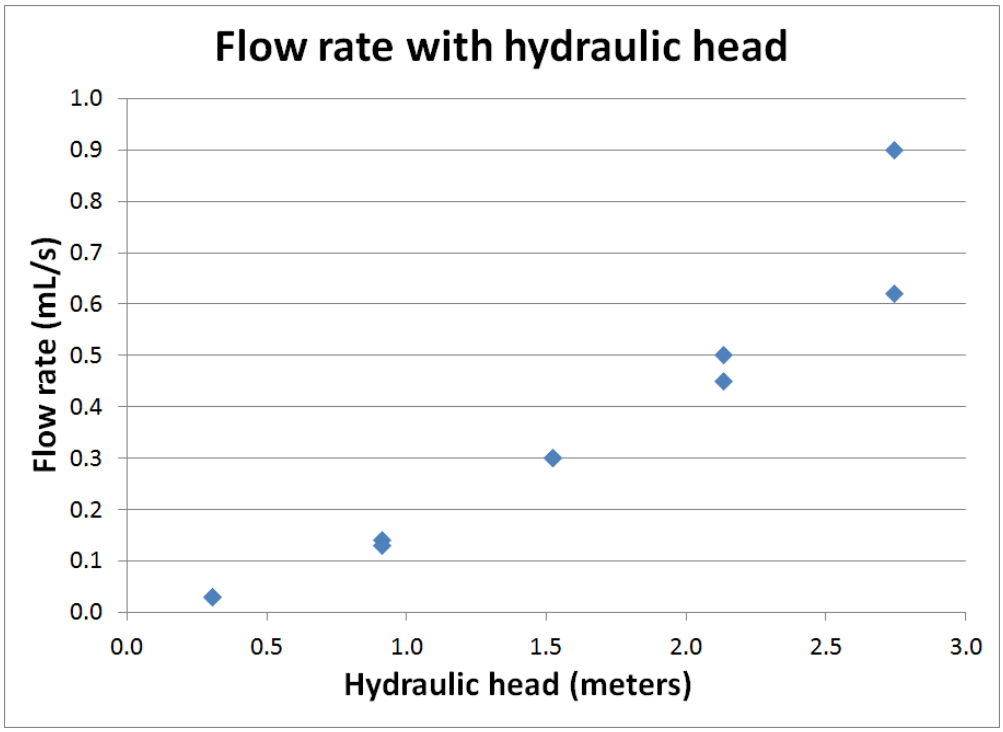

Figure 5-16: Flow rate with respect to hydraulic head.

Given the near linear relationship apparent in Figure 5-16, it is presumed that flow rate is linearly proportional to hydraulic head, a relationship that holds only for laminar flow. The author thus concludes that flow through the CPF is in the laminar regime.

5.3 Effect of incomplete combustion

The effect of incomplete combustion of the rice husk within the CPF is an active area of debate among CPF researchers and manufacturers. Questions remain about how bacteria removal and flow rate are affected by the inhomogeneity caused by incomplete combustion of the rice husk. Figure 5-17 shows a cross-section of a filter made at Hydrologic which exhibits incomplete combustion.

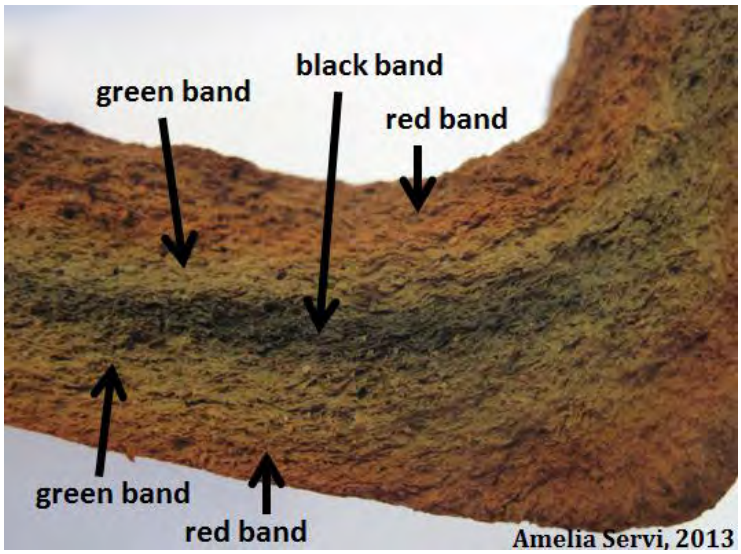

Figure 5-17: Filter cross-section showing incomplete combustion.

The cross-section contains five distinct bands. The central black band contains rice husk that has turned into carbon without fully combusting. In the two green bands, the rice husk is fully combusted, but the clay does not appear to be fully fired. In the two outer red bands, the clay is fully fired and the rice husk is fully combusted[5].

The measurements in the wall thickness tests reported in Figures 4-1 and 4-3 were taken from disks cut from full filters produced at Hydrologic as discussed in Section 3.3.1. The red, green and black layers are visible in the prepared disks as shown in Figure 5-18.

[5] The colors "green" and "red" are used to describe the bands because they are the terms generally used to describe unfired and fired ceramic respectively.

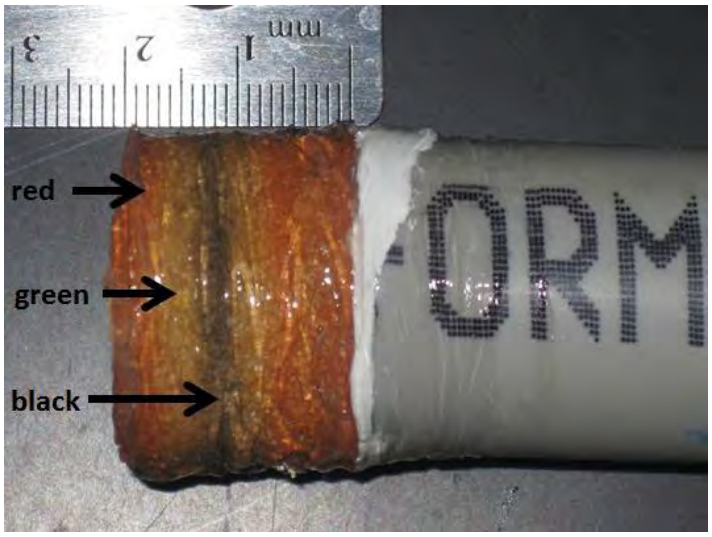

Figure 5-18: Filter disk with red, green and black bands caused by incomplete combustion.

The data from Figures 4-1 and 4-3 showing bacteria removal and flow rate with respect to wall thickness can be plotted against the locations of the bands in those particular samples (Figure 5-19). While the data is limited, based on Figure 5-19, this author concludes that the bands from incomplete combustion have no observable effect on flow rate or bacteria removal throughout the thickness of the CPF. One possible explanation is that, while a carbon layer is a highly visible indicator that the rice husk has left a residue after firing, in the case where the rice husk is fully fired, the rice husk still leaves a residue of ash. It is possible that the carbon from incomplete combustion is not much different from the ash from complete combustion in terms of influence on performance. However, since the ash is white, it is less striking to the viewer and so causes less alarm. More data is needed to confirm these findings. In the meantime, since the bands are taken to not have any effect, they are left out of the theoretical models presented in this chapter.

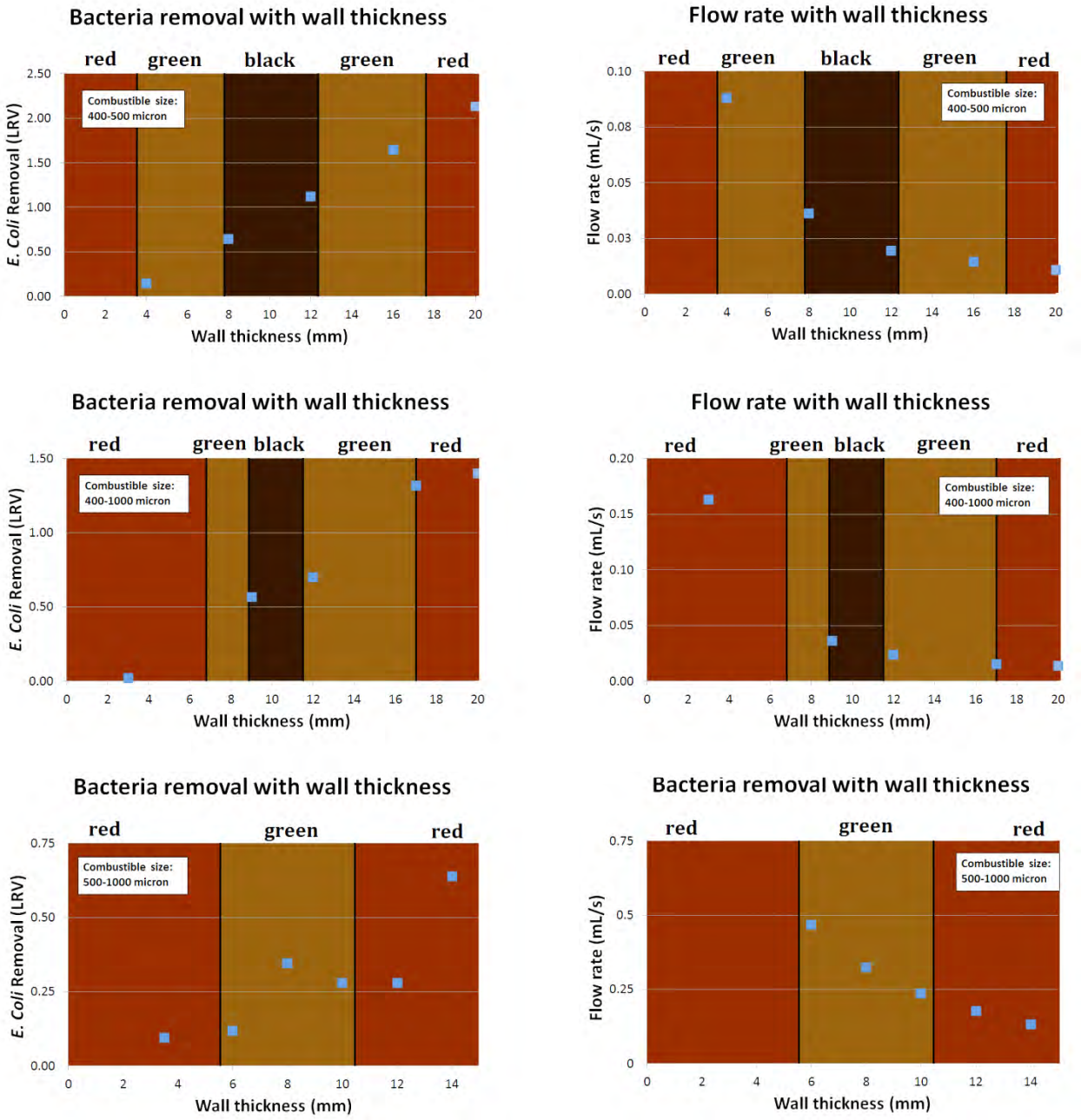

Figure 5-19: Bacteria removal and flow rate for the three filters in Figures 4-1 and 4-3 plotted against the red, green and black bands caused by incomplete combustion.

5.4 Flow rate model

With values for the physical properties and a few assumptions about the filter in place, it is now possible to begin modeling CPF performance. We start with a theoretical model for flow rate. Given the incomplete data available, a definitive model as a function of the manufacturing parameters cannot be reached. However, this author works through the process of developing a model with the intent that it will be useful as a starting point for future models.

5.4.1 Carman-Kozeny

In the scenario where water travels through the filter via the pores left behind by the rice husk, the CPF can be modeled as a bundle of pipes traversing the filter (Figure 5-20). The Carman-Kozeny model introduced in Section 2.2.2 describes this type of flow. The author thinks that this model is fitting because paths such as the one illustrated in Figure 5-11 can easily be imaged as pipes. The Carman-Kozeny model is derived here and then modified to better reflect the behavior of the CPF. The scenario where water travels through the intrinsic clay pores will be discussed in Section 5.4.2.

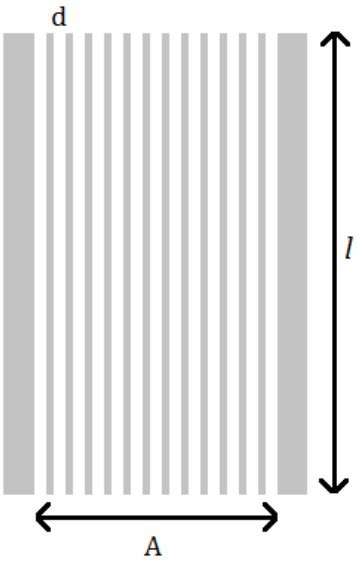

Figure 5-20: Pipe model of the filter.

To model the volumetric flow rate through a filter, we start by calculating the flow rate through a single pipe. Laminar, pressure-driven flow in a circular pipe is described by

Poiseuille's equation which is in turn derived from the Navier-Stokes equation. Poiseuille's equation is given by

$$q = \frac{\pi d^4 \Delta P}{128 \mu l}$$

Equation 5-5

where q is volumetric flow rate, $d$is the diameter of the pipe which is also the characteristic pore size of the filter, ΔP is the pressure drop from one end of the pipe to the other, μ is dynamic viscosity and l is the length of the pipe. The upper limit of the number of pipes spanning the filter (equivalent to the number of "paths" as introduced in Section 3.7) is given by

$$N = \frac{A\varepsilon}{\frac{\pi d^2}{4}} = \frac{4A\varepsilon}{\pi d^2}$$

Equation 5-6

where N is the number of pipes, A is the cross-sectional area of the sample and ε is porosity by volume. This value of N is calculated by dividing the void fraction of the sample cross-section by the cross-sectional area of a single pipe. Multiplying q by N gives the Carman-Kozeny equation for total flow rate Q through the sample

$$Q = \frac{\varepsilon \Delta P A d^2}{32 \mu l}.$$

Equation 5-7

This is the same as Equation 2-1 but rearranged and with capillary radius, r_c, replaced with characteristic pore size, d.

However, this author is skeptical of the value of N calculated when d is interpreted as the hydraulic diameter or the fractional diameter of the rice husk. This calculation of N seems to be a gross over-estimation, with the estimated number of paths for the small disks numbering in the thousands, a situation that goes against this author's observations of the CPF. This value also predicts flow rates significantly higher than those observed experimentally in Figure 4-4, further bringing the value of N into question. Thus this author breaks from the

Carman-Kozeny model to determine a scaling factor for the number of paths which will make for a more accurate value of N and overall flow rate.

The author uses the droplet test as described in Section 3.7 to determine a new estimate for N. Figures 5-21 and 5-22 show filters produced at Hydrologic in Cambodia under regular manufacturing conditions. The filters were submerged in buckets of water such that the water could seep up into the filter through their walls as described in Section 3.7.

Figure 5-21: Droplets appearing on the inside surface of the filter.

Figure 5-22: Droplets appearing on the inside surface of a second filter. This filter has a higher density of distinct droplets indicating a different internal structure.

The number of distinct droplets visible on the inside surface of the filter in Figure 5-21 was recorded over time, reaching a maximum of 263 before the droplets started to coalesce. Each droplet was interpreted by this author to represent a single path that the water could take through the filter. While coalescence of the droplets could indicate that one cannot determine a full count of the number of paths through the filter, it was observed by this author that large areas of the filter surface were droplet-free even after many droplets had appeared on the surface. The coalescence was caused by the distinct droplets getting bigger and joining, not by the whole surface being covered with individual droplets.

The number of distinct droplets visible on the surface of the filter in Figure 5-22 was also monitored over time, but the author found that there were too many small droplets to count accurately using the available images. The author estimates that there were thousands of distinct droplets on its surface.

Since the surface areas of the full filters shown above are approximately fifty times larger than the surface area of the disks used in the flow rate experiments conducted for this thesis, it is expected that the number of distinct pipes through each small sample is on the order of five to fifty. Thus, for this model, a scaling factor of 1/100 is multiplied by N to calculate

$$N' = \frac{N}{100} = \frac{4A\varepsilon}{100\pi d^2} \cong \frac{4A\varepsilon}{\pi D^2}$$

Equation 5-8

Since fractional diameter is equivalent to 1/12 the rice husk size, dividing N by 100 is like using D^2in the calculation of N as opposed to d adding credibility to this modeling decision. Equation 5-8 produces values of N'on the order of ten. Multiplying q by N' and replacing l with LT where L is sample wall thickness and T is the tortuosity of the pipe, we get

$$Q = qN' = \frac{d^2 \Delta P A \varepsilon}{3200 \mu L T}$$

Equation 5-9

where Q is the volumetric flow rate through the sample. We can substitute in $\varepsilon = 1.3P$ where P is percentage rice husk by mass and ε is the volumetric porosity attributed to the rice husk pores to get

$$Q = \frac{d^2 \Delta P A P}{2460 \mu L T}.$$

Equation 5-10

This model is in qualitative agreement with the experimental data for percentage rice husk, P, wall thickness, L, and pressure drop, ΔP (Figures A-4, 4-1, 5-16) since it predicts flow rate to be proportional to pressure drop and percentage rice husk and inversely proportional to wall thickness. The relationship between flow rate and the cross-sectional area of the sample, A, while not tested experimentally, is assumed to be correct. The agreement between the experimental data and rice husk size is less clear and will be addressed in Section 5.4.3.

5.4.2: Packed bed

When calculating predicted flow rate in the scenario where the water flows through the intrinsic clay pores, it is necessary to use a different model for flow rate that is more suitable for packed beds. Instead of modeling the filter as a bundle of pipes, the filter is modeled as a consolidated granular media according to the equation

$$Q = \frac{0.015 \Delta P \varepsilon d^2 A}{L \mu}$$

Equation 5-11

where $d = 2.5\ microns$ and $\varepsilon = 0.16$ represents the porosity due by the intrinsic clay pores. This model for flow through a packed bed is further explained in [25].

5.4.3: Comparing the models to the data

Figure 5-23 shows the predicted flow rates calculated from Equations 5-10 and 5-11 using the different interpretations of characteristic pore size, d. These calculated flow rates are plotted with respect to rice husk size along with the flow rate data from Figure 4-4.

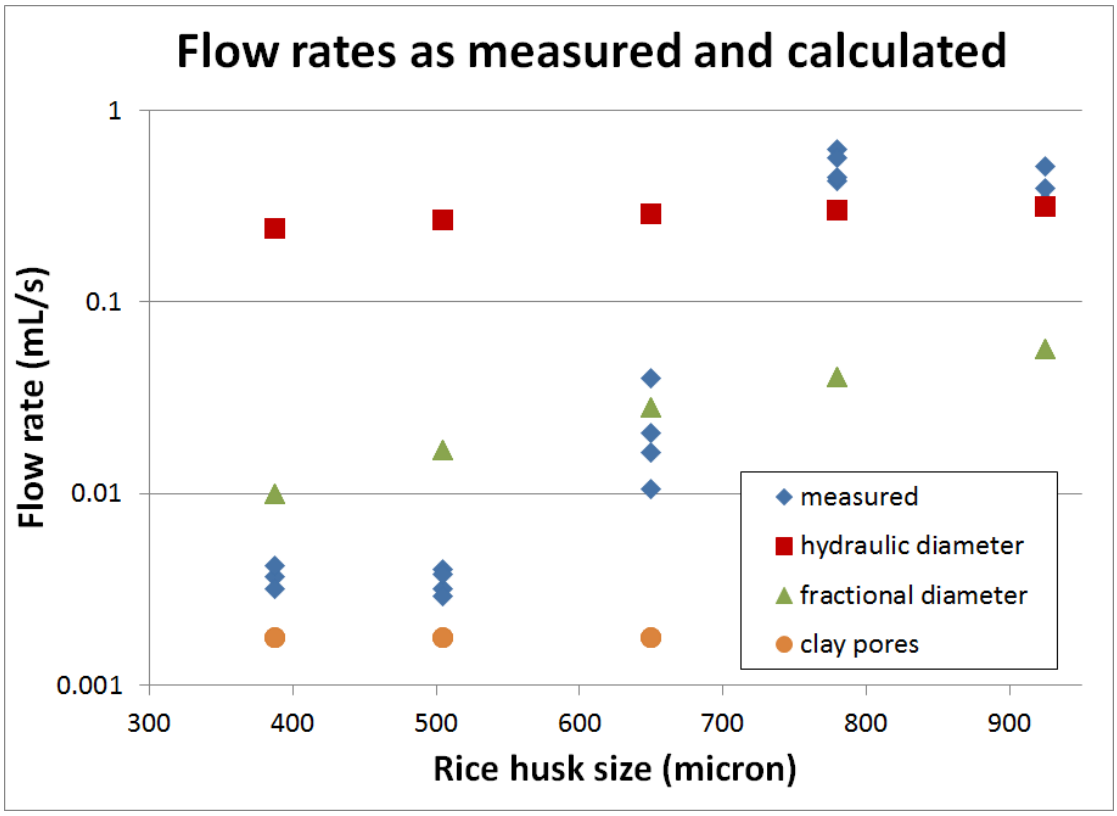

Figure 5-23: Measured and calculated flow rate with respect to rice husk size[6].

In Figure 5-23, it appears that none of the proposed pore sizes coupled with the models fully describe flow through the CPF. The hydraulic diameter and fractional diameter approximately capture the flow rates for the medium and large rice husk sizes, and the intrinsic clay pores approximately capture the flow rates for the smaller rice husk sizes. Based on these results, this author concludes that at least two distinct regions with different flow characteristics exist.

5.5 Bacteria removal model

Moving on from flow rate, we now address bacteria removal. There is little literature about the fine-grained details of filtration for porous media consisting of a solid material with

[6] Assumptions: $\Delta P = 27000Pa$, $A = 0.00043m^2$, $P = 0.2$, $L = .02m$, $\mu = 0.0007Pa \cdot s$, $T = 7$.

distinct pores such as the CPF. Therefore, the author bases her filtration analysis in theory developed for granular media filtration, proposing a modified version to describe the CPF. As with the flow rate model, the proposed filtration model is far from complete and is meant to serve as a starting point for future work.

5.5.1 Possible filtration mechanisms

Many possible mechanisms for bacteria removal in the CPF have been proposed. Key candidates are presented below:

- **Diffusion:** Applicable only for very small particles, diffusion is the result of Brownian motion of a particle within the filter which brings it into contact with the filter walls to which it may stick.
- **Turbulence and inertia:** In turbulent flows, particles are trapped when their momentum pushes them into surfaces within the filter.
- **Sedimentation:** Based on the density difference between the contaminant and the fluid, contaminants which are heavier than the fluid settle onto the floors of the pores within the filter.
- **Mechanical screening:** If the hole-size through which the water travels is smaller than the size of the contaminant, the contaminant will be stopped at the opening of the hole.
- **Adsorption:** Adhesion forces between the contaminants and the filter walls cause the contaminants to stick inside the filter. Since these forces are short-range, sticking only occurs when the contaminant is already close to the filter wall.

Some of the proposed mechanisms can be eliminated in the case of bacterial removal. Diffusion is eliminated as the bacteria are too large to be noticeably affected by diffusion. Turbulence and inertia are also eliminated as the flow was determined to be laminar.

Sedimentation:

Sedimentation is seriously considered because it is a dominant removal mechanism in most biological filtration systems [26]. Sedimentation is heavily dependent on the flow rate of the water through the filter as shown in Figure 5-24.

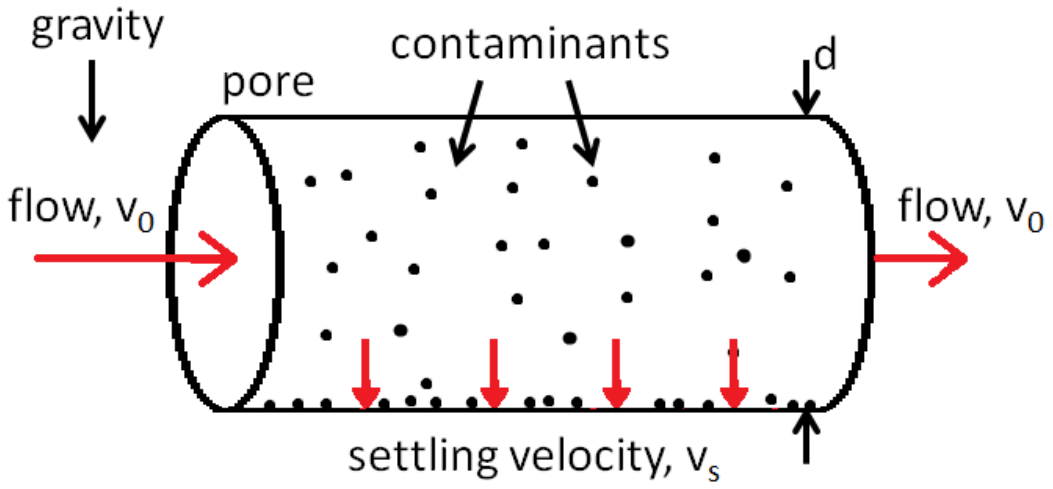

Figure 5-24: Schematic of the sedimentation mechanism of filtration.

In Figure 5-24, v_0 represents the flow velocity within a pore, and v_s represents the settling velocity of the contaminants. The settling velocity is determined by the relative densities of the contaminant and the fluid, the dynamic viscosity of the fluid and the contaminant size. The faster the flow velocity and the larger the pore diameter, the less likely it is that a contaminant will reach the bottom of the pore before it reaches the exit. The amount of contaminant that is caught in the filter due to sedimentation is thus related to the ratio between the flow velocity, v_0, and the settling velocity, v_s, as well as the diameter, d, of the pore.

If sedimentation is an active mechanism of filtration in the CPF, it implies that increasing flow rate through the filter will decrease bacteria removal, regardless of how the flow rate was increased. In order to test the importance of the sedimentation mechanism, this author measured bacteria removal as a function of hydraulic head using the methods described in Section 3.5. Increasing hydraulic head increases flow velocity as was shown in Figure 5-16. Since sedimentation is dependent on the relative velocities of the fluid flow and the settling speed of the contaminants, an independent relationship between hydraulic head and bacteria removal would eliminate sedimentation as a removal mechanism.

Figure 5-25, contains data collected concurrently with the data collected for Figure 5-16.

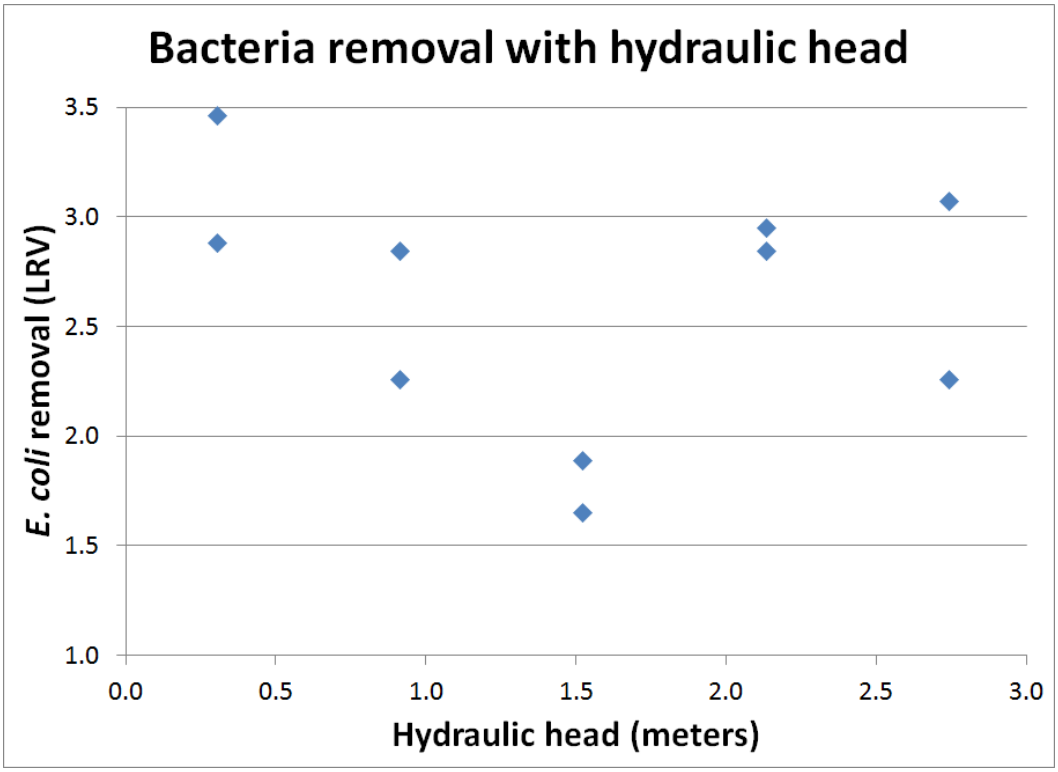

Figure 5-25: Bacteria removal with respect to hydraulic head.

Figure 5-25 shows a minimal net difference in bacteria removal between the lowest and highest hydraulic head values. Between the two extremes, however, there is a downwards slope with increased hydraulic head followed by a jump back up to the original level. This could indicate two different regimes for bacteria removal as a function of hydraulic head, one of which is sedimentation. More data is needed to understand this relationship. For the purposes of the analysis in this study, sedimentation is neglected as a filtration mechanism.

Mechanical screening:

Mechanical screening is also considered as a mechanism for bacteria removal. While the characteristic pore lengths determined by mercury intrusion (Figure 5-6) are larger than the size of the bacteria, it is still possible that some of the bacteria removed within the filter are taken out of solution via mechanical screening. This would be due to the heterogeneous nature of the filter material. If the material of the filter looks something like Figure 5-26, a bacterium

may pass through the filter if it happens to approach a larger hole such as the one labeled “A”. On the other hand, it may get stopped if it happens to approach a smaller hole such as the one labeled “B”. In this way, it is possible that some bacteria could be screened mechanically even if the characteristic pore length for the sample is greater than the diameter of the bacteria.

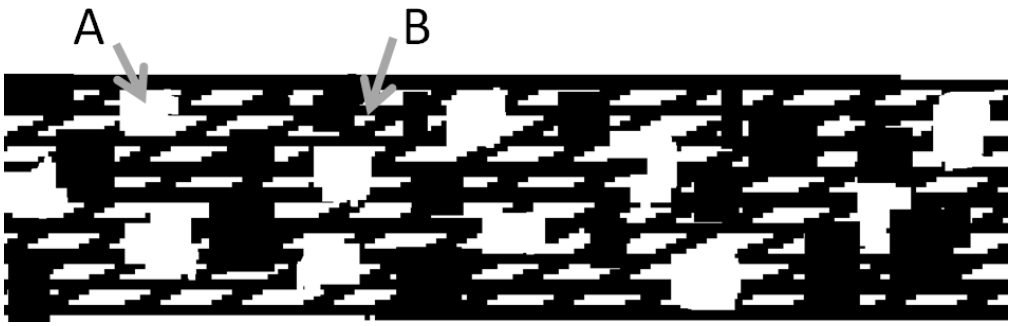

Figure 5-26: A schematic of the CPF material as a heterogeneous mesh.

While mechanical screening is left as a possible mechanism of CPF filtration, this author does not focus on it in the filtration model that follows. This author chose instead to base her filtration model on the adsorption mechanism of filtration. Since adsorption works at close-range, contaminants are only removed from solution when they collide with the pore walls as they make their way through the filter. Given the complexity of the path that the water takes through the filter, as evidenced by the high tortuosity, there are many opportunities for the contaminants to collide with the pore walls as the path narrows, widens, twists and turns. A basic model of adsorption depends only on the relative sizes of the pores and the contaminants to determine the likelihood of collision. This means that the model can be a relatively simple, geometric description that can serve as a good starting point for future refinements.

This author proposes a model of filtration that is loosely based on a model developed by Iwasaki as discussed in [26]. Iwasaki’s model was developed for granular media such as a packed bed of sand. The author considered using Iwasaki’s model directly instead of modifying it for the CPF geometry. However, Iwasaki’s model includes a strong dependence on porosity for determining removal. This is in contrast to the findings in the CPF literature described in Table 2-1 which found a lack of correlation between porosity and bacteria removal. This suggests that Iwasaki’s model needs to be modified to be applicable for the CPF. In 5.5.2,

Iwasaki's model is briefly described followed by a description of a modified model proposed by this author.

5.5.2 Iwasaki model

Iwasaki's model was developed for a granular media filter which he treats as a collection of individual spherical grains that each act independently to remove contaminants from the fluid. Figure 5-27 shows a single grain such as a piece of sand illustrating the adsorption mechanism (called "interception" in [26]). In this scenario, any particle in a streamline which passes through the area W will be intercepted by the grain.

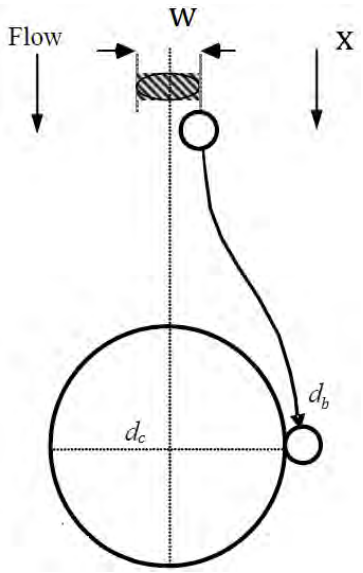

Figure 5-27: A single grain from the Iwasaki model of filtration. Reprinted from [26].

If we say that fluid flow is in the x-direction, then a thin layer of height Δx containing some number of individual grains can be defined within the filter (Figure 5-28).

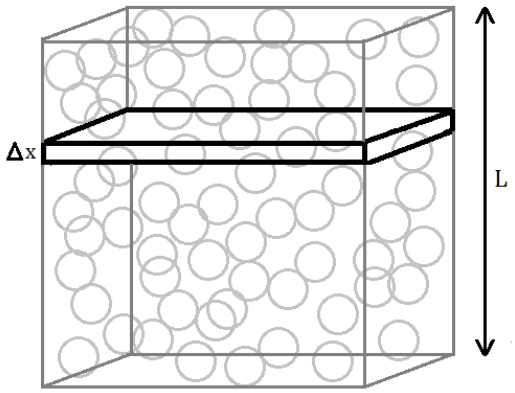

Figure 5-28: A thin layer of length Δx.

Iwasaki's model equates the total removal of contaminants within that layer to the quantity of contaminants removed by a single grain multiplied by the number of grains in the layer.

$$\begin{bmatrix} Total\ removal \\ within\ a\ layer \end{bmatrix} = \begin{bmatrix} removal\ by \\ one\ grain \end{bmatrix} \begin{bmatrix} number\ of\ grains \\ in\ a\ layer \end{bmatrix}.$$

Equation 5-12

Iwasaki fills in the terms in Equation 5-12 as can be seen in detail in [26]. The total removal within a layer is then integrated through the wall thickness of the filter to give a total removal for the filter:

$$-\ln\left(\frac{C_{out}}{C_{in}}\right) = \frac{3}{2}\frac{(1-\varepsilon)\alpha\eta}{d_c}L$$

Equation 5-13

where

C_{out} is the concentration of contaminants exiting the filter

C_{in} is the concentration of contaminants entering the filter

ε is porosity

d_c is grain diameter

L is wall thickness

α is the fraction of particles that collide with the collector that are adsorped. This is called the "removal constant" and is related by surface chemistry. It can range from zero to one.

η is the percentage of particles approaching a grain which collide with it. This is called the "collision percentage" by this author and is determined by geometry.

Yao and Tien [26] calculated η associated with adsorption to be equal to

$$\eta = \frac{3}{2}\left(\frac{d_b}{d_c}\right)^2$$

Equation 5-14

where $d_b$is the diameter of the contaminant and $d_b \ll d_c$.

The Iwasaki model shows some similarities with the experimental data for the CPF. Both this model and the data show increased contaminant removal with increased wall thickness and decreased contaminant removal with increased pore or grain size. However, while the Iwasaki model predicts removal to be dependent on porosity, this is not so for the CPF, and the model must be modified.

5.5.3 Modified Iwasaki

Unlike a granular media filter which consists of many packed grains, the CPF is a solid material with many holes distributed throughout the volume. This author thus modifies Iwasaki's model using a single cylindrical pore left behind by a rice husk particle as the starting point (Figure 68). This cylindrical pore has diameter d and height d_h, and the contaminant has diameter d_b. As with granular media, a contaminant particle approaching the pore may be intercepted and adsorped as shown in Figure 5-29.

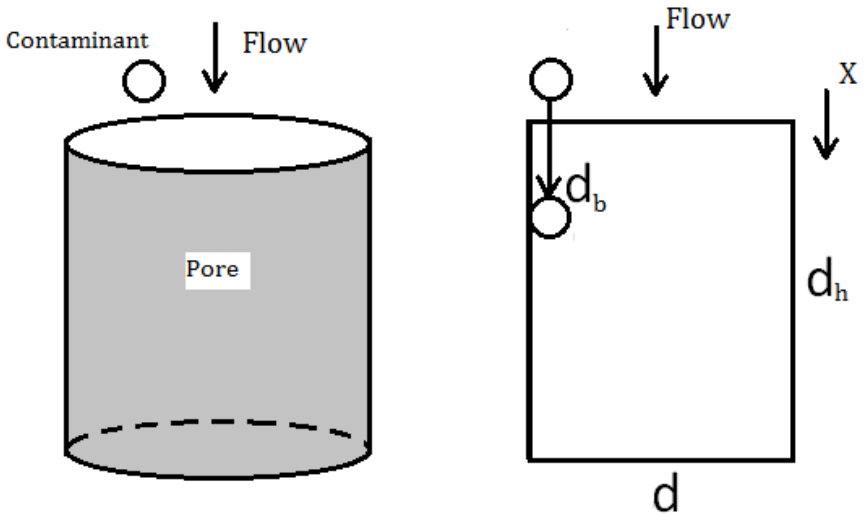

Figure 5-29: A single pore for the modified Iwasaki model of filtration. A contaminant that collides with the pore wall may be adsorped.

A thin layer of length Δx would look like Figure 5-30.

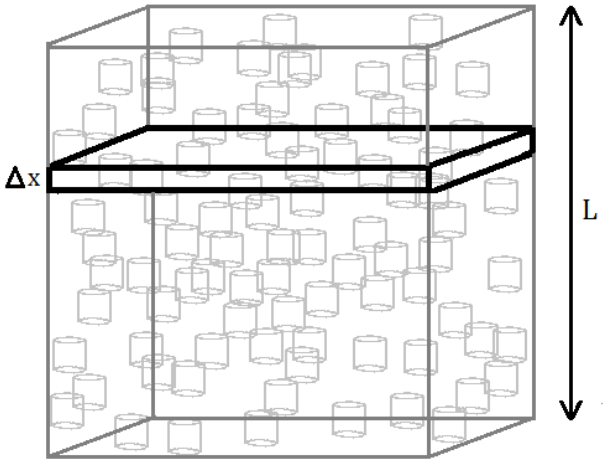

Figure 5-30: A thin layer of length Δx for the modified Iwasaki model.

Similarly to Iwasaki's model, total removal within a layer can be conceptualized as

$$\begin{matrix} \left[\begin{matrix} Total\ removal \\ within\ a\ layer \end{matrix}\right] \\ G \end{matrix} = \begin{matrix} \left[\begin{matrix} removal\ by \\ one\ pore \end{matrix}\right] \\ R \end{matrix} \begin{matrix} \left[\begin{matrix} number\ of\ pores \\ in\ a\ layer \end{matrix}\right]. \\ n \end{matrix}$$

Equation 5-15

where G is the total removal within a layer, R is removal by one pore and n is the number of pores in a layer. The number of pores in the layer is understood to only include pores in the paths that traverse the full filter.

If the pore in Figure 5-29 were viewed from above, it would look like the ring shown in Figure 5-31. Removal of contaminants by one pore is given by the area of the grey ring shown in Figure 5-31 multiplied by the concentration of contaminants, C, at x and the removal constant α as described above. This calculation in based on the assumption that contaminants whose centers are within the grey ring will collide with the pore wall while the contaminants towards the center of the pore will pass through.

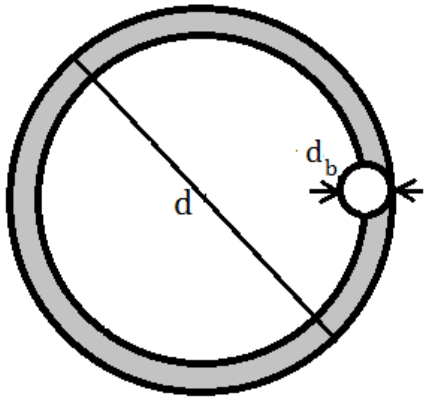

Figure 5-31: A ring along the inside surface of a pore.

Removal by one pore, R, is thus given by

$$R = \left(\frac{\pi d^2}{4} - \frac{\pi(d - d_b)^2}{4}\right) C\alpha = \frac{\pi d_b d}{2} C\alpha.$$

Equation 5-16

where $d_b$is the diameter of the bacteria, d is the cylinder diameter and $d_b \ll d$. R has units of particles/length.

The number of pores in a layer, n is given by

$$n = N' \frac{\Delta x}{d_h}$$

Equation 5-17

where $N'$is the number of paths through the filter as described in Section 5.4.1. The $\Delta x/d_h$ term describes the number of cylinders that would fit vertically into a layer of height Δx.

The left hand side of Equation 5-15, G, is defined as the change in contaminant concentration per unit volume multiplied by the cross-sectional area of the layer. Since this model assumes that the water flows through paths made by a series of pores, the cross-sectional area of the layer is interpreted as the cross-sectional area of a single pore multiplied by the number of paths through the filter. Thus, by definition,

$$G = -N' \frac{\pi d^2}{4} \Delta C$$

Equation 5-18

where G is the total removal of a layer. Equating Equation 5-18 with the product of Equations 5-16 and 5-17,

$$-N' \frac{\pi d^2}{4} \Delta C = \frac{\pi d_b d}{2} \alpha C N' \frac{\Delta x}{d_h}.$$

Equation 5-19

Simplifying and rearranging, we get

$$\frac{\Delta C}{C} = -2 \frac{d_b \alpha}{d_h d} \Delta x$$

Equation 5-20

Integrating over the full wall thickness of the filter and taking into account tortuosity

$$-ln \frac{C_{out}}{C_{in}} = \frac{2 d_b \alpha}{d_h d} LT$$

Equation 5-21

where LT is the wall thickness multiplied by tortuosity. C_{in} is the concentration of contaminants entering the filter and C_{out} is the concentration of contaminants leaving the filter.

The left hand side of Equation 5-21 describes the logarithmic reduction of contaminants as a natural log. In order to convert this to our definition of LRV, which is in base ten, we multiple both sides of Equation 5-21 by $\log_{10}(e)$. We can also set $T = 7$ and $d_b = 2\mu m$ (the

approximate diameter of a bacterium) to produce a first order approximation of bacteria removal in the system

$$LRV = 1.22 \times 10^{-5} \frac{L\alpha}{d_h d}$$

Equation 5-22

where α is left in as the removal constant, which is determined by the chemistry of the bacteria and the filter material.

5.5.4 Choosing pore size values

The next step is to determine values for d and d_h. The diameter, d, describes the cross-sectional area of the cylindrical pore shown in Figure 5-29. The height, d_h, refers to the height of the cylindrical pore. One option is to model removal according to the alignment of the rice husks shown in Figure (5-12). In this case, we can say that d is the hydraulic diameter and d_h is the rice husk size, D (Figure 5-32).

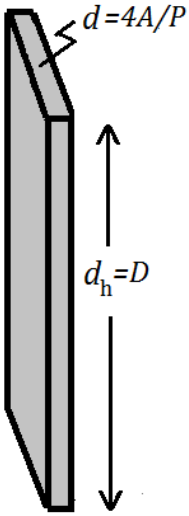

Figure 5-32: Lengthwise alignment of the rice husk.

Another option is to model the alignment of the rice husks as show in Figure (5-13). In this case, we can say that that d is a fractional diameter defined in Equation 5-2 and d_h is the rice husk height (Figure 5-33).

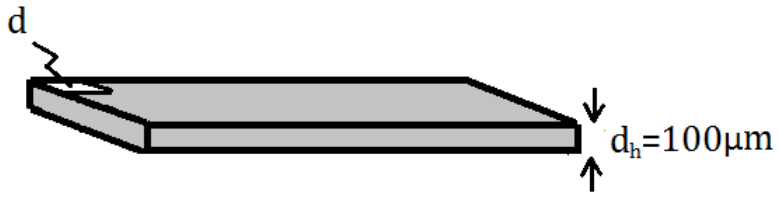

Figure 5-33: Stacked alignment of the rice husk.

The option of characteristic pore size equal to the size of the intrinsic clay pores is not applicable for an adsorption filtration model since the intrinsic pores are on the same order of size as the contaminants. More experimental work is needed to determine if the sizes of the intrinsic clay pores are relevant to the level of contaminant removal. If they are, the filtration model should be modified to include mechanical screening. For now, however, this interpretation of characteristic pore size is not included in the analysis.

Figure 5-34 shows measured and predicted bacteria removal with both interpretations of the characteristic pore sizes (hydraulic diameter and fractional diameter) and a removal constant of $\alpha = 1$. This value of α was chosen in order to show the upper limit of removal possible for the two interpretations of characteristic pore size. However, the value of α can range over several orders of magnitude [26]. Figure 5-35 shows the same data as Figure 5-34 but with $\alpha = 0.01$ for comparison.

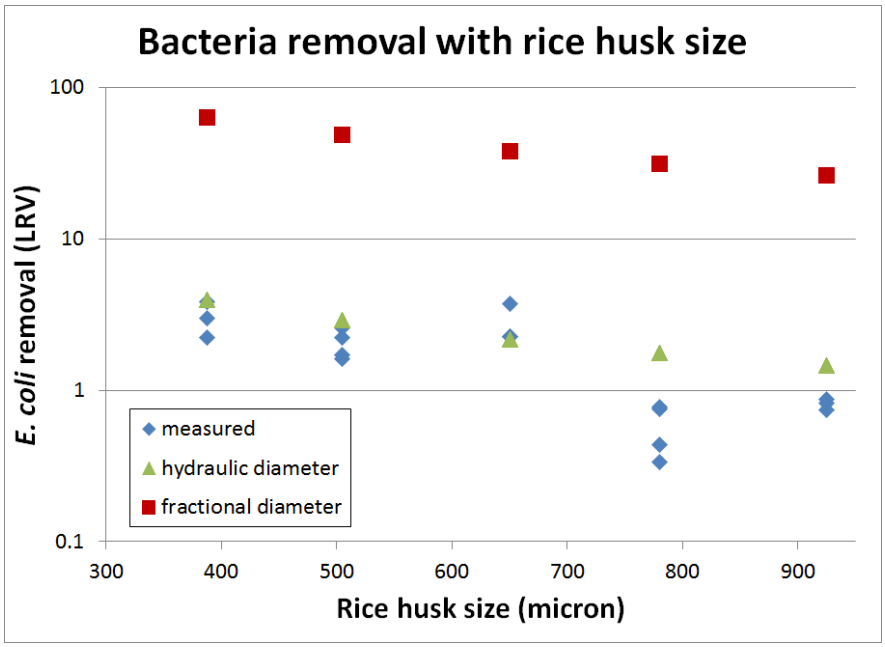

Figure 5-34: Predicted and measured *E. coli* removal with rice husk size. Removal constant, α=1.

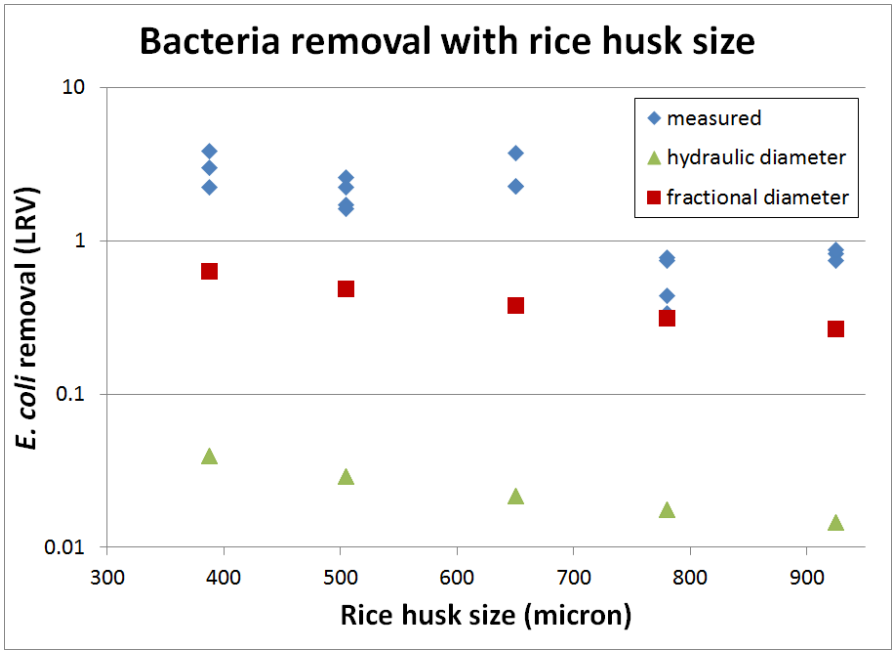

Figure 5-35: Predicted and measured *E. coli* removal with rice husk size. Removal constant, α=0.01.

Figure 5-34 shows that the measured removal values are within the range of possible removal values predicted by Equation 5-22. The level of agreement between the measured and the calculated values depends on the value of α. This value would need to be determined experimentally in order to know if an adsorption-based model is indeed descriptive of the system.

5.6 Strength model

Wall strength is explored in this section one parameter at a time.

5.6.1 Rice husk size

A basic model for modulus of rupture of a brittle material is based on the Griffith's criterion for fracture:

$$\sigma_{max} = \sqrt{\frac{G_C E}{\pi a}}$$

Equation 5-23

where σ_{max} is the modulus of rupture, G_C is the strain energy release rate, a is half the crack length and E is the Young's modulus of the material. This model is normally used to determine the critical crack size that will result in failure of a brittle material. In the case of the CPF, we can set a equal to the rice husk size. In order to compare Equation 5-23 with the data first presented in Figure 4-9, we combine E, G_C and a geometric conversion factor into a constant C such that

$$F_{max} = \frac{C}{\sqrt{a}}$$

Equation 5-24

where $F_{max}$is the load at rupture. By fitting Equation 5-24 to the data, we find $C \cong 35{,}000$. In Figure 5-36, Equation 5-24 is plotted against the experimental data from Figure 4-9.

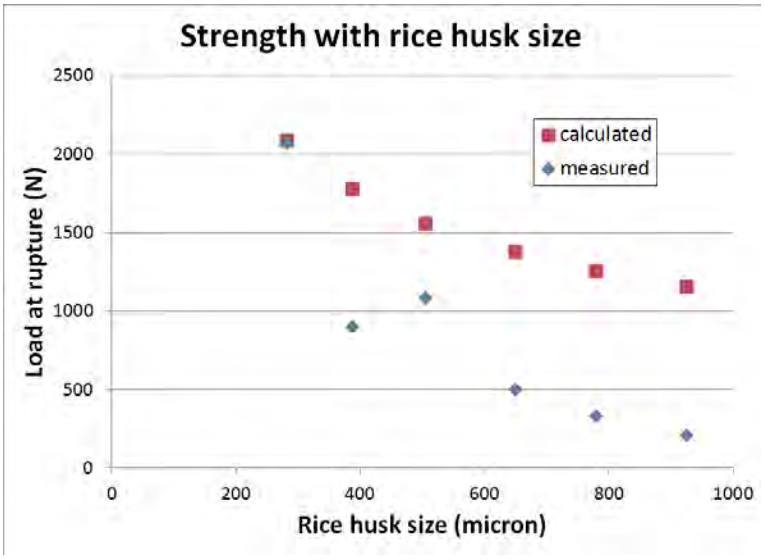

Figure 5-36: Predicted and measured strength with respect to rice husk size.

Figure 5-36 shows that Equation 5-24 is likely not a correct model for strength with respect to rice husk size as the experimental data for strength reduces with increased rice husk size much faster than predicted by the model. This is likely because the CPF contains many more pores than the Griffith's model was meant to support and the interaction between the pores is not reflected in the model. In addition, without determining the values of E or G_C, the order of magnitude agreement between the model and the data cannot be evaluated.

5.6.2 Percentage rice husk

While this author was unable to find previous theoretical studies regarding the strength of ceramic pot filters with respect to percentage rice husk, literature exists relating the strength of concrete, another brittle material, to its porosity. A 1983 paper by Kendall et al [27] presents data and analysis of this relationship. They suggest using Feret's Law

$$\sigma_{max} = C(1 - 1.95\varepsilon)^2$$

Equation 5-25

where σ_{max} is the modulus of rupture, ε is porosity and C is a constant set to equal 10 by this author in order to obtain a good fit. Figure 5-37 shows data from Watters' thesis [19] adapted by this author and plotted against Equation 5-25.

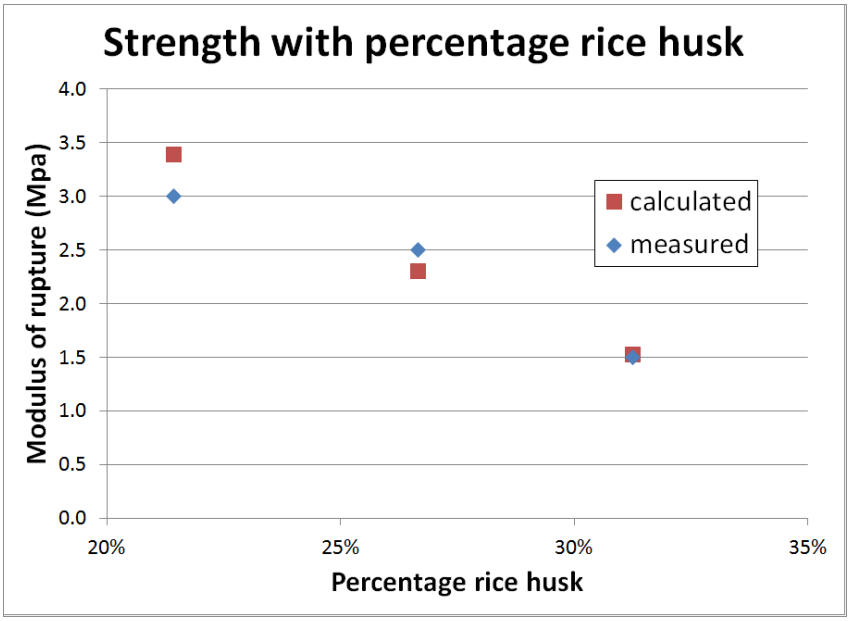

Figure 5-37: Predicted and measured strength with respect to percentage rice husk. Adapted by this author from [19] Figure 5-2.

While the apparent correlation is promising, much more work is needed to test the validity of this model.

5.6.3 Wall thickness

Watters theorized that the moment at rupture of the CPF is proportional to the square of its wall thickness as described in Section 2.2.4 [19]. He compared this result to his experimental data as shown in Figure 5-38. He found that, experimentally, moment at rupture more closely followed wall thickness to the power of 2.6 than it followed a quadratic relationship. However, this author thinks that the quadratic description of strength with respect to wall thickness is still promising and should be further evaluated.

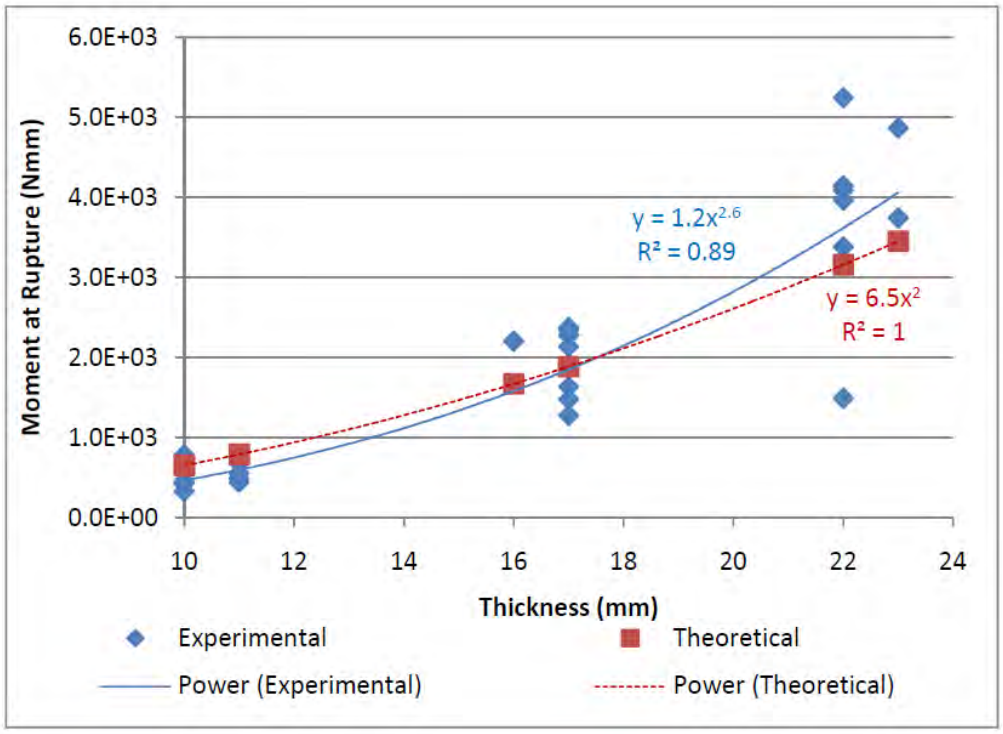

Figure 5-38: Modulus at rupture with respect to wall thickness.

Reprinted from [19] Figure 5-6.

5.6.4 Strength model

Since the first two elements of the strength model presented above are incomplete, no integrated model for wall strength is presented here, and the area is left open for future investigations.

Chapter 6: Discussion

6.1 Full parameter/performance matrix

This chapter addresses design implications for the CPF informed by the data and analysis from the previous chapters. The relationships between the manufacturing parameters (percentage rice husk, rice husk size and wall thickness) and the metrics of performance (flow rate, bacteria removal and strength) are consolidated from the data in Chapters 2 and 4 and the strongest of the theoretical conclusions from Chapter 5 into the complete parameter/performance matrix shown in Table 6-1. Contributions by this author are attributed to Servi. Superscripts have the same meanings as they did for Table 2-1 with the new superscript 4 indicating that the result was arrived at theoretically.

Table 6-1: Full parameter/performance matrix combining prior art and new results.

		Performance metrics		
		Flow rate	Bacteria removal	Strength
Manufacturing parameters	Percentage rice husk	Gensburger[15]: positive linear	Gensburger[15]: no correlation	Plappally[16]: negative correlation[1]
		Miller[17]: positive linear	Miller[17]: no correlation[3]	Watters[19]: negative correlation
		Rayner[14] : positive correlation	Servi: no correlation[4]	
		Plappally[16]: positive correlation[1]		
		Lantagne[18]: positive correlation[1,2]		
		Miller[20]: positive correlation[2]		
		Servi: positive linear[4]		
	Rice husk size	Rayner[14]: positive correlation	Rayner[14]: negative correlation	Servi: negative correlation
		Servi: exponential or positive step	Servi: negative linear or negative step	
	Wall thickness	Servi: inversely proportional	Rayner[14]: positive correlation	Watters[19]: power relationship
		Servi: inversely proportional[4]	Servi: positive linear	Watters[19]: quadratic[4]
			Servi: positive linear[4]	

6.2 Optimization method

6.2.1 Justification

In this chapter, the author converts the generalized relationships in Table 6-1 into a set of equations describing filter performance and uses optimization on those equations to formulate design recommendations. One might argue that the equations for the relationships between manufacturing parameters and performance metrics could be used directly to choose

an optimal set of parameter values. For instance, by trial and error, one could find the combination of parameter values needed to achieve a certain bacteria removal goal or strength target. However, with three manufacturing parameters and three metrics of performance, it is not easy to intuitively determine the best combination of parameter values for optimizing all three performance metrics. This will be even more true if more manufacturing parameters or performance metrics are added to this matrix. For this reason, formal optimization is used to find the best possible values of the manufacturing parameters in order to maximize the performance metrics.

6.2.2 Method

Microsoft Excel Solver was used for all optimizations in this chapter as it uses a standard algorithm and is considered an adequate solver. The plots in this section were produced by iteratively running optimizations in which a bacteria removal value and a minimum allowable strength were specified, and the solver was asked to find the parameter values corresponding to the maximum flow rate possible given those constraints. Thus, each point on the plots in Section 6.5 represents the maximum flow rate that is achievable at the given bacteria removal and strength.

The three metrics of performance and the three manufacturing parameters are listed below with their associated variables and units. The units for strength with be explained in more detail in Section 6.4.1. A screenshot of the solver is shown in Figure 6-1.

Metrics of performance:

- Flow rate: Q [L/hr]
- Bacteria removal: B [LRV]
- Strength: S [multiples of PHW strength]

Manufacturing parameters:

- Percentage rice husk: P [fraction out of 1]
- Rice husk size: D [μm]
- Wall thickness: L [mm]

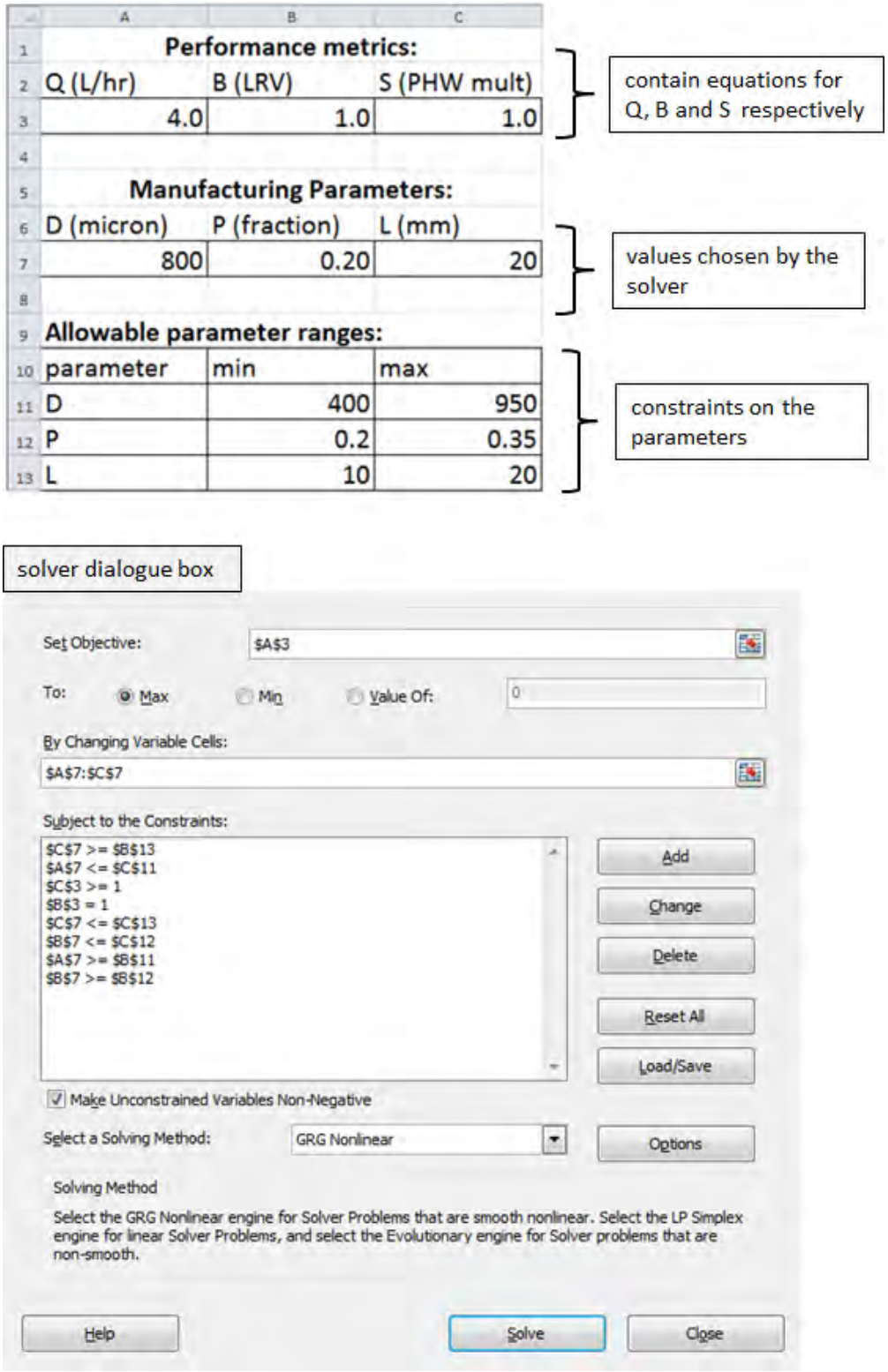

Figure 6-1: Screen shot of the Microsoft Excel Solver.

6.3 Optimization assumptions

Before running the optimizations, it is necessary to convert the information in Table 6-1 into equation form. Where in the previous chapter, the objective was to determine a meaningful theoretical relationship between parameters and performance, this chapter is more pragmatic, and the subsequent equations are developed empirically based on the author's best interpretation of the available data.

Four different sets of assumptions are described below with separate optimizations run for each. These four optimizations were run so that the final results would not dependent on a single interpretation of the available data. After running the four optimizations, the results were synthesized into a single set of design recommendations which are presented in Section 7.1.1. The four sets of assumptions are as follows:

6.3.1 Optimization 1: Continuous model, bounded parameters

The information in Table 6-1 is simplified as shown in Table 6-2 with the relationships between the independent variables (percentage rice husk, rice husk size, wall thickness) and the dependent variables (flow rate, bacteria removal, strength) written inside the appropriate cells.

Table 6-2: Simplified parameter/performance matrix based on continuous assumptions.

	Flow rate	Bacteria removal	Strength
Percentage rice husk	linear	no correlation	negatively linear
Rice husk size	exponential	negatively linear	negatively linear
Wall thickness	inversely proportional	linear	quadratic

When making Table 6-2, the author was presented with multiple options for each cell. She made the decisions as follows:

- **Percentage rice husk/flow rate:** The author chose a positive linear relationship based on the wealth of data in the studies conducted by Gensburger [15] and Miller [17] as well as the convincing logic of the theoretical explanation from Section 5.4.
- **Percentage rice husk/bacteria removal:** While less data exists for this relationship, the cited studies have many data-points supporting that no correlation exists between these two variables.
- **Percentage rice husk/strength:** The author approximated this relationship as negative linear despite this not being quite accurate. This was done because the author does not feel there is enough information available at the moment to propose a more nuanced equation for this relationship. However, for the purposes of this optimization, in the range of percentages of rice husk considered, the author thinks that a linear fit is close enough that it will not compromise the conclusions of the optimization.
- **Rice husk size/flow rate:** For Optimization 1, this author chose the continuous explanation for this cell, describing the relationship between rice husk size and flow rate as exponential. Due to the uncertainty associated with this cell, this assumption will be changed for Optimizations 3 and 4.
- **Rice husk size/bacteria removal:** Similarly, for Optimization 1, this author chose the continuous explanation for this cell, describing the relationship between rice husk size and bacteria removal as negative linear. Due to the uncertainty associated with this cell, this assumption will also be changed for Optimizations 3 and 4.
- **Rice husk size/strength:** For the same reason as for the percentage rice husk/strength relationship, the author approximated this relationship as negative linear despite this not being quite accurate. However, within the range of rice husk sizes under consideration in this study, the author thinks that the approximation will not compromise the conclusions of the optimization.

- **Wall thickness/flow rate:** The author chose an inversely proportional relationship for this cell due to the strength of both the data and the theoretical model as presented in Sections 4.1 and 5.4.
- **Wall thickness/bacteria removal:** The author chose a positive linear relationship for this cell based on the strength of both the data and the model as presented in Sections 4.2 and 5.5.3.
- **Wall thickness/strength:** The author chose to use the quadratic relationship for strength as a function of wall thickness. While Watters' [19] data did not confirm this to be the case, the logic of the model holds more weight to this author than the experimental data.
- **Constraints on the parameters:** For this optimization, the allowable values for the manufacturing parameter are confined to the ranges for which experimental data exists. This was done to avoid the uncertainties introduced by extrapolation.

6.3.2 Optimization 2: Continuous model, unbounded wall thickness

The same relationships as shown in Table 6-2 are used, but instead of bounding all three parameter values, wall thickness is allowed to take on any value. This was done in order to explore the role of wall thickness as a limiting factor of the CPF design.

6.3.3 Optimization 3: Discrete model, bounded parameters

The information in Table 6-1 can also be simplified as shown in Table 6-3, this time using a discrete relationship for rice husk size/flow rate and rice husk size/bacteria removal. This choice was made to reflect the step function interpretation of these performance metrics with respect to rice husk size. The values of the manufacturing parameters are bounded in the same way as for Optimization 1.

Table 6-3: Simplified parameter/performance matrix based on discrete assumptions.

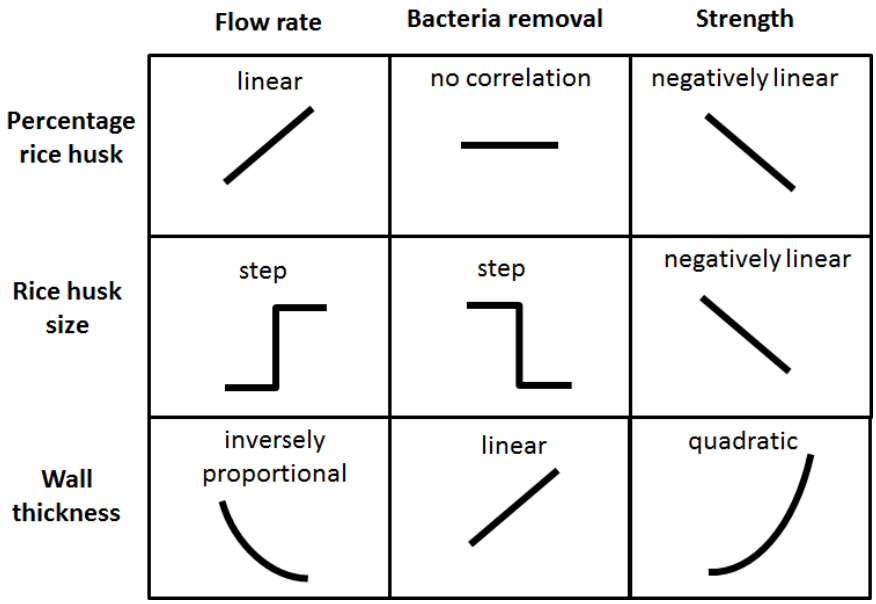

6.3.4 Optimization 4: Discrete model, unbounded wall thickness

The same relationships as shown in Table 6-3 are used, but instead of bounding all three parameter values, wall thickness is allowed to take on any value.

These four sets of assumptions will be shown to produce different results which all share common features. It is likely that none of these sets of assumptions is completely accurate, but rather that together they can teach us something useful about the CPF design.

6.4 Scaling

Before putting numbers to the relationships described in Tables 6-2 and 6-3, appropriate scaling must be done so that the numerical results of the optimizations are a reflection of reality. Since each CPF factory produces filters which differ in many manufacturing parameters besides the three examined here, it is not possible to say that a certain set of these three parameters will give an exact value for flow rate, bacteria removal or strength for a specific filter made at a specific factory. However, the general relationships between these

three parameters and CPF performance should be consistent across factories. In this chapter, calculated flow rates and bacteria removals are scaled to approximate the performance of the current filters produced by the Pure Home Water factory. We can estimate that the Pure Home Water filters are made with parameter values of $P = 20\%$, $L = 20mm$ and $D = 800\ microns$. Average flow rates at that factory are approximately 4L/hr and bacteria removal before the application of silver is approximately 1 LRV. Thus, the equations for flow rate and bacteria removal that follow are scaled to predict 4L/hr and 1 LRV for the above set of parameter values.

However, even if the results presented here are roughly scaled to reflect the performance of the Pure Home Water filters, the absolute numbers presented in this chapter should still be not taken literally. The intention is only to demonstrate trends in filter performance based on manufacturing parameter values.

6.4.1 Scaling strength

While scaling flow rate and bacteria removal is relatively straight-forward given the wealth of data surrounding those two metrics of performance, scaling strength is more difficult. In order to scale the strength results presented in this chapter, this researcher conducted strength tests on filter disks produced at the Hydrologic factory in Cambodia and filter disks produced at the Pure Home Water factory in Ghana. The results from these tests are plotted in Figure 6-2 with each bar representing an individual disk.

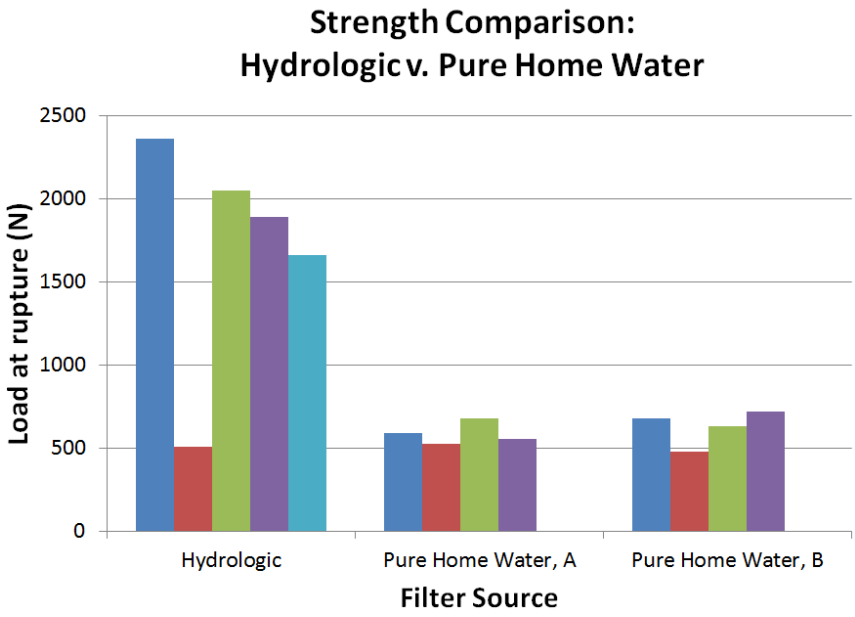

Figure 6-2: A comparison of Hydrologic and PHW filter strengths.

Figure 6-2 shows a significant difference between the strengths of the filters produced at Hydrologic and those produced at Pure Home Water. Table 6-4 compares the values of the manufacturing parameters for the three types of filters shown in Figure 6-2. However, the values of the three parameters give no clues for the observed differences in strengths. This highlights the need for tighter parameter specifications (especially regarding rice husk size) as well as the need for further study of the effects of other manufacturing variables.

Table 6-4: The manufacturing parameters of the Hydrologic and PHW filters.

	percentage rice husk	rice husk size	wall thickness
Hydrologic	26.4%	<1mm	0.74cm
Pure Home Water, A	20%	<1.5mm	0.74cm
Pure Home Water, B	20%	<1mm	0.74cm

The results in Figure 6-2 show why absolute values of strength cannot be determined based on only three manufacturing parameters. Hence, for the purposes of the equations in the following sections, strength is expressed as multiples of current Pure Home Water strength. Thus, a strength value of $S = 1$ indicates that strength is equal to the current Pure Home Water filters.

6.5 Optimization results

6.5.1 Optimization 1: Continuous model, bounded parameters

We can now formulate equations based on the first set of assumptions. Constants were calculated by hand by this author by inspecting the available data. This is considered adequate by the author because the optimizations are meant to show trends of filter performance, not to produce exact values. Constraints on the valid parameter ranges were chosen such that no extrapolation from existing experimental data was needed.

The equations for this optimization are as follows:

Flow rate:

$$Q = 0.108\frac{(P - 0.1) \times 1.0112^{D}}{L}$$

Equation 6-1

valid for

$0.1 < P < 0.6$

$400 < D < 950$ (micron)

$3 < L < 20$ (millimeter)

Thus, a filter with $P = 0.2$, $L = 20mm$ and $D = 800\ microns$ is predicted to have $Q = 4L/hr$.

Bacteria removal:

$$B = 0.000387(950 - D) \times (L - 2.8)$$

Equation 6-2

valid for

$400 < D < 950$ (micron)

$3 < L < 20$ (millimeter)

Thus, a filter with $P = 0.2$, $L = 20mm$ and $D = 800\ microns$ is predicted to have $B = 1LRV$.

Strength:

$$S = 0.000083(0.4 - P) \times (950 - D) \times L^2$$

Equation 6-3

valid for

$0.2 < P < 0.35$

$400 < D < 950$ (micron)

$10 < L < 23$ (millimeter)

Thus, a filter with $P = 0.2$ $L = 20mm$ and $D = 800$ $microns$ is predicted to have $S = 1$.

The plot resulting from Optimization 1 is shown in Figure 6-3. It was produced by using Equations 6-1, 6-2 and 6-3 with Microsoft Excel Solver. As described in Section 6.2.2, each point in Figure 6-3 was determined by using the solver to maximize flow rate at the given levels of bacteria removal and strength. Manufacturing parameters were limited to the ranges of $400 < D < 950$ $micron$, $10 < L < 20mm$, $0.2 < P < 0.35$ to avoid any extrapolation from the experimental data. Figure 6-3 also contains a label for point A, the point corresponding to the current PHW filter design. Full tables of the parameter and performance metric values for this and the following optimizations can be found in Appendix D.

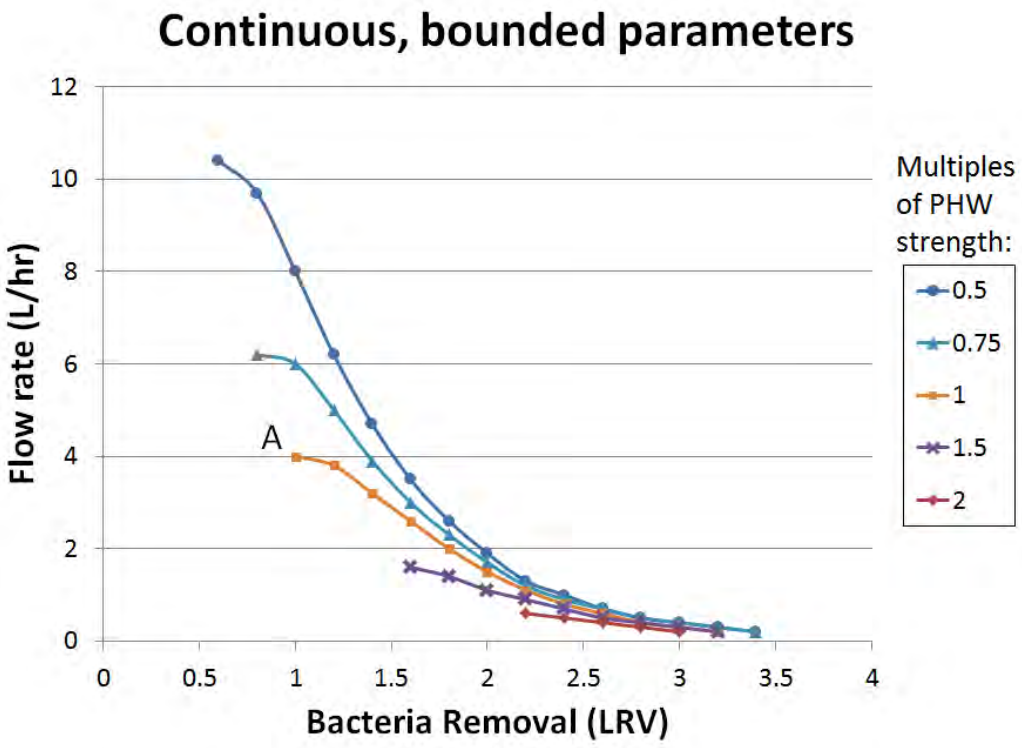

Figure 6-3: Optimization 1: Continuous model, bounded parameters.

Figure 6-3 shows some of the limits of the CPF design. Most striking is the speed at which flow rate reduces with increased bacteria removal. Because of this, there is not a lot of room for improved performance in this scenario and most manufacturers will choose to stay on the left hand side of the curve in order to ensure adequate flow rate. Figure 6-4 shows some of the parameter values for the curve in Figure 6-3 corresponding to strength, $S = 1$.

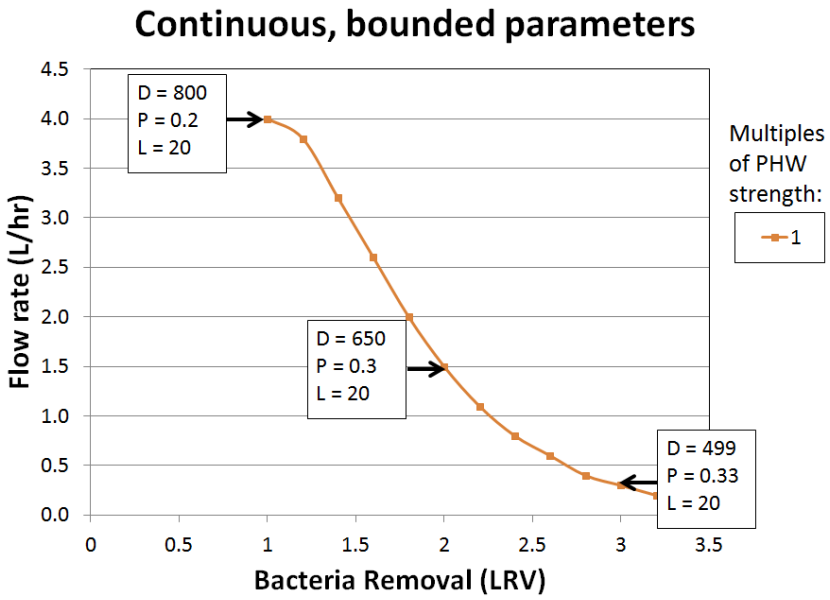

Figure 6-4: Continuous model, bounded parameters. Plotted with the parameter values.

As can be seen by these parameter values, the increase in bacteria removal is achieved by decreasing the rice husk size, D. At the same time, wall thickness, L, is always maximized subject to the imposed constraint of 20mm. While not shown in Figure 6-4, strength increases are increased by lowering the percentage rice husk, P. Because wall thickness is always maximized, this result suggests that wall thickness is a limiting factor in the design.

6.5.2 Optimization 2: Continuous model, unbounded wall thickness

We explore the idea of limiting factors through this next optimization which uses the same governing equations as Optimization 1 but does not have an upper bound on wall thickness. The limits of $400 < D < 950\ micron$ and $0.2 < P < 0.35$ still hold. Figure 6-5 shows the results of Optimization 2. Point A, the current PHW filter design, does not have a corresponding point on any of the curves on this plot because under this set of assumptions, that point would not have the maximum flow rate possible for its bacteria removal and strength.

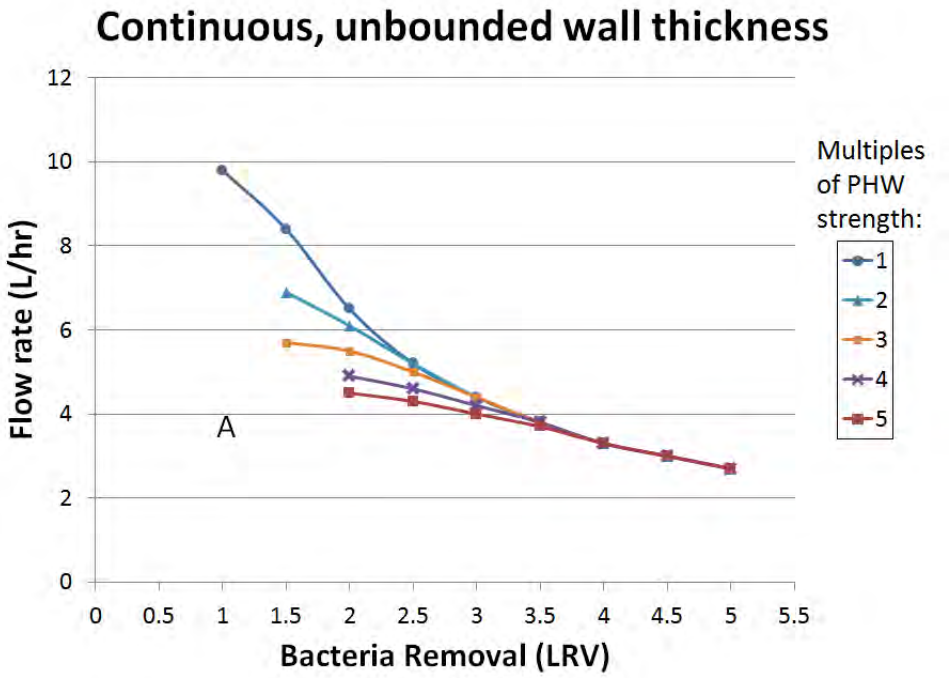

Figure 6-5: Optimization 2: Continuous model, unbounded wall thickness.

In this case, without constraints on wall thickness, flow rate and strength for higher levels of bacteria removal can be increased substantially. The different strength curves are seen to converge for higher values of bacteria removal indicating that these two aspects of performance are correlated at these higher values. Figure 6-6 shows some of the parameter values for the curve in Figure 6-5 corresponding to strength, $S = 1$.

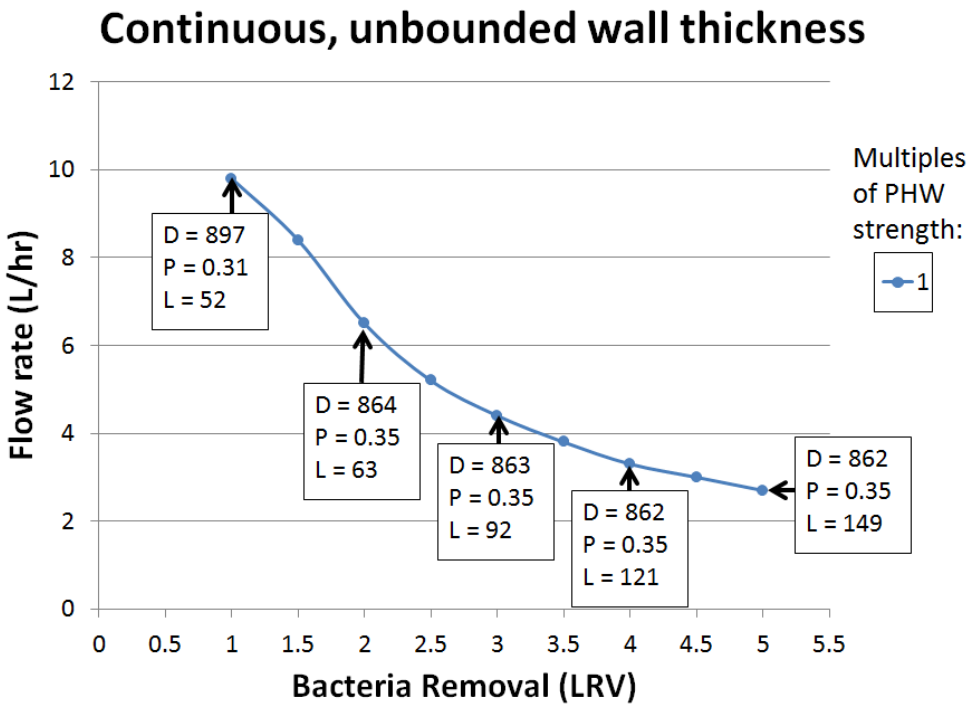

Figure 6-6: Continuous mode, unbounded wall thickness. Plotted with the parameter values.

As seen in Figure 6-6, in this scenario, bacteria removal is increased primarily by increasing wall thickness, L. These wall thicknesses are so large that they are not feasible for ceramics manufacturing. However, the lesson that increasing wall thickness improves overall performance is still useful to know. In this optimization, percentage rice husk converges to its maximum limit of 0.35 and rice husk size converges to 862µm as bacteria removal is increased. This indicates that, in this scenario, percentage rice husk is a limiting factor. Increasing wall thickness also contributes substantially to increased strength which is why the strength curves converge as bacteria removal increases.

6.5.3 Optimization 3: Discrete model, bounded parameters

For Optimization 3, the step-function relationships for flow rate and bacteria removal with respect to rice husk size are used. It is important to test these assumptions because they represent a different interpretation of the data available to us. The original constraints on the manufacturing parameters from Optimization 1 are included.

A model for flow rate can be built as follows with the values of the constants determined based on the experimental data:

$$Q = 8\frac{(P - 0.1)}{L} \; for \; D \leq 650 \; microns$$

Equation 6-4

$$Q = 800\frac{(P - 0.1)}{L} \; for \; D > 650 \; micron$$

Equation 6-5

for

$0.1 < P < 0.6$

$400 < D < 950$ (micron)

$3 < L < 20$ (millimeter)

A filter with $P = 0.2$, $L = 20mm$ and $D = 800 \; micron$ is predicted to have $Q = 4L/hr$.
A filter with $P = 0.2$, $L = 20mm$ and $D = 400 \; micron$ is predicted to have $Q = 0.04L/hr$.
This reflects the hundred-fold difference in flow rates between the regions of smaller and larger rice husk size.

A model for bacteria removal can be presented as follows:

$$B = 0.15(L - 2.8) \; for \; D \leq 650 \; microns$$

Equation 6-6

$$B = 0.04(L - 2.8) \; for \; D \leq 650 \; microns$$

Equation 6-7

for

$400 < D < 950$ (micron)

$3 < L < 20$ (millimeter)

A filter with $P = 0.2$, $L = 20mm$ and $D = 800\ micron$ is predicted to have $B = 2.58LRV$.
A filter with $P = 0.2$, $L = 20mm$ and $D = 400\ micron$ is predicted to have $B = 0.688LRV$.

Equation 6-3 is again used to describe filter strength. The same constraints of $400 < D < 950\ micron$, $10 < L < 20mm$, $0.2 < P < 0.35$ are imposed on the manufacturing parameters in order to avoid any extrapolation from the experimental data. A plot of Optimization 3 is shown in Figure 6-7 with point A corresponding to the PHW filter.

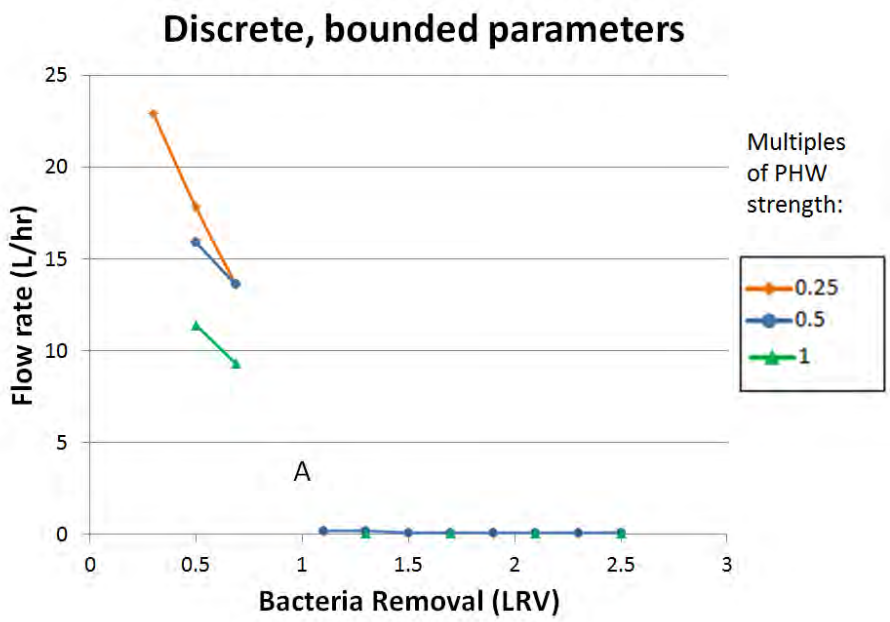

Figure 6-7: Optimization 3: Discrete model, bounded parameters.

In this case, filters with a rice husk size above 650µm have flow rates in the higher range (9 to 23L/hr) while filters with a rice husk size below 650µm have flow rates in the lower range (0.1 to 0.2L/hr). The blank area between the two regimes is an artifact of the sharp transition used in this model. Figure 6-8 shows some of the parameter values associated with Figure 6-7.

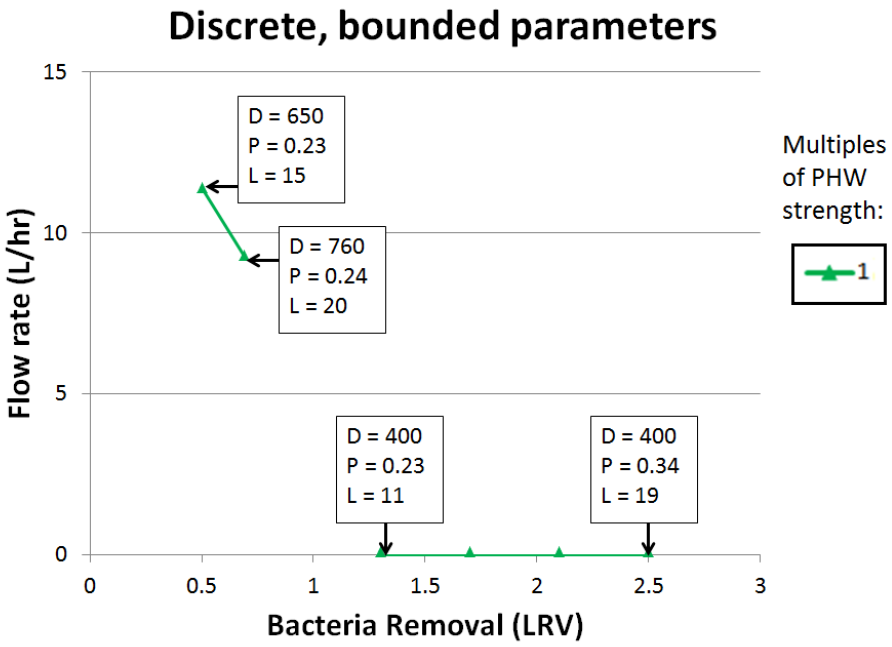

Figure 6-8: Discrete model, bounded parameters. Plotted with the parameter values.

As with Optimization 2, bacteria removal is increased by increasing wall thickness, L. Decreasing rice husk size also increases removal but causes flow rates to plummet to almost zero. Because of this, with the limits imposed on wall thickness, there is not much room in this scenario for design improvement

6.5.4 Optimization 4: Discrete model, unbounded wall thickness

For this optimization, we remove the limit on wall thickness while keeping the same governing equations as for Optimization 3. The limits of $400 < D < 950\ micron$ and $0.2 < P < 0.35$ still hold. Figure 6-9 shows the results of this optimization. Point A, the current PHW filter design, is again included for reference. The parameter values associated with the strength, $S = 1$ curve are shown in Figure 6-10.

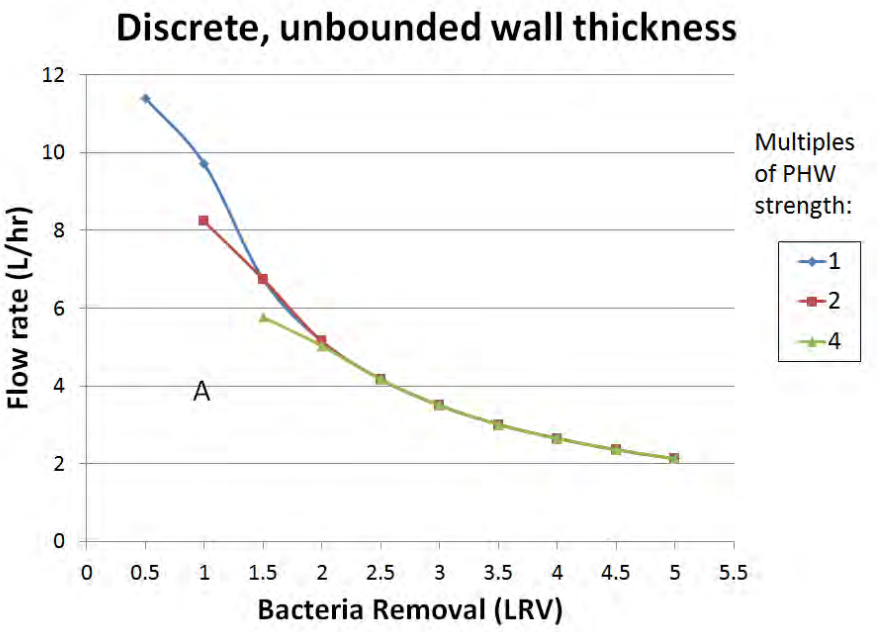

Figure 6-9: Optimization 4: Discrete model, unbounded wall thickness.

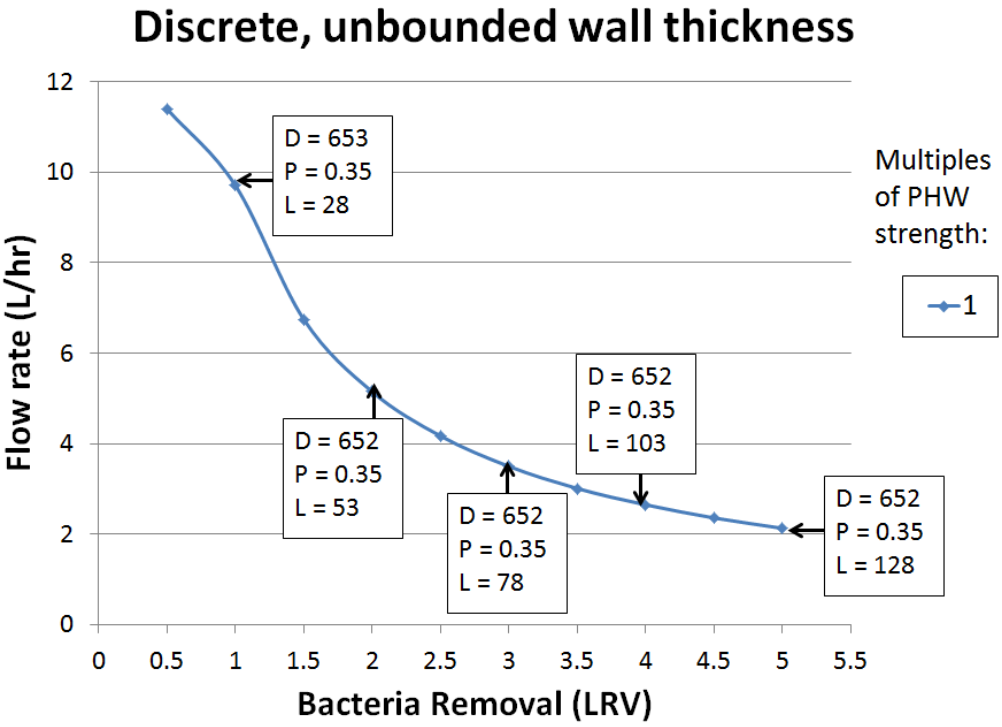

Figure 6-10: Discrete model, unbounded wall thickness. Plotted with the parameter values.

In this scenario, the rice husk size never leaves the larger range and, like with Optimization 2, bacteria removal is increased solely by increasing wall thickness. Again, the wall thicknesses are impossibly high for filters made out of ceramic. In Figure 6-9, the different strength curves collapse into a single line indicating that strength is not a limiting factor. Percentage rice husk is always maximized indicating that it could likely be increased further without hurting performance.

6.5.5 Synthesis of the optimizations

The results from the four optimizations show similar features. These optimizations show that when reducing rice husk size is relied upon to increase bacteria removal, flow rate is heavily penalized. This problem is circumvented by allowing wall thickness to increase, though the optimal wall thickness values are substantially larger than can be supported by the ceramic manufacturing process. The design implications of these optimizations are found in Chapter 7.

One of the objectives of this chapter is to demonstrate the use of optimization in the study of the CPF. While the design appears to be rather limited with just these three manufacturing parameters, with more parameters, it is expected that more and promising solutions will emerge.

Chapter 7: Conclusions, recommendations and future work

The goal of this thesis was to improve our understanding of the effects of manufacturing parameters on filter performance and so help the millions of people who lack access to safe drinking water. Chapters 2-6 addressed this goal through experimental studies, theoretical analysis and optimizations. This chapter synthesizes these findings into a set of design recommendation. These recommendations are followed by suggestions for future work and a summary of the contributions of this thesis.

7.1 Design recommendations

7.1.1 Choice of manufacturing parameter values

In this study, we considered three aspects of filter performance: flow rate, bacteria removal and strength, and three manufacturing parameters: percentage rice husk, rice husk size and wall thickness. The best choice of manufacturing parameter values depends on the relative importance of the different performance goals to the given manufacturer. As can be seen in Figures 6-3 to 6-10, improving one aspect of performance reduces performance in the other areas[7]. Therefore, the design recommendations must be tailored to the manufacturers' goals.

The author's design recommendations are as follows:

- If you want to increase **bacteria removal**, the best way is to increase wall thickness. Considering that increasing wall thickness makes firing more difficult and the filter heavier, wall thickness should only be increased within reasonable bounds likely determined by trial and error. If wall thickness cannot be increased further, but higher bacteria removal is still needed, it may be necessary to decrease rice husk size, even though this would substantially decrease flow rate.

[7] The exception is for very high bacteria removal levels which also exhibit high strength values (see Figure 6-5 especially).

- If you want to increase **flow rate**, the best way is to increase percentage rice husk. If flow rate is still significantly slower than desired, it may also be necessary to increase rice husk size, though this would be at the expense of bacteria removal.
- If you want to increase **strength**, the best way is to decrease percentage rice husk and/or increase wall thickness. If additional strength is still needed, it may be necessary to decrease rice husk size, though this would substantially decrease flow rate.

While the above are not the only ways to achieve these goals, they are the best ways to achieve them via manipulation of the three manufacturing parameters as informed by this author's current understanding of the CPF.

7.1.2 Controlling rice husk size

In order to keep a consistent flow rate between filters produced at the factory, the size of the rice husk should be tightly controlled. This recommendation is made in light of the sensitivity of flow rate to rice husk size as shown throughout this thesis. Keeping rice husk size consistent is important in order to avoid high rejection rates at the factory due to highly varying flow rates. If a factory is having quality assurance issues, the cost of removing rice husk particles that are too large or too small is likely to be negligible in comparison to the cost savings from having a higher percentage of filters pass quality control.

Control of rice husk size can be achieved in two ways:

- Sieve the rice husk at the top and bottom of a **narrow range** of sizes (a few hundred microns). This method ensures that even if the distribution of rice husk sizes is inconsistent within the allowable size range, the range is narrow enough that the inconsistency will not significantly affect performance.
- Use a wider range of rice husk sizes (closer to a thousand microns) but carefully **control the distribution** of sizes within that range. This may mean sieving the rice husk into a few narrow ranges and then mixing rice husk from each pile in the desired ratio.

The former method would be easier to implement but involves discarding more rice husk due to the narrower acceptable range. In addition, the implications of using a narrow range of rice

husk sizes as opposed to the wider ranges currently used at the factories has not yet been determined making it unclear at this time if this method will produce the desired results. The latter method would be more difficult to maintain, though if achievable, it would improve consistency with the least change in current production.

7.1.3 Additional design recommendations

- **Monitor wall thickness and percentage rice husk:** While it may go without saying, wall thickness and percentage rice husk should also be tightly controlled. Most factories already achieve this, although issues such as press misalignment should be monitored.
- **Hydraulic head and surface area:** While many factories already consider hydraulic head and surface area when designing the shapes of their filters, the results from Section 5.5.1 confirm that hydraulic head can be increased without hurting bacteria removal.
- **Completeness of rice husk combustion:** While complete combustion may be desired, the findings in Section 5.3 suggest that it is not necessary to prioritize this aspect of the CPF manufacturing process.

7.2 Future work

The study of the CPF is an active one, and this author has identified a number of areas where additional work is needed. This work can be organized by the original objectives of this thesis.

7.2.1 Objective one: Relationships between manufacturing parameters and performance

- **Expand the matrix:** A number of studies of the CPF have emerged over the last few years which explore the relationships between manufacturing parameters and aspects of filter performance other than the ones studied in this thesis. The parameter/performance matrix should thus be expanded to include columns and rows for these other variables of study, and these new cells should be populated with the results from these existing studies. An example of an expanded matrix is shown in Table 7-1.

Table 7-1: Extended parameter/performance matrix.

Manufacturing parameters	Performance metrics: Flow rate	Bacteria removal without silver	Bacteria removal with silver	Virus removal	Protazoa removal	Turbidity removal	Strength	...
Percentage rice husk or sawdust								
Rice husk or sawdust size								
Combustible shape								
Maximum firing temperature								
Clay chemistry								
Clay powder size and shape								
Wall thickness								
...								

- **Fill in the gaps:** Additional experimental and theoretical studies should be conducted to continue to fill in the gaps in the expanded matrix and to strengthen the results in the existing cells of the matrix. When adding to the existing cells in the matrix, a wider range of parameter values should be studied in order to determine the upper and lower limits for parameters such as percentage rice husk and wall thickness. In the case of new areas of the matrix, efforts should be made to study parameters in such a way that the results are continuous and expandable. For instance, instead of studying clay from one country versus clay from another country, effort should be made to continuously vary the composition of the clay (possibly by mixing two types of clay in a series of different ratios) in order to find an analytical relationship between clay characteristics and filter performance.
- **Further investigate rice husk size:** This author identified rice husk size as an extremely important and inadequately understood manufacturing parameter. This author would like to see significant work towards understanding this parameter, including strengthening the

results in this thesis and investigating the effects of the distribution of rice husk sizes within a wider size range.

- **Investigate parameter interactions:** The interactions between manufacturing parameters should be studied. While this author only looked at one parameter/performance relationship at a time, the interactions among parameters is expected to be meaningful.

7.2.2 Internal mechanisms

A number of questions surrounding the internal mechanisms of the CPF were addressed in detail in Chapter 5 of this thesis. Substantative investigations into these questions were conducted in this thesis, but more work is needed to provide definitive answers. Through addressing these questions, a more definitive understanding of the CPF can be built which can be used to make further improvements to the design. Outstanding research questions are presented below along with suggestions for directions of future work:

- **Does increasing flow rate reduce bacteria removal?** If so, flow rate cannot be increased without hurting removal effectiveness, regardless of the way in which it is increased. In this thesis, the author found no net change in removal over a wide range of flow rates varied by adjusting the hydraulic head. However, removal levels varied within the range tested, and more data is needed to understand this effect.
- **Does incomplete combustion harm or help bacteria removal and flow rate?** CPF manufacturers spend significant effort trying to control the completeness of firing. A better understanding of the effects of incomplete combustion will help channel those efforts more effectively. In this thesis, the author found no correlation between incomplete combustion and bacteria removal and flow rate. More data is needed to verify or refute this finding. In addition, the effect of incomplete combustion on strength was left untested.
- **How does hydraulic head affect flow rate?** A linear relationship between hydraulic head and flow rate implies laminar flow. This in turn affects the flow rate and filtration models which should be considered when modeling the CPF. While this study determined a linear relationship, more data would help to verify this finding.

- **How does rice husk size translate into pore size and shape?** Understanding this relationship could explain the differences between rice husk and sawdust and could suggest an ideal rice husk size to use. In this thesis, the author proposes three possible pore size models based on hydraulic diameter, a fractional diameter and intrinsic clay pore size. She also suggests that two or more pore size regimes may exist as a function of rice husk size. Further exploration of this topic is needed as pore size greatly impacts CPF performance.
- **What is the correct scaling factor (if any) for the Carman-Kozeny model of flow rate?** The Carman-Kozeny model for flow through a porous media seems to be a logical model to use for the CPF. However, without knowing if and how large a scaling factor should be used, it is not possible to verify the applicability of the model. In this study, the author used the droplet test to determine a scaling factor of 1/100. However, a more rigorous study is needed to solidify this aspect of the flow rate model.
- **What is the value of the removal constant of filtration, α?** In a collision-based filtration model or any filtration model besides mechanical screening, filtration effectiveness is scaled by a removal constant. Because of this, increasing the removal constant increases contaminant removal efficiency. This author did not investigate the value of α and a full study of its value, how it can be increased and the effects of increasing it is needed.
- **How is tortuoisty affected by rice husk size?** Changes in tortuosity have large effects on both flow rate and bacteria removal. This author's preliminary results show tortuosity to be constant for rice husk sizes above 400μm. However, further analysis and explanation of this finding is needed. In addition, a study of the effects of percentage rice husk on tortuosity would be valuable. If tortuosity can be manipulated, it will have implications for both flow rate and bacteria removal.

7.2.3 Design recommendations

- The design recommendations in Section 7.1 should be tested in a laboratory and in a pilot factory setting.

- As the parameter/performance matrix is expanded and improved, optimizations such as the ones described in Chapter 6 should be rerun with the new information in order to yield additional design recommendations.

7.3 Summary of contributions

Numerous contributions to the field of ceramic pot filters were made in this thesis through asking new questions about the CPF and making progress in determining the answers to those questions. The contributions are listed below:

- **Choosing important variables for study:** Three manufacturing parameters and three metrics of performance were identified as important for study. The three parameters are percentage rice husk, rice husk size and wall thickness. The three metrics of performance are flow rate, bacteria removal and strength. Both wall thickness and rice husk size were previously largely unstudied. Similarly, strength was relatively unstudied (Chapter 1).
- **Creating a framework for the relationships between variables:** The manufacturing parameters and performance metrics were organized into a matrix, effectively showing the current state of knowledge and the areas where more work is needed (Chapter 2).
- **Consolidating results from the literature:** Previously determined relationships between variables were consolidated from the literature into the matrix (Chapter 2).
- **Collecting new experimental data:** The author collected new experimental data for five cells of the matrix:
    - Wall thickness/flow rate;
    - Wall thickness/bacteria removal
    - Rice husk size/flow rate;
    - Rice husk size/bacteria removal;
    - Rice husk size/strength.

  Through this effort in combination with the consolidated results from the literature, all of the cells of the three by three parameter/performance matrix were populated (Chapter 4).

- **Compiling a set of questions about the CPF internal structure and mechanisms:** In order to build a theoretical model of the CPF, a number of questions about the internal structure and mechanisms of the CPF were addressed (Chapter 5).
- **Building theoretical models for flow rate, bacteria removal and strength:** Preliminary models for flow rate, bacteria removal and strength were proposed and tested against the experimental data (Chapter 5).
- **Designing and running optimizations:** The experimental and theoretical relationships between manufacturing parameters and performance metrics were translated into equation form. An expandable method for running optimizations for the CPF was introduced and four optimizations using different sets of assumptions were run (Chapter 6).
- **Design recommendations:** The findings from the experimental data, the theoretical analysis and the optimizations were consolidated into testable design recommendations (Chapter 7).

As ceramic pot filter production continues to scale-up, it is hoped that the work presented this thesis will help to push the design forward.

Appendix A: Studies from the literature included in Table 2-1

A.1 Percentage rice husk and flow rate

Rayner [14]: "Flow rate was increased with an increased burn-out material to clay ratio by weight and with increased particle size of the same ratio." This result is shown in Figure A-1 reprinted from [14] with the original caption. The numbers in the legend refer to the US sieve numbers of the meshes between which the rice husk or sawdust was sieved as described in Table A-1, reprinted from [14] below.

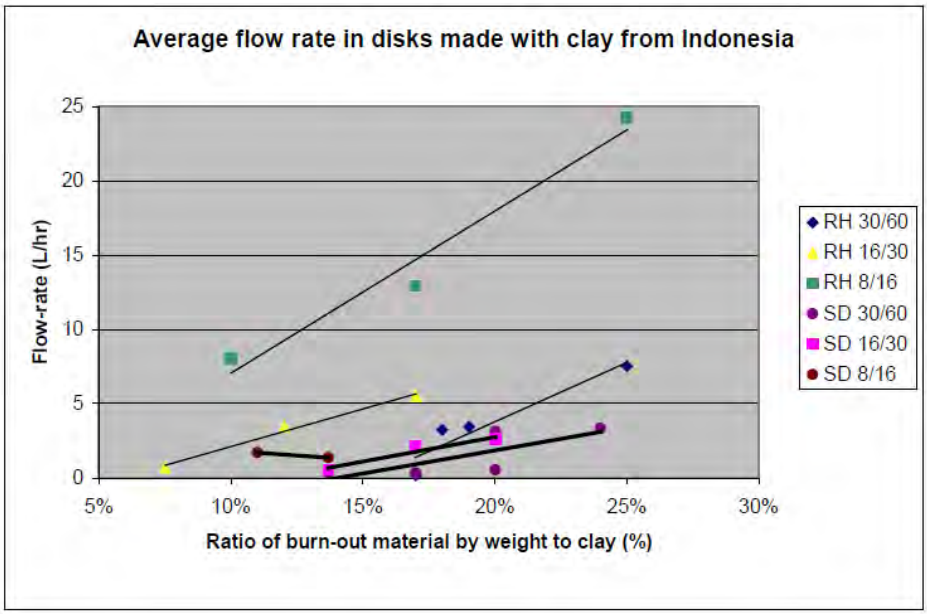

Figure A-1: Average flow rate in relation to particle size and ratio with clay from Indonesia and rice husk (RH) or sawdust (SD). Reprinted from [14] Figure 18.

Table A-1: Sieve size conversions. Reprinted from [14] Table 1.

US sieve	Tyler equivalent	Opening (mm)
8	8	2.38
16	14	1.19
30	28	0.595
60	60	0.25

Gensburger [15]: "Flow rate is linearly related to rice husk quantity." This result is shown in Figure A-2 reprinted from [15] with the original annotations.

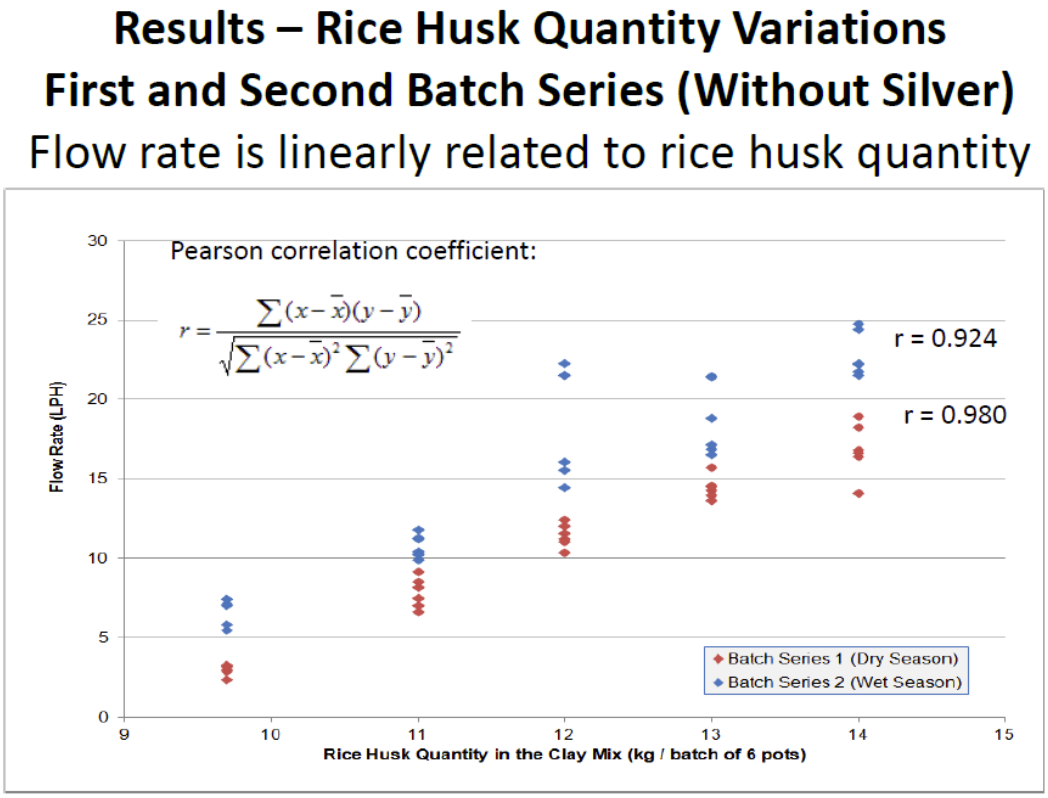

Figure A-2: Rice husk quantity and flow rate. Reprinted from [15] page 11.

Plappally [16]: "Average cumulative discharge… is seen to increase with increases in amount of sawdust." This result is shown in Figure A-3, reprinted from [16] with its original caption. The filters in this study were made with sawdust, not rice husk as the combustible. The numbers in the legend refer to the ratio of clay to sawdust, for example the "65-35" filter is composed of 35% sawdust by mass.

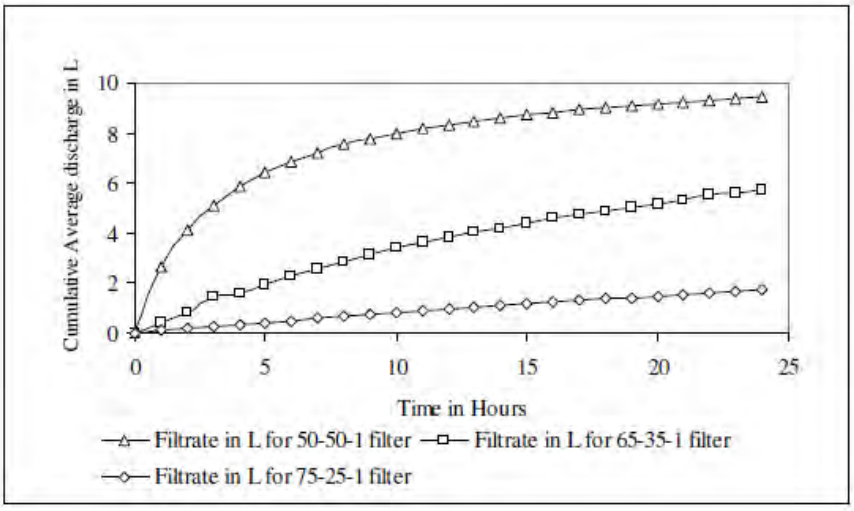

Figure A-3: Measurement of discharge from three distinct filters for a duration of 24 hours. Reprinted from [16] Figure 3.15.

Miller [17]: "As the percentage of rice husk increases, the flow rate increases." This result is shown in Figure A-4, reprinted from [17] with its original caption. This author interprets the linear regression to mean that Miller interpreted the data as having a positive linear relationship between percentage rice husk and flow rate.

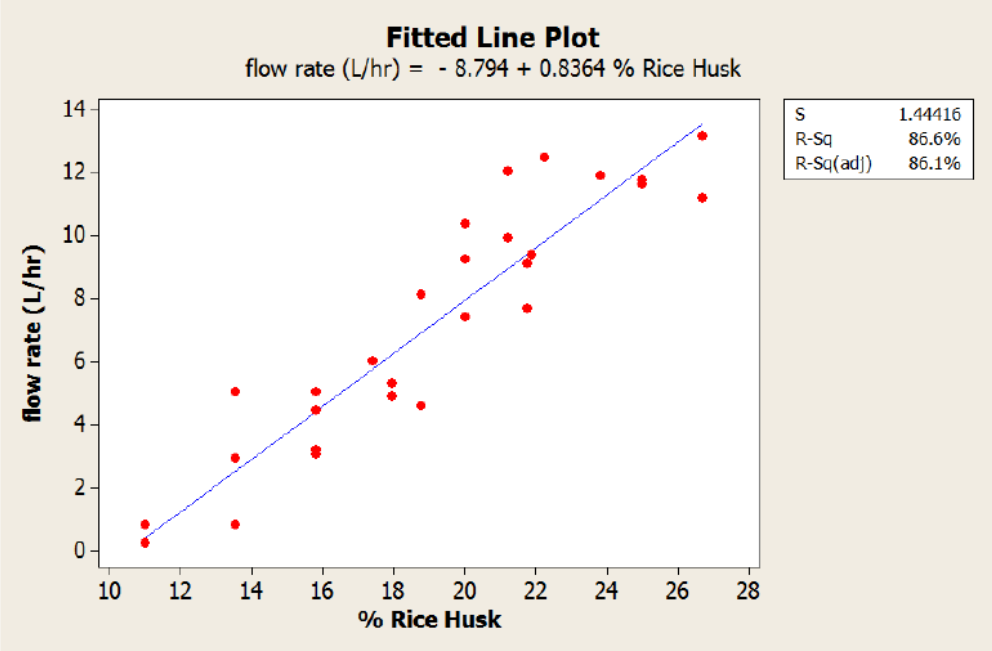

Figure A-4: Flow rate vs. percent rice husk. Reprinted from [17], Figure 4-17.

Lantagne [18]: "Higher percentage sawdust [leads] to higher flow rates." This result is shown in Figure A-5, reprinted from [18] with the original caption. The filters in [18] were painted with silver and used sawdust as the combustible.

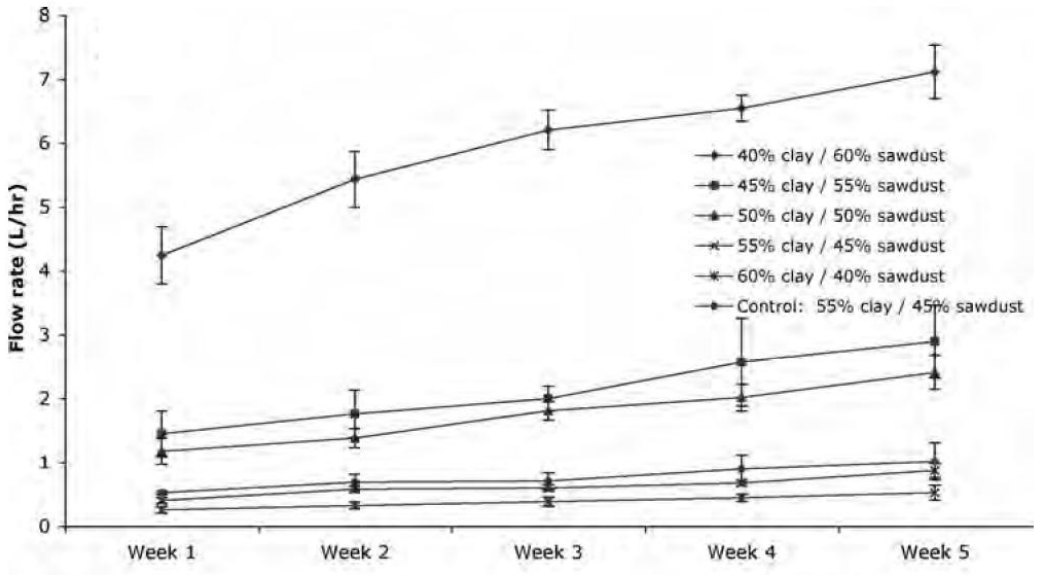

Figure A-5: Flow rate in clay : sawdust ratio testing filters. Note: Results presented are averages of triplicate samples. Reprinted from [18] Figure 5a.

Miller [20]: "A series of two-sample T-tests assuming unequal variances with 95% confidence showed a direct relationship between increasing flow rate and increasing percent combustible by mass for filters 1 through 6 with rice husk. A similar relationship was not found for filters 7 through 12 with sawdust, however, the two filters with the highest percent combustible by mass, 11 and 12, had statistically higher flow rates than the other four filters with lower percent combustible by mass." These results are shown in Figure A-6 reprinted from [20] with its original caption. The filters from this study were painted with silver.

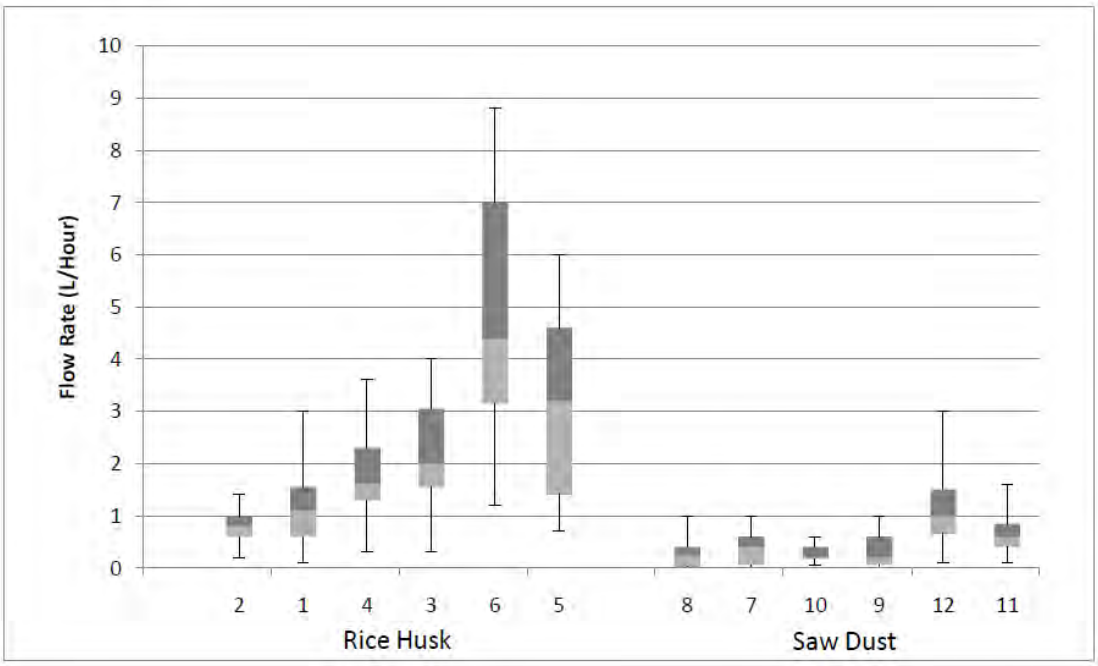

Figure A-6: Flow rate of filter pairs 1-12, increasing percent combustible by mass, sorted by combustible type. Reprinted from [20] Figure 5-52.

A.2 Percentage rice husk and bacteria removal

Gensburger [15]: Gensburger found "no correlation" between rice husk percentage and bacteria removal. This result is shown in Figure A-7, reprinted from [15] with the original annotations.

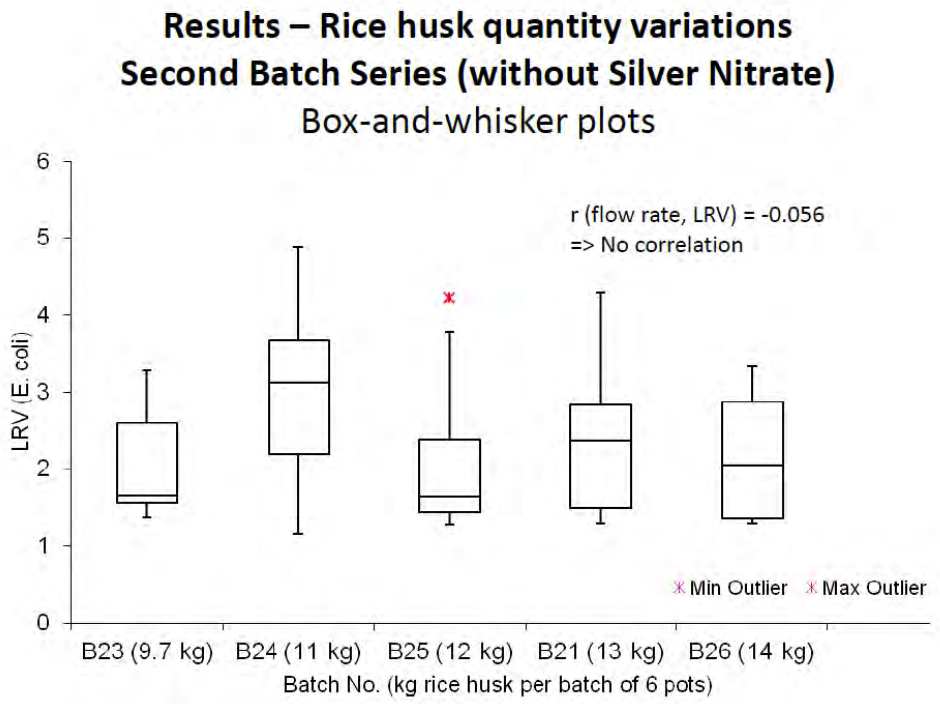

Figure A-7: Bacteria removal with mass of rice husk. Reprinted from [15] page 15.

Miller [17]: "The results…showed that, in a simple regression test, none of these production variables [including percentage rice husk] predict how well a CPF removed total coliform bacteria." These results are shown in Figure A-8, reprinted from [17] with the original caption. Miller's experiments used total coliform instead of *E. coli* as the indicator for bacteria removal.

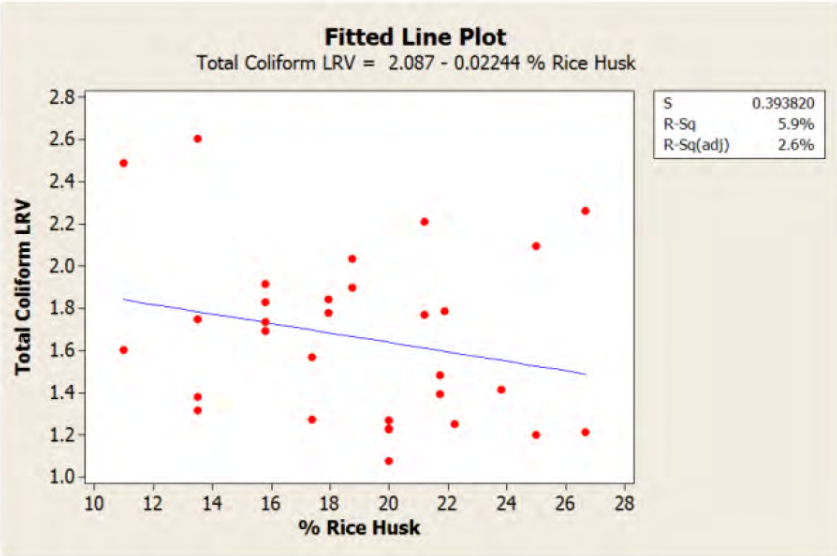

Figure A-8: Total coliform LRV vs. percent rice husk. Reprinted from [17] Figure 4-1.

A.3 Percentage rice husk and strength

Plappally [16]: "[There was a] non-linear decrease in fracture toughness…with increase in the volumetric content of sawdust." This is shown in Figure A-9, reprinted with the original caption. The filters in this study were made with sawdust and fracture toughness was used instead of moment at rupture to indicate strength.

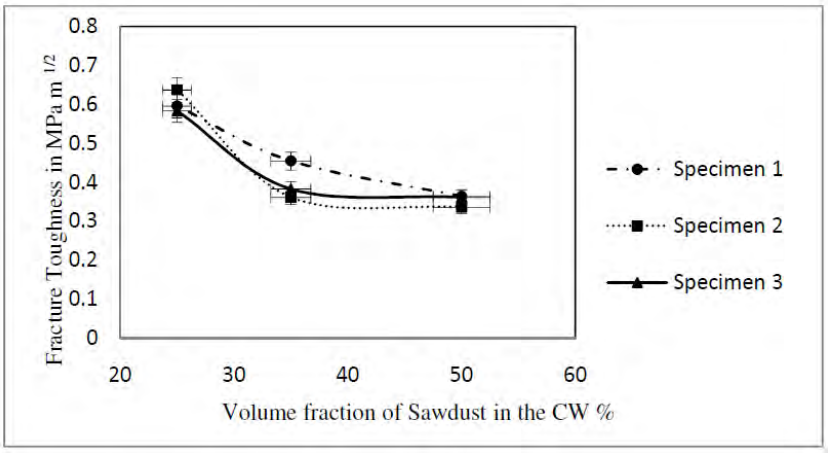

Figure A-9: Fracture toughness as a function of the volume fraction of sawdust for the three different T-specimens of clay ceramicware containing 25, 35 and 50% sawdust by volume, respectively. Reprinted from [16] Figure 4.6.

Watters [19]: "All four categories [of filters] display a decreasing relationship between the amount of combustible and bending strength." These results are shown in Figure A-10, reprinted from [19] with the original caption.

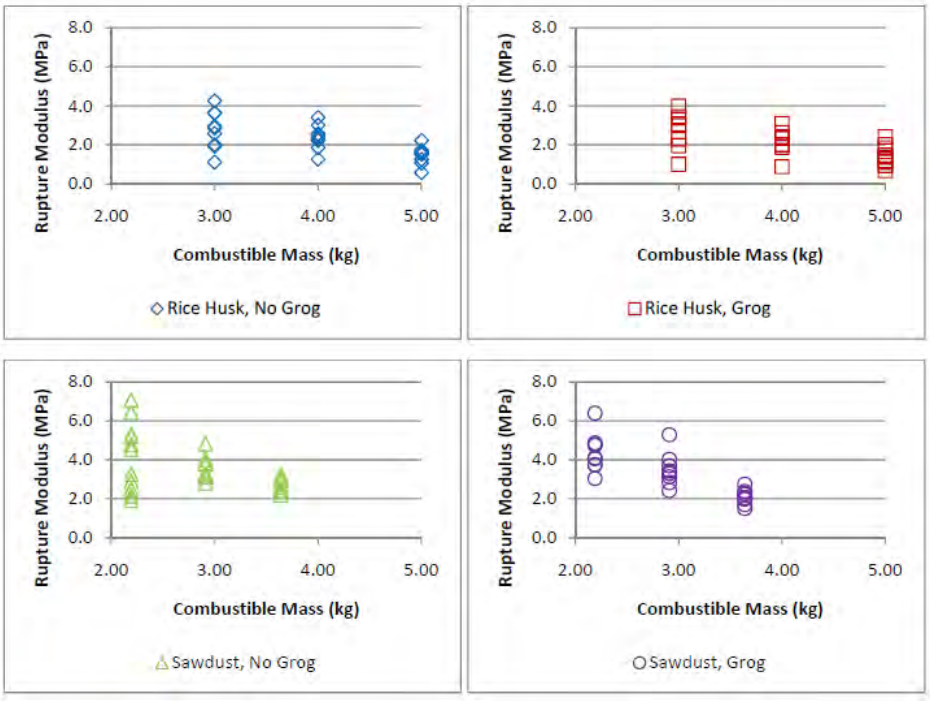

Figure A-10: Modulus of rupture vs. combustible mass, separate categories. Reprinted from [19] Figure 5-2.

A.4 Rice husk size and flow rate

Rayner [14]: "Flow rate was increased with an increased burn-out material to clay ratio by weight and with increased particle size of the same ratio." The results from this study can be seen in Figure A-1.

A.5 Rice husk size and bacteria removal

Rayner [14]: "A smaller particle size with sawdust seemed more reliably effective and seemed better able to accommodate more variation in [burn-out] ratio than disks manufactured with larger particle sizes." This result can be seen in Figure A-11, reprinted from [14] with the original caption. The mesh sizes in Figure A-11 are explained above in Table A-1. While the

conclusions presented are for sawdust, no conclusions were reached for similar data gathered for filters made with rice husk because, “none of the disks manufactured with rice husk met both LRV and flow-rate criteria.”

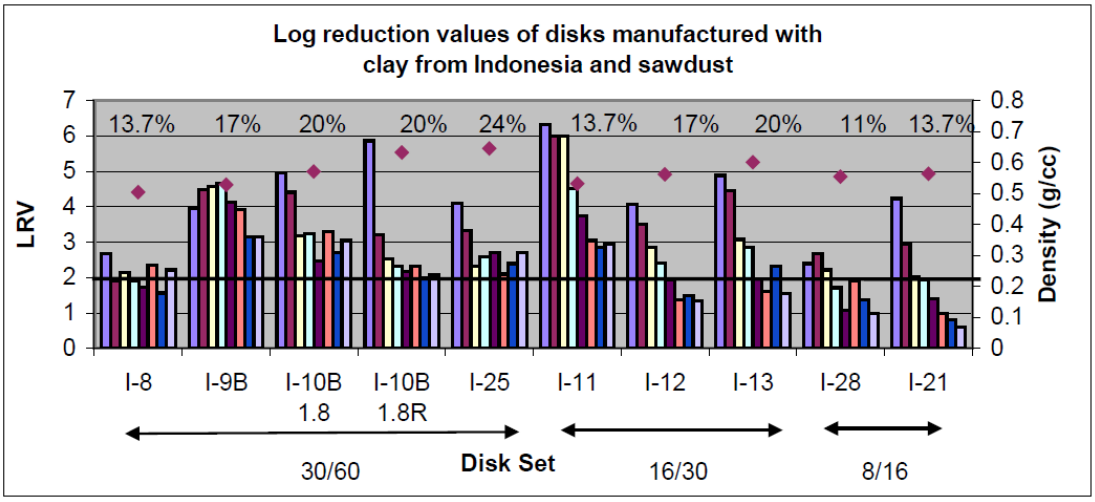

Figure A-11: Log reduction value of disks manufactured with Indonesian clay and sawdust. Reprinted from [14] Figure 28.

A.6 Rice husk size and strength

No studies were found.

A.7 Wall thickness and flow rate

No studies were found.

A.8 Wall thickness and bacteria removal

Rayner [14]: “A reduction in disk thickness resulted in a reduction in [bacteria removal] effectiveness.” This result is shown in Figure A-12, reprinted from [14] with the original caption. In Figure A-12, wall thickness decreases from left to right for each set of disks.

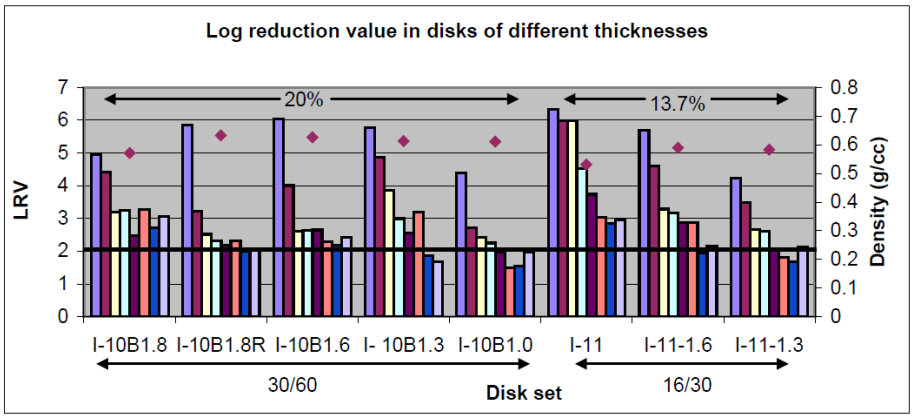

Figure A-12: Log reduction value of disks manufactured to different thicknesses. Reprinted from [14] Figure 30.

A.9 Wall thickness and strength

Watters [19]: "The R^2 value for the given power relationship exceeds the R^2 values obtained by assuming a linear, exponential, or order-2 polynomial relationship, suggesting that the power relationship is the best fit for the data." Watters' data along with a trend line for the power relationship and one for the theoretical quadratic relationship are shown in Figure A-13, reprinted from [19] with the original caption. The derivation of the theoretical quadratic relationship is found in Equation 5-1 of Watters' thesis [19].

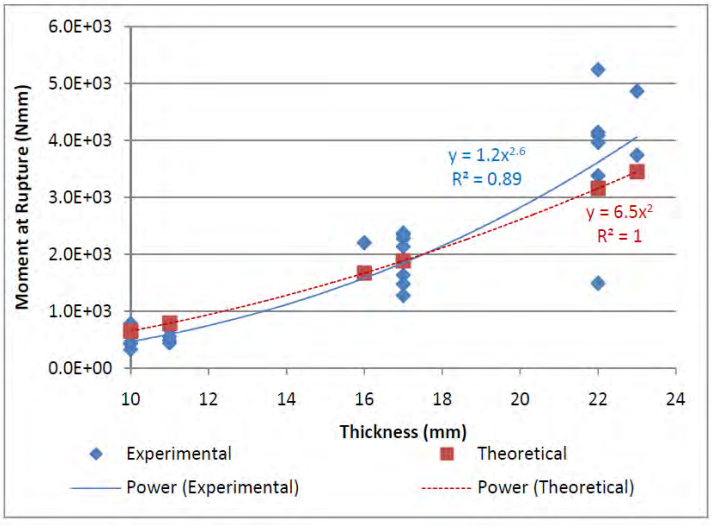

Figure A-13: Moment at Rupture vs. thickness for samples manufactured from recipe #4. Reprinted from [19] Figure 5-6.

Appendix B: Bacteriological testing details

B.1 Standard method for culturing *E. coli* K12

The following standard method was modified from a protocol written by Andrew Jones, a graduate student in the Mechanical Engineering Department at MIT:

Standard method for culturing *E. coli* K12

Chemicals/Organisms:

- Tryptone (8.0g)
- NaCl (0.5g)
- LB media plates (10)
- LB broth (500 mL, supports 10^9/mL *E. coli*)
- Freeze-dried *E. coli* K12[8] (1 vial)
- Distilled water (1.0L)

Equipment:

- Refrigerator (4°C)
- Incubator (37°C)
- Autoclave (121°C)
- Hood

Metal/Glassware:

- Glassware (>1L)
- Test tube (>5mL)
- Vial (>10mL)
- Test tube holder
- Pipettes (0.5mL, 5mL, 10mL)
- Sterile mix-sticks

Prepare the freeze-dried K12

- Mix Tryptone (8.0g), NaCl (0.5g) and distilled water (1.0L) in a 1.5L glassware.
- Autoclave the mix at 121°C for 15 minutes

[8] ATCC product code: 10798 Escherichia coli

To be done in the hood:

- Pipette 0.5mL broth into the vial containing *E. coli* K12
- Mix the liquid in the vial into a slurry
- Add this slurry to 4.5mL additional broth
- Incubate broth on a shake table at 37°C for 8 hours
- Store broth at 4°C, the broth will keep for one month

Streak a plate

- Dip a sterile mix-stick into the broth and streak it onto the plate
- Incubate plate at 37 °C for 8 hours
- Store plate at 4°C, the colonies will keep for one month

Prepare broth

- Pipette 10mL LB broth into vial
- Dip sterile mix-stick into a colony on the plate
- Dip mix-stick into the broth
- Incubate the broth on a shake table at 37°C for 24 hours
- Store broth at 4°C, the *E. coli* will keep for 1 month
- When nearing the end of the month, streak a plate with *E. coli* from the broth and repeat the above steps

B.2 Agar plate preparation

The following protocol was modified from [28]:

Agar Plate Preparation

(Makes approximately 40 plates)

Making the LB agar

1. Add 500 mL of dH2O to a 1L Pyrex jar.
2. Add to this:
    - 5.0 g Tryptone
    - 2.5 g yeast extract
    - 5.0 g NaCl
    - 7.5 g agar
3. Mix powder well to bring into solution.
4. Autoclave at liquid setting for 20 minutes making sure to loosen top.
5. Let agar cool to approximately 55°C (you should be able to pick up the jar without a glove).

Pouring the Plates

1. Make sure the bench top has been wiped down with bleach/EtOH.
2. Remove sterile Petri dishes from plastic bag (save the bag for storage).
3. Pour a thin layer (5mm) of LB agar (~10mL) into each plate being careful to not lift the cover off excessively (you should be able to just open up enough to pour).
4. Swirl plate in a circular motion to distribute agar on bottom completely.
5. Let each plate cool until solid (approximately 20 minutes) then flip so as to avoid condensation on the agar.
6. Store plates in plastic bags in fridge, upside down to avoid condensation on the agar.

Time to make two batches:

10 minutes to mix ingredient
90 minutes to autoclave
45 minutes to cool
20 minutes to pour

Appendix C: Experimental data

Wall thickness / Flow rate

Percentage rice husk: 26.4%
Rice husk size: 400-1000micron
Surface area: 600 mm^2
Hydraulic head: 30cm

sample	wall thickness (mm)	flow rate (mL/s)
23e5	18.8	0.0133
23e5	17.6	0.01529
23e5	15	0.01987
23e5	10	0.03531
23e5	5	0.089
23d4	18	0.01108
23d4	16	0.01402
23d4	14	0.01851
23d4	12	0.02547
23d4	10	0.04256
23d4	8	0.05726
23d4	6	0.07282
23d4	4	0.08886
23e7	19	0.01064
23e7	18	0.01333
23e7	16	0.01518
23e7	14	0.0202
23e7	12	0.02698
23e7	10	0.03736
23e7	8	0.04741
23e7	6	0.05887
23e7	4	0.1018
23c5	20	0.01345
23c5	17	0.01501
23c5	12	0.02383
23c5	9	0.03624
23c5	3	0.1632

Wall thickness / Bacteria removal

Percentage rice husk: 26.4%

Surface area: 600 mm^2

Hydraulic head: 30cm

sample	rice husk size (micron)	wall thickness (mm)	measured LRV	median LRV
3d4	400-500	20	2.26	2.14
3d4	400-500	20	2.13	
3d4	400-500	20	2.19	
3d4	400-500	20	2.14	
3d4	400-500	20	2.1	
3d4	400-500	16	1.61	1.64
3d4	400-500	16	1.64	
3d4	400-500	16	1.67	
3d4	400-500	12	0.93	1.12
3d4	400-500	12	1.12	
3d4	400-500	12	1.16	
3d4	400-500	8	0.64	0.64
3d4	400-500	8	0.76	
3d4	400-500	8	0.59	
3d4	400-500	4	0.8	0.14
3d4	400-500	4	0.14	
3d4	400-500	4	0.2	
3d4	400-500	4	0.02	
3d4	400-500	4	-0.16	
23c5	400-1000	20	1.62	1.4
23c5	400-1000	20	1.4	
23c5	400-1000	20	1.1	
23c5	400-1000	17	1.19	1.32
23c5	400-1000	17	1.4	
23c5	400-1000	17	1.32	
23c5	400-1000	12	1.19	0.7
23c5	400-1000	12	0.51	
23c5	400-1000	12	0.7	
23c5	400-1000	9	0.63	0.57
23c5	400-1000	9	0.52	

sample	rice husk size (micron)	wall thickness (mm)	measured LRV	median LRV
23c5	400-1000	9	0.57	
23c5	400-1000	3	0.17	0.02
23c5	400-1000	3	0.02	
23c5	400-1000	3	-0.39	
2e4	500-1000	14		0.64
2e4	500-1000	14		
2e4	500-1000	14	0.64	
2e4	500-1000	12		0.28
2e4	500-1000	12	0.28	
2e4	500-1000	12		
2e4	500-1000	10		0.28
2e4	500-1000	10	0.26	
2e4	500-1000	10	0.3	
2e4	500-1000	8		0.35
2e4	500-1000	8		
2e4	500-1000	8	0.35	
2e4	500-1000	6	0.42	0.12
2e4	500-1000	6	-0.27	
2e4	500-1000	6	0.12	
2e4	500-1000	3.5	0.1	0.1
2e4	500-1000	3.5		
2e4	500-1000	3.5		

Rice husk size / Flow rate

Percentage rice husk: 20%

sample	rice husk size (micron)	wall thickness (mm)	area (mm^2)	flow rate (mL/s)	hydraulic head (m)	hydraulic conductivity (m/hr)
121	355-420	20.21	431	0.0037	2.74	0.0002269
122	355-420	20.23	411	0.003	2.74	0.0001944
123	355-420	20.34	403	0.0039	2.74	0.0002578
124	355-420	19.53	432			
131	420-590	19.8	435	0.0041	2.67	0.000252
132	420-590	20.39	417	0.0031	2.67	0.0002018
133	420-590	19.12	440	0.0032	2.67	0.0001844
134	420-590	20.34	439	0.0038	2.67	0.0002381
141	590-710	20.39	413	0.0374	2.68	0.002487
142	590-710	21.04	434	0.0158	2.68	0.0010321
143	590-710	19.67	460	0.0115	2.68	0.0006609
144	590-710	21.11	412	0.0188	2.68	0.0012983
151	710-850	21.78	430	0.5783	2.75	0.0383739
152	710-850	20.95	439	0.55	2.75	0.0343937
153	710-850	20.52	419	0.4087	2.75	0.0261929
154	710-850	21.28	435	0.4277	2.75	0.0273731
161	850-1000	20.26	437	0.512	2.78	0.0306998
162	850-1000	20.49	453	0.344	2.78	0.0201543
163	850-1000	21.64	437	0.3695	2.78	0.0236646
164	850-1000	20.25	473			

Rice husk size / Bacteria removal

Percentage rice husk: 20%

sample	rice husk size (micron)	wall thickness (mm)	measured LRV	median LRV
121	355-420	20.21	2.26	2.26
121	355-420	20.21	2.44	
121	355-420	20.21	2.21	
122	355-420	20.23	3.86	3.86
122	355-420	20.23	3.48	
122	355-420	20.23	3.95	
123	355-420	20.34	2.80	3.04
123	355-420	20.34	3.04	
123	355-420	20.34	3.33	
131	420-590	19.8	1.72	1.70
131	420-590	19.8	1.67	
131	420-590	19.8	1.70	
132	420-590	20.39	2.31	2.62
132	420-590	20.39	2.81	
132	420-590	20.39	2.62	
133	420-590	19.12	2.07	2.13
133	420-590	19.12	2.23	
133	420-590	19.12	2.13	
134	420-590	20.34	1.63	1.63
134	420-590	20.34	1.63	
134	420-590	20.34	1.98	
141	590-710	20.39	2.50	2.30
141	590-710	20.39	2.16	
141	590-710	20.39	2.30	
143	590-710	19.67	4.45	3.68
143	590-710	19.67	3.68	
143	590-710	19.67	2.15	
144	590-710	21.11	2.24	2.38
144	590-710	21.11	2.99	
144	590-710	21.11	2.38	
151	710-850	21.78	0.70	0.47
151	710-850	21.78	0.41	

151	710-850	21.78	0.47	
152	710-850	20.95	0.35	0.35
152	710-850	20.95	0.31	
152	710-850	20.95	0.80	
153	710-850	20.52	0.77	0.77
153	710-850	20.52	0.73	
153	710-850	20.52	0.78	
154	710-850	21.28	0.82	0.82
154	710-850	21.28	0.68	
154	710-850	21.28	1.07	
161	850-1000	20.26	0.83	0.83
161	850-1000	20.26	0.91	
161	850-1000	20.26	0.50	
162	850-1000	20.49	0.83	0.76
162	850-1000	20.49	0.76	
162	850-1000	20.49	0.59	
163	850-1000	21.64	0.94	0.89
163	850-1000	21.64	0.83	
163	850-1000	21.64		

sample	rice husk size (micron)	wall thickness (mm)	measured LRV	median LRV

Rice husk size / Strength

Percentage rice husk: 20%

Wall thickness: 7.4mm

(Approximate calculations not reported in the text)

sample	rice husk size (micron)	load at rupture (N)	moment arm (m)	width (m)	max stress (Mpa)
11	208-355	2069	0.01432	0.0220	150
12	355-420	898	0.01706	0.0220	78
13	420-590	1083	0.01495	0.0239	75
14	590-710	499	0.0136	0.0234	32
15	710-850	333	0.01233	0.0241	19
16	850-1000	207	0.0164	0.0228	16

Factory / Strength

Wall thickness: 7.4mm

sample	rice husk size (micron)	percentage rice husk (%)	max force (N)
Hydrologic 1	0-1000	26.4	2363
Hydrologic 2	0-1000	26.4	506
Hydrologic 3	0-1000	26.4	2051
Hydrologic 4	0-1000	26.4	1890
Hydrologic 5	0-1000	26.4	1664
PHW 1	0-1500	20	588
PHW 2	0-1500	20	528
PHW 3	0-1500	20	676
PHW 4	0-1500	20	557
PHW 5	0-1000	20	680
PHW 6	0-1000	20	479
PHW 7	0-1000	20	630
PHW 8	0-1000	20	718

Throughput: first prelim test

Percentage rice husk: 26.4%

Rice husk size: 400-1000micron

Surface area: 600 mm^2

Wall thickness: 20.06mm

Hydraulic head: 30cm

sample	flow rate (mL/s)	median LRV
23c5	0.01047	1.97
23c5	0.01137	2.00
23c5	0.01184	1.74
23c5	0.01238	1.14
23c5	0.01288	1.40
23c5	0.01359	1.32

Throughput: second prelim test

Percentage rice husk: 20%

Rice husk size: 590-850micron

Surface area: 412mm^2

Wall thickness: 24.67mm

Hydraulic head: 2.74m

sample	flow rate (mL/s)	median LRV
321	0.45	2.17144635
321	0.29	2.18078638
321	0.26	2.0546691
321	0.24	1.84354421
321	0.24	1.89906154
321	0.24	1.80413009
321	0.24	1.83070699

Hydraulic head

Percentage rice husk: 20%

Rice husk size: 590-850micron

sample	wall thickness (mm)	area (mm^2)	hydraulic head (m)	flow rate (mL/s)	median LRV
323	21.93	375	2.74	0.90	2.26
323	21.93	375	2.13	0.50	2.95
323	21.93	375	1.52	0.30	1.65
323	21.93	375	0.91	0.14	2.26
323	21.93	375	0.30	0.03	2.88
324	12.38	375	2.74	0.62	3.07
324	12.38	375	2.13	0.45	2.84
324	12.38	375	1.52	0.30	1.89
324	12.38	375	0.91	0.13	2.84
324	12.38	375	0.30	0.03	3.46

Droplet test

time (s)	number of droplets	time (s)	number of droplets
0	0	359	27
15	0	364	39
165	0	372	68
175	0	380	90
184	0	383	132
190	0	384	99
245	0	385	117
320	1	386	103
324	2	387	141
328	3	397	160
341	4	454	211
344	5	514	220
347	7	574	263
351	9	634	190
355	11		

Appendix D: Optimization data

D.1 Optimization 1

For S>=0.5

set B solver finds F, D, P, L

B	F	D	P	L
0.6	10.4	860	0.23	20
0.8	9.7	830	0.27	20
1	8	800	0.3	20
1.2	6.2	770	0.32	20
1.4	4.7	740	0.33	20
1.6	3.5	710	0.34	20
1.8	2.6	680	0.34	20
2	1.9	650	0.35	20
2.2	1.3	619	0.35	20
2.4	1	589	0.35	20
2.6	0.7	559	0.35	20
2.8	0.5	529	0.35	20
3	0.4	499	0.35	20
3.2	0.3	469	0.35	20
3.4	0.2	439	0.35	20

For S>=0.75

set B solver finds F, D, P, L

B	F	D	P	L
0.8	6.2	830	0.21	20
1	6	800	0.25	20
1.2	5	770	0.27	20
1.4	3.9	740	0.29	20
1.6	3	710	0.31	20
1.8	2.3	680	0.32	20
2	1.7	650	0.32	20
2.2	1.2	619	0.33	20
2.4	0.9	589	0.34	20
2.6	0.7	559	0.34	20
2.8	0.5	529	0.35	20
3	0.4	499	0.35	20
3.2	0.3	469	0.35	20
3.4	0.2	439	0.35	20

For S>=1

set B solver finds F, D, P, L

B	F	D	P	L
1	4	800	0.2	20
1.2	3.8	770	0.23	20
1.4	3.2	740	0.26	20
1.6	2.6	710	0.27	20
1.8	2	680	0.29	20
2	1.5	650	0.3	20
2.2	1.1	619	0.31	20
2.4	0.8	589	0.32	20
2.6	0.6	559	0.32	20
2.8	0.4	529	0.33	20
3	0.3	499	0.33	20
3.2	0.2	469	0.34	20

For S>=1.5

set B solver finds F, D, P, L

B	F	D	P	L
1.6	1.6	710	0.21	20
1.8	1.4	680	0.23	20
2	1.1	650	0.25	20
2.2	0.9	619	0.26	20
2.4	0.7	589	0.27	20
2.6	0.5	559	0.28	20
2.8	0.4	529	0.29	20
3	0.3	499	0.3	20
3.2	0.2	469	0.31	20

For S>=2

set B solver finds F, D, P, L

B	F	D	P	L
2.2	0.6	619	0.22	20
2.4	0.5	589	0.23	20
2.6	0.4	559	0.25	20
2.8	0.3	529	0.26	20
3	0.2	499	0.27	20

D.2 Optimization 2

For S>=1

set B solver finds F, D, P, L

B	F	D	P	L
1	9.8	897	0.31	52
1.5	8.4	881	0.25	59
2	6.5	864	0.35	63
2.5	5.2	863	0.35	77
3	4.4	863	0.35	92
3.5	3.8	863	0.35	106
4	3.3	862	0.35	121
4.5	3	862	0.35	135
5	2.7	862	0.35	149

For S>=2

set B solver finds F, D, P, L

B	F	D	P	L
1	6.9	916	0.28	78
1.5	6.9	895	0.32	73
2	6.1	883	0.34	80
2.5	5.2	863	0.35	77
3	4.4	863	0.35	92
3.5	3.8	863	0.35	106
4	3.3	862	0.35	121
4.5	3	862	0.35	135
5	2.7	862	0.35	149

For S>=3

set B solver finds F, D, P, L

B	F	D	P	L
1.5	5.7	905	0.3	90
2	5.5	891	0.33	90
2.5	5.0	882	0.34	98
3	4.4	863	0.35	92
3.5	3.8	863	0.35	106
4	3.3	862	0.35	121
4.5	3	862	0.35	135
5	2.7	862	0.35	149

For S>=4

set B solver finds F, D, P, L

B	F	D	P	L
1.5	4.9	913	0.29	108
2	4.9	898	0.31	103
2.5	4.6	888	0.33	106
3	4.2	881	0.35	115
3.5	3.8	863	0.35	106
4	3.3	862	0.35	121
4.5	3	862	0.35	135
5	2.7	862	0.35	149

For S>=5

set B solver finds F, D, P, L

B	F	D	P	L
2	4.5	904	0.3	115
2.5	4.3	893	0.32	116
3	4	885	0.34	122
3.5	3.7	878	0.35	130
4	3.3	862	0.35	121
4.5	3	862	0.35	135
5	2.7	862	0.35	149

D.3 Optimization 3

For S>=0.25

set B solver finds F, D, P, L

B	F	D	P	L
0.3	22.9	651	0.31	10
0.5	17.8	651	0.35	15
0.688	13.6	651	0.35	20
1.1	0.2	600	0.32	10
1.9	0.1	400	0.35	15
2.3	0.1	400	0.35	18

For S>=0.5

set B solver finds F, D, P, L

B	F	D	P	L
0.3	15.6	650	0.21	10
0.5	15.9	651	0.31	15
0.688	13.6	650	0.35	20
1.1	0.2	400	0.29	10
1.3	0.2	400	0.32	11
1.5	0.1	400	0.33	13
1.7	0.1	400	0.35	14
1.9	0.1	400	0.35	15
2.1	0.1	400	0.35	17
2.3	0.1	400	0.35	18
2.5	0.1	400	0.35	19
2.5	0.1	400	0.35	19

For S>=1

set B solver finds F, D, P, L

B	F	D	P	L
0.5	11.4	650	0.23	15
0.688	9.3	760	0.24	20
1.3	0.1	400	0.23	11
1.7	0.1	400	0.31	15
2.1	0.1	400	0.32	17
2.5	0.1	400	0.34	19

D.4 Optimization 4

For S>=1

set B solver finds F, D, P, L

B	F	D	P	L
0.5	11.4	651	0.23	15
1	9.71	653	0.35	28
1.5	6.75	652	0.35	40
2	5.15	652	0.35	53
2.5	4.17	652	0.35	65
3	3.5	652	0.35	78
3.5	3.01	652	0.35	90
4	2.65	652	0.35	103
4.5	2.36	652	0.35	115
5	2.13	652	0.35	128

For S>=2

set B solver finds F, D, P, L

B	F	D	P	L
1	8.23	650	0.3	28
1.5	6.75	652	0.35	40
2	5.15	652	0.35	53
2.5	4.17	652	0.35	65
3	3.5	652	0.35	78
3.5	3.01	652	0.35	90
4	2.65	652	0.35	103
4.5	2.36	652	0.35	115
5	2.13	652	0.35	128

For S>=4

set B solver finds F, D, P, L

B	F	D	P	L
1.5	5.8	651	0.3	40
2	5.0	651	0.34	53
2.5	4.2	724	0.35	65
3	3.5	791	0.35	78
3.5	3.0	832	0.35	90
4	2.7	859	0.35	103
4.5	2.4	877	0.35	115
5	2.1	891	0.35	128

Glossary

Adsorption: The adhesion of particles to a surface.

Agar plate: A petri dish filled with a growth medium for culturing micro-organisms.

Bacteria removal: The percentage of bacteria removed by a filter, often expressed as a logarithmic reduction value (LRV).

Biocide: A substance which damages a harmful organism through chemical or biological means.

Bubble point test: A test where air is forced against the inside of a submerged filter. The pressure corresponding to the first bubbles seen on the outside of the filter is used to calculate a characteristic pore length.

Bulk Reynold's number: A dimensionless number used to determine whether flow through porous media is laminar or turbulent.

Capillary radius: When modeling a porous media as a bundle of pipes, the capillary radius can be used to describe the radius of one of those pipes.

Characteristic pore length: A measure of characteristic pore size that corresponds to the minimum diameter through which a liquid needs to pass in order to breach the sample.

Characteristic pore size: The size in units of length that best describes the dimensions of the pores in the filter.

Collision percentage: The percentage of particles that approach a filter surface that collide with it.

Colony-forming unit (cfu): The number of viable bacterial cells in a unit of liquid typically reported as cfu/mL.

Combustible: A material incorporated into the unfired ceramic pot filter (CPF) that combusts upon firing leaving a void in its place. In this study, ground rice husk is used as the combustible. Saw dust has been used in other studies.

Continuous model: A model of a system that assumes behavior varies smoothly with changes in the variables.

Diffusion: When particles are brought into contact with a filter surface as a result of the random movement of particles suspended in a fluid (also called Brownian motion).

Discrete model: A function whose adjacent points are not necessarily on the same curve.

Disease burden: The total impact of public health problems on society including the financial cost, mortality, morbidity and other indicators.

Disk: In this study, a small circular sample cut from the bottom of a ceramic pot filter or produced specially for use in the experiments.

Escherichia coli K12: A rod-shaped bacterium commonly found in the lower intestine of warm-blooded organisms. The K12 strain is non-toxic for humans.

Effluent: Fluid flowing out of a filtration system. In this case, water that has passed through the ceramic pot filter.

Fecal-oral route: The route of transmission of diseases in which pathogens in feces are passed to new hosts through the mouth, often from drinking contaminated water.

Filtration mechanism: The process by which contaminants are removed from the water. Mechanisms include sedimentation, adsorption and screening among others.

Fine-grain model: A model that addresses the micro-structure of the system.

Flow rate: Volume of liquid per unit time exiting the ceramic pot filter.

Fractional rice husk size: An interpretation of characteristic pore size as a fraction of the rice husk size.

Granular media filtration: Water filtration that works by passing liquid through a layer of sand (or other media) such that particles suspended in the liquid are caught in the media.

Half crack length: The length of a crack within a brittle material. Given an applied stress, if the half crack length exceeds a critical value, the material will fracture.

Hydraulic conductivity: The ease with which a fluid can move through a porous media measured in units of length per unit time. Hydraulic conductivity is independent of characteristics of the fluid.

Hydraulic diameter: A measure of a characteristic diameter of an irregular shape. It is defined as four times the cross-sectional area divided by the perimeter.

Hydraulic head: A measure of water pressure at a point. It is reported in units of length corresponding to the height of water above the point.

Improved water: Water from a source which is protected from outside contamination, especially fecal matter.

Incomplete combustion: Occurs when there is not enough oxygen to allow the fuel to react completely. The result is a carbon residue.

Inertia: In turbulent flows, collision of particles with the internal surface of the filter caused by momentum.

Influent: Fluid flowing into a system. In this case, contaminated water before it has passed through the ceramic pot filter.

Intrinsic clay pores: Microscopic pores in a ceramic material that arise from open space in the alignment of the clay particles during firing. These pores exist independently of the pores produced by introducing a combustible.

Laminar flow: Fluid flow whose motion is dominated by viscous forces. Flow in porous media is almost always laminar due to the small sizes of the pores and the low flow rates.

Load cell: A device that is used to convert a force into an electrical signal.

Load at rupture: The amount of force applied to the ceramic pot filter disk that resulted in material failure within the disk, expressed in units of force.

Logarithmic reduction value (LRV): A measure of the removal of micro-organisms from contaminated water. An increase of one LRV corresponds to an order of magnitude increase in contaminant removal.

Lysogeny/Luria (LB) broth: A nutrient-rich liquid in which to cultivate bacteria.

Manufacturing parameter: A manufacturing choice made when producing the ceramic pot filter. In this study, the manufacturing parameters of interest are percentage rice husk, rice husk size and wall thickness.

Maximum firing temperature: The maximum temperature reached in the kiln when firing the ceramic pot filters.

Mechanical screening: Separation of particles based on size by pushing them against a mesh. The particles that are larger than the holes in the mesh will be stopped.

Mesh: A woven material with many small holes that can be used for separating out particles based on size.

Modulus of rupture: The level of internal stress that results in the failure of a brittle material, expressed as force per unit area.

Moment at rupture: The amount of torque applied to a brittle object which results in material failure within the object, expressed as force multiplied by distance.

Non-wetting: When a liquid resists contact with a solid. When a drop does not wet to a surface, it will not spread out on the surface but instead keeps its drop-like shape.

Parameter/performance matrix: A chart for organizing information about the ceramic pot filter where each cell contains information about the relationship between a manufacturing parameter and a metric of performance.

Path through the filter: Flow through a porous media can be modeled as flow through a bundle of narrow pipes. A "path" through the filter is defined as one of those pipes.

Percentage rice husk: The mass of rice husk as a percentage of the mass of the dry ingredients (clay powder and rice husk) used in production of the ceramic pot filter. Not to be confused with porosity which is the volume percentage of void space within the total volume of the fired filter.

Performance metric: A measure of the product's fulfillment of specific design goals. The metrics of performance for the ceramic pot filter studied here are flow rate, bacteria removal and strength.

Permeability: A measure of the ability of a porous media to allow fluids to pass through it measured in units of length squared. Permeability is dependent on the characteristics of the fluid as well as the characteristics of the porous media.

Phosphate buffered saline (PBS): A water-based salt solution used in biological research which maintains an ion concentration level which is non-toxic to cells.

Physical properties: Measurable characteristics of the filter. These include characteristic pore size, porosity and wall thickness.

Plating: Spreading a liquid sample of known quantity onto an agar plate in order to determine the number of colony forming units (cfu) present in the sample.

Pore height: When modeling contaminant removal, the vertical dimension of a pore left behind by a rice husk particle.

Porosity: The volume percentage of void space within the total volume of the fired filter.

Pressure drop: The difference in total pressure between two points on a pipe. For this application, pressure drop refers to the difference in pressure between the inside surface and the outside surface of the filter.

Quality assurance: Efforts taken to increase the percentage of manufactured units which are within the desired specifications. This is in contrast to quality control which is the removal of out of specification units before distribution or sale.

Removal constant: The percentage of particles that collide with a filter surface which are adsorped.

Rice husk: The hard, protective covering on a grain of rice.

Rice husk height: The length of the thin dimension of the rice husk, approximated in this study as 100µm.

Rice husk pores: When the rice husk combusts during firing, void spaces are left where the rice husk used to be.

Rice husk size: The length dimension of the openings of the mesh used to sieve the rice husk before incorporation in the filter. Since the rice husk is sieved between two meshes (thus discarding combustible that is too big or too small) rice husk size is the average of the top and bottom mesh sizes. This term is not to be confused with "characteristic pore size" which is the length value associated with the size of the pores within the filter.

Rice husk size range: The difference in size between the top and bottom meshes that were used to sieve the rice husk.

Scanning electron microscope: A microscope that uses a beam of electrons to produce an image of a sample with resolution down to the nanometer range.

Sedimentation: When contaminants which are heavier than a fluid settle to the bottom over time.

Sieving: Separating particles based on size using a mesh.

Step function: A function that equals a different constant in different parts of the domain.

Strain energy release rate: The energy dissipated during fracture per unit of newly created fracture surface area. The higher this value, the more energy is needed to fracture the material.

Throughput: Total volume of fluid that has passed through the filter.

Tortuosity: The ratio between the length of the path that water must travel to traverse a material and the wall thickness of that material.

Total coliform: A set of bacteria genera including *E. coli* whose presence in water indicates fecal contamination.

Triplicate: Independent tests on three water samples from the same source are conducted. This is done so that an average value from the three tests can be determined.

Turbid water: Water that appears cloudy due to the presence of suspended solids including dirt and biological contaminants.

Turbulent flow: Fluid flow whose motion is dominated by inertial forces. Turbulent flows are common when the fluid velocity is high.

Too numerous to count: When so many bacteria are present on an agar plate that it is not possible to count the number of colonies accurately. This indicates that the incorrect dilution was used.

Wall strength: In this case, strength is defined as the moment at rupture. Filters need to be strong enough that they do not break when handled.

Wall thickness: The distance between the inside and outside surface of a ceramic pot filter or the top and bottom surface of a filter disk.

Worm gear jack: A mechanism capable of exerting large forces through the mechanical advantage produced by a worm gear.

Young's modulus: A measure of the stiffness of a material defined as the ratio of stress to strain.

Zero readings: When no bacteria are detected in a sample of water. This indicates either an absence of bacteria in the sample or an error in the testing procedure.

Bibliography

[1] World Health Organization and UNICEF (2012). Progress on drinking water and sanitation: 2012 update. *WHO/UNICEF Joint Monitoring Programme for Water Supply and Sanitation*. http://www.unicef.org/media/files/JMPreport2012.pdf (accessed May 17, 2013).

[2] Pruss, A., Kay, D., Fewtrell, L., Bartram, J. (2002). Estimating the burden of disease from water, sanitation, and hygiene at a global level. *Environmental Health Perspectives*, 101(5). http://www.ncbi.nlm.nih.gov/pmc/articles/PMC1240845/pdf/ehp0110-000537.pdf (accessed May 17, 2013).

[3] Kosek, M., Bem, C., Guerrant, R. (2003). The global burden of diarrhoeal disease, as estimated from studies published between 1992 and 2000. *Bulletin of the World Health Organization*, 81, 197–204. http://www.ncbi.nlm.nih.gov/pmc/articles/PMC2572419/pdf/12764516.pdf (accessed May 17, 2013).

[4] Waddington, H., Snilstveit, B. (2010). Effectiveness and sustainability of water, sanitation, and hygiene interventions in combating diarrhea. *Journal of Development Effectiveness*, 1:3. 295–335.

[5] Clasen, T. (2011) Household water treatment and safe storage in low-income countries. Wiley-Blackwell.

[6] The Ceramics Manufacturing Working Group (2011). Best Practice Recommendations for Local Manufacturing of Ceramic Pot Filters for Household Water Treatment. *Center for Disease Control and Prevention*. http://waterinstitute.unc.edu/media/Best%20Practice%20Recommendations%20for%20Manufacturing%20Ceramic%20Pot%20Filters%20June2011.pdf (accessed May 17, 2013).

[7] Brown, J. (2007). Effectiveness of Ceramic Filtration for Drinking Water Treatment in Cambodia. PhD Dissertation in Environmental Sciences and Engineering, University of North Carolina at Chapel Hill. http://potterswithoutborders.com/wp-content/uploads/2011/06/joe-brown-dissertation.pdf (accessed May 17, 2013).

[8] Hunter, P. (2009). Household water treatment in developing countries: comparing different intervention types using meta-regression. *Journal of Environmental Science and Technology*, 43, 8991–8997.

[9] Potters for Peace (2013). pottersforpeace.com (accessed May 17, 2013).

[10] Lantagne, D.S. (2001). Investigation of the potters for peace colloidal silver impregnated ceramic filter report 1: intrinsic effectiveness. Alethia Environmental: Allston, MA, USA. http://web.mit.edu/watsan/Docs/Other%20Documents/ceramicpot/PFP-Report1-Daniele%20Lantagne,%2012-01.pdf (accessed May 17, 2013).

[11] Donachy, B. (2011) Summaries of Reports and Studies of the Ceramic Water Purifier (CWP): A Colloidal Silver (CS) Impregnated Ceramic Water Filter. http://www.ide-cambodia.org/download/Review-and-summary-of-studies-and-reports-english-Jan112.pdf (accessed May 17, 2013).

[12] World Health Organization (2011). Guidelines for drinking-water quality, fourth edition. *Water, Sanitation and Health (WSH) Programme*. http://www.who.int/water_sanitation_health/publications/2011/dwq_guidelines/en/index.html (accessed May 17, 2013).

[13] Brown, J., Sobsey, M. (2011). Evaluating household water treatment options: heath-based targets and microbiological performance specifications. *World Heath Organization*. http://whqlibdoc.who.int/publications/2011/9789241548229_eng.pdf (accessed May 17, 2013).

[14] Rayner, J., Oyanedel-Craver, V., Zhang, H. (2012). Impact of Manufacturing Variables on the Effectiveness of Ceramic Pot Filtration: Report for the Global Ceramic Water Pot Industry, PATH, Seattle. http://www.ceramicwaterfilter.org/wp-content/uploads/manufacturing_variables_final_report.pdf (accessed May 17, 2013)

[15] Gensburger, I (2011). Investigation of the Critical Parameters in the Production of Ceramic pot filters. University of Oklahoma International Water Conference, October, 2011. https://www.ou.edu/content/dam/CoE/WaTER%20Center/documents/conference2011/Presentations/Gensburger.pdf (accessed May 17, 2013).

[16] Plappally, A. (2010). Theoretical and Empirical Modeling of Flow, Strength, Leaching and Micro-Structural Characteristics of V Shaped Porous Ceramic Pot Filters. PhD Dissertation in Food, Agricultural and Biological Engineering, Columbus, Ohio. http://etd.ohiolink.edu/send-pdf.cgi/Plappally%20Anand.pdf?osu1276860054 (accessed May 17, 2013).

[17] Miller, M. (2012). Hemispheric Ceramic Pot Filter Evaluation and Quality Assurance Program in Northern Ghana. Masters of Engineering thesis in Environmental Engineering, MIT. http://web.mit.edu/watsan/Docs/Student%20Theses/Ghana/2012/Thesis_MattMiller_FINAL-5-18-12.pdf (accessed May 17, 2013).

[18]: Lantagne, D. (2010). Effect of production variables on microbiological removal in locally-produced ceramic filters for household water treatment. *International Journal of Environmental Health Research*, 1–17.

[19] Watters, T. (2010). The Effect of Compositional and Geometrical Changes to the Bending Strength of the Ghanaian Ceramic Pot Filter. Masters of Engineering Thesis in Environmental Engineering, MIT. http://web.mit.edu/watsan/Docs/Student%20Theses/Ghana/ Thesis%20FINAL%20Travis%20Watters%205-23-10.pdf (accessed May 17, 2013).

[20] Miller, T. (2010). Optimizing Performance of Ceramic Pot Filters in Northern Ghana and Modeling Flow through Paraboloid-Shaped Filters. Masters of Engineering Thesis in Environmental Engineering, MIT. http://web.mit.edu/watsan/Docs/Student%20Theses/Ghana/Thesis%20FINAL%20Travis%20Reed%20Miller%205-24-10.pdf (accessed May 17, 2013).

[21]: Van Halem, D. (2006). Ceramic silver impregnated pot filters for household drinking water treatment in developing countries. Master of Science thesis in Civil Engineering, Delft University, Netherlands. http://potterswithoutborders.com/wp-content/uploads/2011/06/ finalcsfreport_29-10-2-van-dalem1.pdf (accessed May 17, 2013).

[22] Webb, P. (2001). An introduction to the physical characterization of materials by mercury intrusion porosimetry with emphasis on reduction and presentation of experimental data. Micromeritics Instrument Corp. Norcross, GA. http://www.particletesting.com/docs/intro_mip.pdf (accessed May 17, 2013).

[23] Jeol USA (2013). Jeol Guide to Scanning Microscope Observation. http://www.geology.wisc.edu/~johnf/g777/JEOLguide.pdf (accessed May 17, 2013).

[24] Nimmo, J. R. (2004). Porosity and pore size distribution. *Encyclopedia of Soils in the Environment*, 3, 295–303. http://wwwrcamnl.wr.usgs.gov/uzf/abs_pubs/papers/nimmo.04.encyc.por.ese.pdf (accessed May 17, 2013).

[25] Scheffler, M., Colombo, P. (2005). Cellular ceramics: structure, manufacturing, properties and applications. Wiley-VCH, Weinheim, Germany.

[26] Benjamin, M., Lawler, D. (2013). Water quality engineering: physical/chemical treatment processes. Chapter 14. Wiley.

[27] Kendall, K., Howard, A., Birchall, J., Pratt, P., Proctor, A. Jefferis, S. (1983). The relation between porosity, microstructure and strength, and the approach to advance cement-based materials [and discussion]. *Philosophical Transactions of the Royal Society of London*. 310, 139–153.

[28] The Barber Lab, UCLA Department of Ecology and Evolutionary Biology https://www.eeb.ucla.edu/Faculty/Barber/Web%20Protocols/LB%20Agar%20Plates.pdf (accessed May 17, 2013).